Alma Mater Studiorum – Università di Bologna

DOTTORATO DI RICERCA IN

BIOCHIMICA

*Ciclo **XXIV***

Settore Concorsuale di afferenza: 05/E1

Settore Scientifico disciplinare: BIO/10

Characterization of new molecular targets involved in iodide flux in the thyroid gland: the anoctamins

Presentata da: Dott.sa Carmela Iosco 0000376278

Coordinatore Dottorato	**Relatore**	**Correlatore**
Chiar.mo Prof.	**Chiar.mo Prof.**	**Prof.sa**
Giorgio Lenaz	**Giovanni Romeo**	**Kerry Rhoden**

Esame finale anno 2012

INDEX

ABSTRACT

Iodide transport is necessary for the synthesis of thyroid hormones following accumulation in the follicular lumen out of thyroid cells, via channels unknown with the exception of pendrin.

According to our hypothesis, TMEM16A could be the main molecular identity of the channel mediating iodide efflux in the thyroid gland. TMEM16A is the prior candidate for calcium-activated chloride conductance (CaCC). TMEM16A belongs to the TMEM16/anoctamin family comprising ten members (TMEM16A-K). Higher affinity of TMEM16A for iodide and predicted expression in the thyroid gland suggest its mediation of iodide efflux.

The aim of this project was to identify the role of TMEM16A in iodide transport in the thyroid gland, by characterizing its molecular expression and functional properties.

We demonstrated that TMEM16F, H, K transcripts are expressed in FRTL-5 thyroid cells, as well as TMEM16A, which is TSH-independent. Tumor tissue from human thyroid maintains TMEM16A expression.

Functional *in vivo* experiments in FRTL-5, stably expressing YFP-H148Q/I152L fluorescent protein as a biosensor, showed that iodide efflux is stimulated by agonists of purinergic receptors with an order of potency of ATP>UTP>ADP (compatible with an involvement of P_2Y purinergic receptors), and by agonists of adrenergic receptors (epinephrine, norepinephrine and phenylephrine). Iodide efflux was blocked by α-receptor antagonists prazosin and phentolamine, consistent with a role of α1 adrenergic receptors. Iodide efflux was specifically dependent on calcium mobilized from intracellular compartments and induced by the calcium ionophore ionomycin. CaCC blockers suppressed ionomycin-/ATP-/epinephrine-stimulated iodide efflux.

Heterologous expression of TMEM16A in CHO K1 cells induced calcium-activated iodide fluxes.

All these results support the hypothesis of the involvement of TMEM16A in calcium-dependent iodide efflux induced by receptor agonists in thyroid cells. TMEM16A may represent a new pharmacological target for thyroid cancer therapy, since its blockade may enhance the retention of radioiodide by tumour cells enhancing the efficacy of radioablative therapy.

CHAPTER 1

INTRODUCTION

1.1 THYROID GLAND

1.1.1 STRUCTURAL AND MORPHOLOGICAL CHARACTERISTICS

Thyroid gland is an endocrine gland specialized in synthesis, storage and secretion of hormones essential for regulation of metabolism and for thermogenesis.

It is localized at under- hyoid region of neck, on the front surface of trachea. Thyroid gland contacts laterally sternocleidomastoid muscle and carotid arteries, rear-recurrent laryngeal nerve, trachea and esophagus. Above thyroid gland there is larynx.

Thyroid gland consists of two side lobes joined in the midline by a thin portion of tissue, isthmus. Like all endocrine glands, thyroid is richly vascularised, in particular branches of internal carotid artery: two superior thyroid arteries. Each lobe has a length of about 4 cm and a width of about 1-2 cm. In adults, normal thyroid gland weighs between 15 and 25 grams. Its size, however, may be different according to individual, environmental, nutritional factors.

Secretory epithelial cells produce thyroid peptide hormones T_3 (tri-iodothyronine) and T_4 (tetra-iodothyronine or thyroxin), calcitonin. These cells are classified into two types, follicular and parafollicular. Follicular cells (thyrocytes) are organized as a single layer of cubic hollow structures called follicles (50-500 uM in diameter), representing unity of structure and function of thyroid gland (Fig.1.1). Thyroid gland is the only body follicular gland. Thyrocytes synthesize, accumulate and secrete thyroid hormones. In fact, it is enclosed in follicular lumen thyroid colloid, a protein matrix which acts as a deposit of T_3 and T_4 thyroid hormones, secreted by thyrocytes in response to hormonal stimuli, as the glycoprotein thyroglobulin (TG).
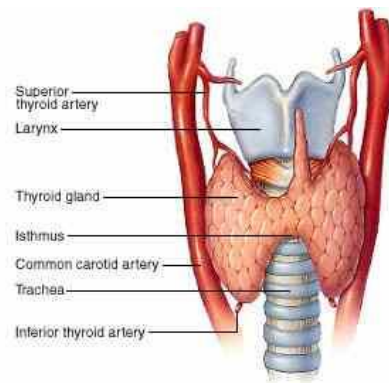
Fig. 1.1 Anatomy and follicular structure of human thyroid gland. (pyroenergen.com)

Thyroid gland is the only body gland to accumulate hormones outside the cells that synthesize them. Due to their active secretion of protein molecules, thyrocytes are characterized by a large number of mitochondria and a rough endoplasmic reticulum of considerable size.

Thyrocytes parafollicular cells ("clear" or "C") are among follicular thyrocytes and in interfollicular interstitium. Parafollicular cells are not organized into defined structures such as follicles, but scattered in small groups. These cells secrete calcitonin hormone, which helps body metabolism of calcium, in antagonism with parathyroid hormone secreted by dark chief cells of parathyroid glands. The latter are in contact with rear side lobes of thyroid gland. Calcitonin inhibits the release of minerals from bones causing hypocalcaemia and ipophosphoremia, whereas PTH promotes their release causing hypercalcaemia and hyperphosphatemia.

Hormones T_3 and T_4 produce rather wide-ranging effects by interacting with several districts of organism: they increase basal metabolic rate, oxygen consumption and thermogenesis, stimulate metabolism of carbohydrates and lipids, accelerate metabolism of cholesterol, decrease liver glycogen levels.

Hormones T_3 and T_4 also play a role in growth and development of organism not only in general, since they stimulate protein synthesis, proliferation and cell differentiation, but also, particularly, in cardiovascular parameters such as frequency, heartbeat, myocardial contractility and vasodilatation.

Thyroid hormones triiodothyronine (T_3) and thyroxin (T_4) are the only endogenous molecules to contain iodine element, on which thyroid gland depends for its proper function. In fact, thyroxin contains two molecules of tyrosine and four iodine atoms while triiodothyronine two molecules of tyrosine and three atoms of iodine.Through

bloodstream, dietary iodine is transported into thyroid follicular cells as iodide anion. In this manner thyroid hormones can be synthesized.

1.1.2 INNERVATION

Innervation of thyroid gland is supplied by cervical sympathetic and vagus nerve, mainly through superior inferior laryngeal nerve (recurrent), responsible for phonation.

Superior laryngeal nerves have an internal branch, which is distributed in supraglottic laryngeal mucosa and in the two faces of epiglottis, and an external branch, which innervates cricothyroidal muscle and is distributed in subglottic and laryngeal mucosa up to laryngeal ventricle of Morgagni mucosa. Lesion of external branch of superior laryngeal nerve causes paralysis of cricothyroidal muscle and consequently loss of ipsilateral true vocal cord tension, which leads to resulting dysphonia (voice impairment).

Laryngeal nerves below, known as "recurrent" (because of their course that embraces arch of aorta to the left and the right subclavian artery), are the main nerves, with phonatory function, because innervate all the muscles endolaryngeal that determine vocal cords motility.

Experimental evidences showed thyroid innervations and signalling pathways for thyroid hormone synthesis in details.

Cholinergic nerve fibers take contacts with follicle cells and cholinergic mediators enhance cGMP accumulation in human normal thyroid gland. A muscarinic receptor antagonist, atropine, blocked this activity, effect that suggested involvement of parasympathetic nervous system in regulation of human thyroid function (Van Sande et al., 1980)

In a cell model, FRTL-5 thyroid cells, a muscarinic receptor was found to inhibit phospholipase C activity. Carbachol, a cholinergic agonist, decreases the steady-state iodide content, an effect correlated with iodination of thyroglobulin and with thyroid hormone synthesis. Carbachol potentiated thyrotropin-induced stimulation of adenylyl cyclase enzyme, without alteration of cAMP basal levels (Di Girolamo et al., 1991).

Histochemistry and cytospectrofluorometry studies in calf thyroid cells revealed that sympathetic nerve fibres, located around vessels as a network and close to thyroid follicles as single fibres, contained norepinephrine.

Mast cells, located around follicles and vessels, contain histamine and dopamine and the latter was found also in parafollicular cells. Numerous acetylcholine-containing nerve fibres were found around vessels and between follicles.

Isolated thyroid cells, exposed to several amines, showed a increase in iodine uptake and organification stimulated by norepinephrine and dopamine. Also epinephrine, isoproterenol, and S-hydroxytryptamine produced responses with the same entity. Phentolamine, an α adrenergic blocking agent, blocked iodine organification. Thyroid hormone synthesis was suggested to be regulated with contribution of norepinephrine released from intrathyroidal sympathetic terminals and of dopamine released from intrathyroidal mast cells (Melander et al., 1973)

Comparison between fetuses, young (20-45), and elderly (greater than 60) euthyroid people with thyroid cancer or hyperparathyroidism, revealed a reduction in the number of interfollicular adrenergic nerve terminals and lower norepinephrine concentration with increasing age, suggesting functional role of catecholamines in thyroid gland (Melander et al., 1978).

1.1.3 CATECHOLAMINES

 Structure of catecholamines consists of a catechol (1-2 dihydroxy-benzene), and an amino group (fig. 1.2). Central nervous system, sympathetic nerve endings and cromaffin cells of adrenal medulla synthesize adrenaline/epinephrine, noradrenaline/norepinephrine and dopamine from tyrosine aminoacid.

 Many cells possess adrenergic receptors, and binding of an agonist will generally cause a sympathetic (or sympathomimetic) response (e.g. fight-or-flight response). For instance, heart rate will increase and pupils will dilate, energy will be mobilized, and blood flow diverted from other non-essential organs to skeletal muscle.

 Adrenergic receptors are classified into 2 types, α and β, divided into 5 subtypes:

- ❖ $\alpha1$ and $\alpha2$, with different affinity to antagonists;
- ❖ $\beta1$, with equal affinity for epinephrine and norepinephrine;
- ❖ $\beta2$, with greater affinity for epinephrine than norepinephrine;
- ❖ $\beta3$.

 Dopaminergic receptors are classified into 2 types, D1 and D2, divided into 5 subtypes:

- ❖ D1 and D5;
- ❖ D2, D3, D4.

Adrenergic $\alpha1$ receptors are coupled to Gq proteins; when activated, hydrolysis of phosphatidylinositol (3,4,5)-trisphosphate (PIP3) leads to formation of 1,4,5-triphosphate (IP_3) and diacylglycerol (DAG). IP_3 induces Ca^{2+} release from intracellular stores increase Ca^{2+} influx across plasma membrane. Ca^{2+}dependent protein kinase activated may mediate free Ca^{2+} effects. DAG actives protein kinase C.

 Adrenergic $\alpha2$ receptors are coupled to Gi proteins, when activated lead to inhibition of adenylate cyclase with consequent intracellular cAMP decrease.

 β receptor activation induces adenylate cyclase activation with intracellular cAMP increase. Final effect is activation of glycogen phosphorylase.

 Adrenergic receptors can undergo slower or faster desensitization after exposure to catecholamines or sympathetic mimetics drugs. Receptors can be phosphorylated by protein kinase GRK and increase their affinity for β-arrestins, once bound to them are no longer able to activate G protein.

Isoproterenol is the main β-adrenergic agonist.

Among α-adrenergic antagonists there are:

❖ phentolamine, competitive antagonists against α1 α2 adrenergic receptors and inhibitor of serotonin-dependent responses; phentolamine can be agonist on muscarinic receptors and histamine H1 and H2 receptors;

❖ prazosin, highly selective for α1-adrenergic receptors, 1000 fold more than α2-adrenergic receptors.

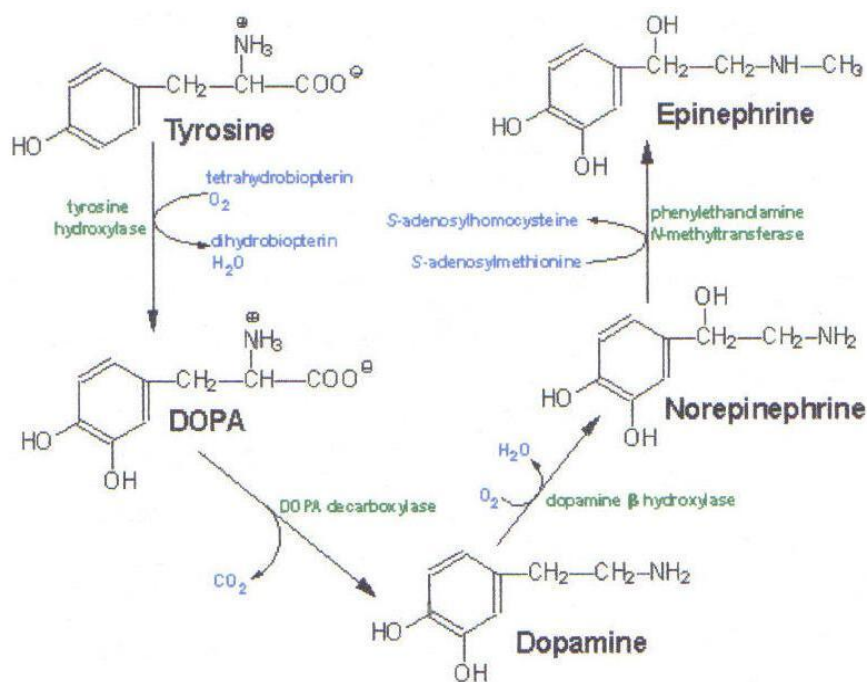The most important β-antagonist is propranolol, non-selective antagonist against all subtypes of β receptors.

Fig. 1.2 Structure of catecholamines scientific-training.it

1.1.4 EFFECT OF CATECHOLAMINES ON THYROID GLAND

Catecholaminergic system functional role in thyroid gland was examined in several studies.

Thyrotropin increases number of adrenergic α1- receptors by inducing their biosynthesis, a cAMP-mediated effect (Corda et al, 1985). Adrenergic α1- receptors on FRTL-5 thyroid cells have been functionally linked to iodide efflux into follicular lumen and to thyroglobulin iodination and, subsequently, thyroid hormone synthesis; adrenergic α1-receptor signal was mediated by Ca^{2+} rather than by cAMP, with involvement of arachidonic acid intermediates. Specifically, this studies employed norepinephrine. (Corda et al, 1985). According to other studies, biosynthesis of adrenergic α1- receptors in FRTL-5 cells depends on TSH action, which induces a signaling mechanism cAMP dependent, since binding of radioactive prazosin, α-adrenergic agonist, was dependent on TSH concentration in culture medium (Rope and Khon, 1985).

1. 2 IODIDE TRANSPORT

According to studies carried out so far, molecular responsible for transport from basolateral to apical membrane of thyrocytes, within the follicular lumen, are mainly two proteins: Sodium Iodide symporter (NIS) (Rodriguez, 2002) and pendrin (Royaux, 2000) (fig. 1.3).

NIS transporter is able to accumulate iodide within thyrocytes up to 30-40 fold compared to plasma compartment (nM), taking it at concentrations of the order of mM (Carrasco, 1993). Transport is active: iodide transport against electrochemical gradient is allowed by transport of sodium according to gradient concentration maintained from Na^+/ K^+ ATPase pump with consume of ATP. In this manner, iodide can be transported from interstitial fluid to thyrocyte cytoplasm.
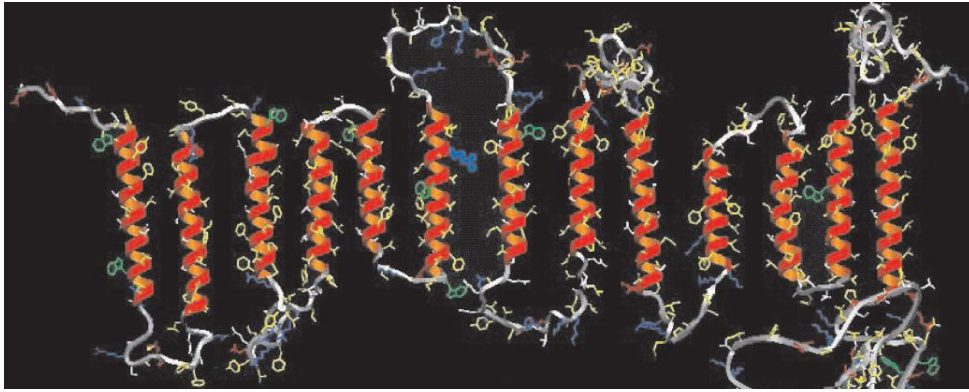
Fig. 1.3 NIS (Sodium Iodide Symporter, Dohán et al., 2003)

Iodide is then transported into follicular lumen through apical membrane by means of pendrin, an anion exchanger which carries iodide and chloride into thyroid gland, in a passive manner, according to concentration gradient (Soleimani, 2001, Scott, 2000).

Once in follicular lumen, iodide undergoes a oxidation process with tyrosine residues to form MIT (monoiodiotyrosine) and DIT (diiodiotyrosine) ("organification", since iodine is incorporated into an organic compound, the iodinated thyroglobulin) . At the interface between apical membrane and follicular lumen there are the enzymes that allow organification process of iodide to be accumulated in colloid, with more details a NADPH tireossidasi (ThOX), which generates peroxide (H_2O_2), substrate of thyroid peroxidase (TPO). Thyroglobulin, a protein found in most of the colloid, provides tyrosine residues that undergo iodination to form thyroid hormones, it acts as "scaffolding" for their synthesis. Thyroglobulin also allows their accumulation after synthesis.

Thyroglobulin monoiodiotyrosine and diiodiotyrosine, formed by oxidation of iodide, together constitute triiodiotyrosine (T_3) and tetraiodiotyrosine or thyroxin (T_4) via an ether bond (Cahman, 1977, Virion, 1981). Thyroglobulin may contain from four to eight molecules of hormones.

Thyroid hormones are released as a result of external stimuli, in particular, TSH (Thyroid-Stimulating Hormone), to activate processes described below. Thyroglobulin related to T_3 and T_4 hormones is internalized by endocytosis, hydrolyzed in fagolisosomes, so hormones can be released. Thyroglobulin undergoes a process of recycling being re-transported into colloid or degraded, hormones are

secreted into bloodstream with a mechanism still not well defined or metabolised by microsomal iodotyrosine dehalogenase, to recover as much as possible iodine not secreted.

Iodide metabolism, synthesis and release of thyroid hormones are possible thanks to follicular organization and thyroid follicular cell polarization in basolateral and apical area, each with its own proteins properly placed and not free to move laterally, also thanks to presence of tight junctions between cells; the latter, moreover, allow the maintenance of iodide concentration gradient between the inside and the outside of follicle and retention of luminal content which otherwise would diffuse.

TSH is the main regulator of thyroid hormones T_3 and T_4. Control occurs via hypothalamic-pituitary-thyroid axes. TRH hormone (thyrotropin releasing hormone) is secreted by hypothalamus, reaches anterior pituitary where it stimulates TSH release (thyroid stimulating hormone or thyrotropin) from thyrotropic cells. TSH, thus synthesized and poured into bloodstream, acts on a specific membrane receptor (the TSHR, TSH receptor, coupled to a stimulatory G protein), which undergoes a conformational change activates stimulatory G protein resulting in the increase AMP levels of 3'-5 'cyclic (cAMP) intracellular, which leads to activation of a cAMP-dependent protein kinase (PKA). Finally process leads to activation of thyrocyte, which internalises cells by phagocytosis of colloid. Phagosomes, once formed, fuse with lysosomes, which split the bond between thyroglobulin and thyroid hormones, then released into bloodstream via basolateral membrane .

T4 is secreted about 20% more than in T3 in the bloodstream. Hormones released from thyroglobulin but not secreted are deiodinated from iodothyrosine dehalogenase to allow all of iodide to be reabsorbed and recycled.

TSH, through activation of these processes, stimulates thyroid gland to synthesize thyroid hormones and increase its volume.

Elevated levels of T_4 and T_3 inhibit the secretion of TRH and TSH, with a negative feedback mechanism. Drugs that inhibit T_4 and T_3 synthesis increase TSH circulating levels, which stimulates thyroid gland hyperplasia (goiter).

Thyroid hormone release can also be stimulated indirectly through blood vessels by nerve fibers of cervical sympathetic ganglia.

As with all components contained in the plasma, thyroid hormone molecules free and reversibly bounds with plasma transport proteins, thyroxine binding globulin (or TBG) and transthyretin.

The main form of thyroid hormones is T_3. In peripheral districts most of free T_4, in fact, is deiodinated and converted into T_3, which binds on nuclear receptors of thyroid hormones in the target cells, with an affinity ten fold higher compared to T_4. A hormone-receptor complex is created, thus, which translocates to nucleus and regulates transcription of target genes by binding to specific thyroid hormone response elements (TRE), contained in them. The effects exerted are manifold, in general, body metabolism speed increase, catabolism of carbohydrates and lipids and protein synthesis stimulation.

Thyroid gland is among the most responsive organs of the body: in response to specific stimuli that increase cell metabolism, such as occurs during puberty or pregnancy, there is increased physiologically volume and activity of the gland, transitional epithelial hyperplasia (follicular cells become tall and columnar and thyroglobulin is reabsorbed). Stimulus cessation produces the reverse process: glandular epithelium is flattened, cuboidal, and resumes colloid accumulation in the follicular lumen.

According to studies carried out so far, molecular mediators for iodide transport from basolateral to apical membrane of thyrocytes within follicular lumen, are mainly two proteins: Sodium Iodide Symporter (NIS) (Rodriguez, 2002) and pendrin (Royaux, 2000) .

Synthesis of thyroid hormones requires iodide uptake by thyroid follicular cells across basolateral membrane and, after passing through the cell, ion efflux into follicular lumen through apical membrane. The mechanisms that mediate iodide transport through thyroid cells basolateral membrane are well known (Dohan et al., 2003). Less it is known about the mechanism iodide efflux across apical membrane, efflux which is dependent on continuous iodide uptake, to maintain the high ion intracellular concentration. Carriers certainly involved in iodide transport in the thyroid gland are NIS and pendrin.

1.2.1 NIS

NIS (Na^+/ I^- symporter) is a membrane intrinsic glycoprotein that actively cotransports two ions and a sodium iodide ion. NIS belongs to solute transporters SLC5A family (Bizhanova and Kopp, 2009), and represents the member number 5, and is encoded by SLC5A5 gene (solute carrier family 5), located on chromosome 19 (19p12-13.2) and contains 15 exons and 14 introns (Smanik et al., 1997). All members of this family of proteins exploit the electrochemical gradient of sodium as a driving force for anion transport across plasma membrane (Reizer et al., 1994). NIS has a high affinity for iodide and is able to also carry other ions (Eskandari et al., 1997).

1.2.1.1 Molecular characterization

Molecular characterization of NIS protein started in 1996, when cDNA encoding rat NIS was isolated by cloning of expression in oocytes of Xenopus laevis (Dai et al., 1996). Subsequently, it was also cloned human cDNA by RT-PCR (Reverse Transcriptase - Polymerase Chain Reaction), taking advantage of homology with rat NIS (Smanik et al., 1996). Human protein contains 643 amino acid residues, while rat 618; amino acid sequence identity between the two proteins is 84% (Smanik et al., 1997; Dai et al., 1996).

According to currently accepted structural model, NIS contains thirteen transmembrane domains and has the amino-terminal end located outside the cell, while the carboxy-terminal end is located in the cytosol (Dohan et al., 2003) .Mature protein weighs about 87 kDa and has three asparagine residues that are glycosylation sites (Dohan et al., 2003). Glycosylation does not seem to be required for stability, activity or correct location of NIS on plasma membrane (Levy et al., 1998).

TSH is the main regulator of thyrocyte proliferation and differentiation and functions, including iodide uptake (Vassart and Dumont, 1992). Then, TSH stimulates iodide accumulation in thyroid gland, regulating positively NIS expression, both at protein level and at mRNA level, via activation of cyclic AMP pathway (cAMP) (Weiss et al., 1984a). This has been demonstrated by *in vitro* studies on a highly differentiated cell line of rat thyroid gland (FRTL-5) (Weiss et al., 1984a) and on primary cultures of human thyroid gland (Saito et al., 1997), but also through studies on animals *in vivo*. In fact, hypophysectomised rats showed greatly reduced levels of protein expression of NIS and a single injection of TSH has led to recovery of normal expression levels (Levy et al., 1997). Moreover, rats fed a diet low in iodine or treated with 6-propyl-2-thiouracil, an agent capable of blocking iodide organification, have a high concentration of TSH, which correlates with an increase in NIS protein expression in thyroid gland (Bizhanova and Kopp, 2009). FRTL-5 cells, grown in medium TSH-free, have decreased intracellular concentration of cAMP and impaired ability to transport iodide; when TSH is provided to cells again, increases expression of NIS mRNA and protein, and subsequently also iodide uptake (Weiss et al., 1984a). TSH not only regulates NIS transcription and biosynthesis but, through post-translational mechanisms, it also stimulates its activity and expression on thyrocyte basolateral membrane (Riedel et al, 2001). In FRTL-5 cells deprived of TSH, NIS half-life is reduced from five to three days and the protein translocates from plasma membrane to intracellular compartments (Riedel et al, 2001). Intracellular distribution regulation of NIS have been only partially elucidated.

Iodide itself regulates its accumulation in thyroid gland. In 1948, Wolff and Chaikoff reported that high doses of iodide (beyond a critical threshold) block process of

organification in thyroid gland of rats *in vivo* (Wolff and Chaikoff, 1948). This phenomenon is known as Wolff-Chaikoff's acute effect and is a reversible process, since once organification resumes, serum iodide concentration decreases. In fact, this effect, rather than depending on plasma iodide concentration, depends on intracellular: it has been demonstrated, in fact, that the acute effect is deleted by inhibitors of NIS (Raben, 1949). Mechanisms underlying the effect of Wolff-Chaikoff are very complex and affecting regulation of several genes and proteins. In particular, high iodide concentrations influence NIS expression and activity, determining *in vivo* and *in vitro* a reduction mRNA and protein levels, and not through post-translational mechanisms (such as the increase in the turnover of the protein) (Eng et al., 1999; Eng et al., 2001).

Finally, NIS expression is deleted, at transcriptional level, from the follicular thyroglobulin (in fact, when this protein accumulates in follicular lumen, it is induced by reduction of iodide uptake *in vivo*) (Koichi et al., 1999) .

1.2.1.2 Inhibitors

Thiocyanate (SCN^-) and perchlorate ($ClO4^-$) are two major anions able to inhibit iodide accumulation in the thyroid gland, by competing with iodide for interaction with NIS (Carrasco, 1993; Wolff, 1964). Perchlorate is between 10 and 100 foldmore potent than thiocyanate (Dohan et al., 2003) and has been used in the treatment of hyperthyroidism (pathological condition caused by an excessive synthesis of thyroid hormones) for a long time, despite the severe side effects. Perchlorate is also used to detect defects in iodide organification (Baschieri et al., 1963). Some studies claim that perchlorate is simply a NIS inhibitor (Eskandari et al, 1997), but, in more recent publications, it was demonstrated that is actively transported by NIS and is, therefore, one of its substrate (Dohan et al., 2007). Sodium and perchlorate transport mediated by NIS is electroneutral (1 Na^+: 1 $ClO4^-$), while iodide transport is electrogenic (2 Na^+: 1 I^-), then NIS is capable of carrying different substrates with different stoichiometry (Dohan et al., 2007). Perchlorate, a widely used pollutant, is transported by NIS in breast milk, with great risk to infant health (Dohan et al., 2007).

<u>1.2.1.3 NIS gene mutations</u>

 Biallelic mutations in gene encoding NIS is responsible for a rare congenital defect in iodide transport (or ITD, Iodide Transport Defect), autosomal recessive and characterized by reduced or absent iodide uptake in the thyroid gland, hypothyroidism (i.e. clinical condition characterized by insufficient thyroid hormone synthesis), goiter and low ratio of iodide concentration in saliva and plasma (Dohan et al., 2003; Wolff, 1983). Congenital hypothyroidism has deleterious and irreversible effects on developing babies and, if untreated, results in cretinism (hypothyroidism and associated disease characterized by altered development of skeletal and central nervous system, with severe mental retardation, low stature and coarse facial features). Absence or deficiency of functional NIS molecules reduces iodide uptake from thyrocytes and thyroid hormone synthesis, resulting in increased levels of circulating TSH and induction of morphological and biochemical processes that result in development of goiter. In most cases, heterozygous subjects are euthyroid and have normal size of the gland, and then a single healthy copy of gene encoding NIS is however sufficient to ensure a normal transport of iodide in thyroid follicular cells. So far, twelve NIS mutations were identified causing the ITD and some have been well characterized.

 Thanks to NIS transporter, the thyroid gland is able to accumulate radioiodide, and this property is essential for diagnosis and treatment of thyroid disorders, such as neoplastic diseases, whose therapy is generally radioiodide administration, which, being a radioactive isotope, is toxic for the cells able to pick it up, such as tumor cells of thyroid origin.

1.2.2. APICAL IODIDE TRANSPORT: PENDRIN

1.2.2.1 Expression and function

 Among the proteins expressed in apical membrane of thyrocytes, pendrin is one of most studied. It is involved in iodide efflux. The encoding gene is SLC26A4 (first called PDS Pendred Syndrome, a disease which is responsible of), a member of family of "multifunctional anion exchangers" SLC26A (Mount and Romero, 2004). It is located on chromosome 7 (7q31) and consists of 21 exons (Kopp et al., 2008).

 Encoded protein consists of 780 amino acids, is 86 kDa, has 11 or 12 transmembrane domains and is highly hydrophobic. Both the amino-terminal segment and the carboxy-terminal are located within the cytosol (Kopp et al., 2008).

 Initially it was believed to be a sulphate transporter, given its similarity with this family of transporters. It has been shown, however, that pendrin is a iodide-independent sodium transporter (Scott et al., 1999).

In patients with Pendred's syndrome, have not been shown alterations of sulphate transport in thyroid tissue (Kraiem, 1999).

 Pendrin has the function of transporting iodide, entered in cytoplasm of thyrocyte by means of NIS, towards follicular lumen. One of the evidence that confirm is its ability to carry it only if concentrated more than 1 mM, as observed in CHO cells and COS-7 transfected with SLC26A4cDNA.

 This feautre of pendrin is characteristic of a channel, rather than a transporter.

Several studies have shown that pendrin was involved in iodide efflux. Most effective approach has been the use of a dual-chamber culture system: NIS and pendrin were made to express in polarized cells MDCK (Madin-Darby canine kidney epithelial), grown at the interface of a semi-permeable cell culture double chamber; pendrin could allow concentration of iodide from one compartment to another, while in cells expressing only NIS, with high intracellular iodide concentration, this phenomenon was not observed (Yoshida, 2004).

 Cells expressing only pendrin showed, however, lower levels of intracellular iodide compared to not transfected cells, but higher levels in apical chamber. (Gillam et al.,

2004). Results of this type are in favour of hypothesis that sees pendrin involved in iodide transport across the apical membrane of thyroid follicular cells.

It has been shown property of pendrin to be exchanger chloride/ base in different cell types, for example chloride/ format, if it is expressed in Xenopus laevis oocytes (Scott DA., Karniski LP., 2000), or carrier of bicarbonate, hydroxide ion formed cells and human embryonic kidney (Soleimani, 2001). It should be noted, however, that expression of exogenous transporters and ionic channels can lead to alteration of features: for example chloride and iodide transport seemed competitive in oocytes of Xenopus laevis and Sf9 (Scott et al., 1999) but was not confirmed in other studies.

Pendrin would be a transporter of chloride, bicarbonate and iodide (Yoshida et al., 2002), in particular a exchanger chloride/ iodide, according to electrophysiological studies (Rillema, Melissa, 2003). Through pendrin, chloride and iodide would enter thyrocyte and emerge towards follicular lumen. Both the ions would activate transport. Chloride reabsorption in thyrocyte would play a role similar to that covered in cells of other tissues: maintaining the "tone" phone (volume) of water distribution and concentrations of elements in the follicle.

SLC26A4 transcript is present in the thyroid gland and in the kidney (Northern blot experiments) and in the fetal cochlea (experiments screening of a cDNA library).

Pendrin is present on apical membrane of epithelial cells of the thick ascending of Henle's loop and the distal convoluted tubule (immunohistochemical experiments) but 200 fold less than in the thyroid gland(Lacroix et al., 2001), and with heterogeneous expression, both qualitatively and quantitatively.

Pendrin is also expressed in several other districts of nephron: was detected in cortical collecting ducts (Soleimani, 2001), especially in intercalated cells, which regulate excretion of acid/ base transporting bicarbonate. Knock-out mice for SLC26A4 have cortical collecting ducts lack the capability to secrete bicarbonate. An earlier study (Scott et al., 1999) had shown, among other things, that pendrin expressed in oocytes of Xenopus laevis, has transport properties similar to those of the exchanger chloride/ format, which absorbs 60% of the chloride filtrate and is localized to the apical membrane of proximal tubule cells.

In the inner ear, pendrin has similar functions: the endolymph present therein has a low sodium concentration, but potassium and chloride high concentrations compared to plasma and perilymph, gradients guaranteed by transporters expressed by the

surrounding cells. Since gene mutationsof these transporters are associated with forms of deafness, it is clear their involvement in homeostasis of electrolyte composition of the inner ear as an essential factor for normal hearing function.

Pendrin is also expressed in placental syncytiotrophoblast and in lactating mammary gland (immunohistochemistry experiments) (Rillema et Hill, 2003).

1.2.2.1 Regulation

NIS and TPO (thyroid peroxidase) genes are more sensitive to stimulation by TSH induced with respect to SLC26A4 gene, however, even if levels of TSH and TG (thyroglobulin) show a regulatory function: pendrin expression would be induced by low levels of TG (Bidart et al., 2000), antagonist of stimulating effect of TSH on other genes: NIS and TSHR are less expressed with high levels of TG. Regulation is complex: according to an accepted model, TG inhibits NIS expression in a follicle with a lumen rich in TG accumulated, thereby reducing iodide uptake. Functional pendrin would carry all the iodide already concentrated within the cell into follicular lumen, despite low level of SLC26A4transcription in the situation described. In this follicle, TSH would promote reabsorption and degradation of follicular TG and secretion of T3/T4 in the blood stream. The concentration of TG would decrease as the reabsorption of follicle and degradation in lysosomes of newly synthesized TG was higher than TG. A lower concentration of follicular TG would then re-challenge NIS, TG, pendrin expression (Kohn, 2001).

Recent studies, however, showed that TG, however, causes an increase in transcriptional gene activity (Kopp et al., 2008), in contrast with what previously found and with its function as a suppressor of thyroid-specific expression.

Against this hypothesis, however, TSH accelerates iodide apical efflux into follicular lumen (Weiss et al., 1984b; Nilsson et al., 1990), both in rat thyroid cells than in the pig. TSH stimulates the metabolic pathway of PKA (protein kinases A), leading to, in thyroid cells, regulation of pendrin, primarily regulated by pituitary hormone: phosphorylation of pendrin leads to increase in its membrane translocation, recruited from endosomal pool (Royaux et al., 2000).

TTF1 transcription factor specific for thyroid cells appears to be involved in positive regulation of the activity of pendrin gene promoter, while does not seem that iodide,

at least in vitro, can regulate gene expression of pendrin gene (Suzuki and Kohn, 2006) .

1.2.2.3. Pendred's syndrome

Pendred's syndrome is an autosomal recessive disorder caused by mutation biallelic (homozygous or heterozygous compound) of gene encoding pendrin. The main feature is the association between sensor-neural hearing loss (bilateral) and goiter, with highly variable phenotype. Name "pendrin" derivers from the researcher, Vaughan Pendred, who first described this syndrome between endemic goiter and deafness family in 1896, a century before the responsible gene was identified (Kopp, 1999) .

Hypothyroidism is usually subclinical and present in 30-40% of cases, while most of the patients is euthyroid (with or without goiter), especially with adequate supply of iodine in diet. Among syndromic deafnesses is the most common form and represents 10% of hereditary deafness (Fraser, 1965). Inner ear is presented morphologically altered, a feature probably also due to alteration of ionic transport associated with the syndrome, in particular water and solutes flow, which would lead to the expansion of cochlea and loss of its functional architecture.

Despite pendrin plays an important role in chloride transport in the nephron, Pendred's syndrome does not involve renal alterations at clinical level, probably due to presence of multiple and compensating transport systems.

In thyroid tissue of patients, iodide is not completely organified, presumably to lower transport of iodide in thyroid colloid through the pendrin, thyroid hormone biosynthesis may therefore undergo various consequences (Royaux et al., 2001). Most of the numerous gene mutations are missense; known mutations are almost 150 (Kopp et al., 2008) predominantly missense mutations (a few are nonsense or inside the intron); protein undergoes some alteration in translocation to plasma membrane, probably due to an abnormal folding, finally remaining in endoplasmic reticulum (Taylor et al., 2002; Rotman-Pikielny et al., 2002). This retention (Endoplasmatic Reticulim Storage Disorders, ESRD) has been confirmed by functional studies of localization of mutated and wild type protein with tags (GFP, Green Fluorescent Protein) in HeLa cells (Taylor er al., 2002) .

Despite the numerous studies that have confirmed its role in iodide transport, pendrin seems not to be essential for apical iodide transport of in the thyroid gland (efflux into follicular lumen): carriers of mutations in SLC26A4 gene do not always develop goiter (Kopp et al. , 2008), while studies in knock-out mice for pendrin showed no thyroid abnormalities (Everett et al., 2001). With greater probability, iodide flows through thyrocyte apical membrane according to concentration gradient, by means of different channels permeable anionic iodide, such as the pendrin (Wolff, 2005) .

1.2.3. OTHER CHANNELS IN THYROID GLAND

There are also other channels permeable to iodide anion expressed in thyrocytes, CFTR and ClC-5, their function is still controversial as far as it regards iodide transport in thyroid gland, maybe involvement in apical transport.

1.2.3.1 CFTR

CFTR (Transmembrane Conductance Regulator in Cystic Fibrosis) is a chloride channel expressed in epithelial cells of various organs and tissues, in the apical membrane, e.g. in thyroid gland (Devuyst et al., 1997), respiratory tract, pancreas , intestine, testes, and sweat glands (only in the latter, transporter is responsible for chlorine absorption and its secretion, as occurs in other organs) (Verkman et Galietta, 2009) . This channel allows and regulates the transepithelial transport of water and solutes and is mainly responsible for epithelial chloride (Cl^-) permeability. CFTR can carry, in addition to chloride, also other anions, such as iodide and nitrate, for which, however, permeability is smaller. Gene encoding CFTR, identified in 1989 and located on chromosome 7, is mutated in cystic fibrosis, deadly genetic disease and more common in Caucasians. This is an inherited autosomal recessive and the main events are chronic and recurrent lung infections and pancreatic exocrine insufficiency.

CFTR is an integral membrane protein which consists of 1480 amino acid residues. Has twelve transmembrane segments, which are grouped to form two domains (MSD1 and MSD2, Membrane-Spanning Domain) (Figure) and constitute the channel pore. It also has two binding domains to nucleotides (NBD1 and NBD2, Nucleotide

Binding Domain) to which ATP molecules bind, separated by a large regulatory domain polar (R domain), which is phosphorylated at multiple sites (Figure). cAMP-dependent phosphorylation results in channel activation (Figure), therefore, its activity is stimulated by agents that elevate intracellular levels of cAMP, such as phosphodiesterase inhibitors, enzyme that degrades cAMP, and activators of the enzyme adenylate cyclase (including forskolin) which catalyzes synthesis of cAMP from ATP. CFTR is a member of ABC transporter superfamily (ATP-Binding Cassette): channel activation requires, in addition to phosphorylation, binding and hydrolysis of ATP (Figure), which determines conformational changes required for channel opening control and ion transport according to concentration gradient across the plasma membrane.

CFTR expression in human thyroid gland has been demonstrated both for mRNA with RT-PCR, and for protein, with Western blot performed on membrane extracts (Devuyst et al., 1997). Immunohistochemical studies also showed that 64% of follicular thyroid tests are positive for CFTR, but that, for each follicle, only 16% of thyrocytes is labelled with anti-CFTR (Devuyst et al., 1997) . High heterogeneity of follicular cell population in CFTR expression seems to reflect the different state of cell metabolism: follicular cells expressing CFTR are those particularly active in the secretion or reabsorption of thyroglobulin (Devuyst et al., 1997) .

Role of CFTR in many secretory epithelia is still unclear. With regard to the thyroid gland, it is believed that CFTR may directly or indirectly influence iodide efflux into follicular epithelium because subclinical hypothyroidism was found in patients with cystic fibrosis (De Luca et al., 1982). As in many other secretory epithelia, fluid secretion into thyroid follicle lumen appears to be driven, at least in part, by the transport of Cl^- mediated by a cAMP-activated channel (Armstrong et al., 1992), whose molecular identity, however, has not yet been characterized. So if it were shown that this channel is CFTR, subclinical hypothyroidism in patients with cystic fibrosis could be explained by presence of slight alterations in secretion or absorption of colloid (Devuyst et al., 1992) .

<u>1.2.3.2 CLC-5</u>

ClC-5 is a chloride channel voltage-dependent, belonging to ClC protein family. It is expressed predominantly in the kidney and is responsible for electrogenic exchange of ions H^+/ Cl^- (Scheel et al., 2005): chloride influence is coupled to outflow of protons with a stoichiometry of $2Cl^-$: $1H^+$. It is expressed in intracellular compartment and its function is to facilitate endosome acidification: in fact, it is necessary to maintain electroneutrality during electrogenic pumping of H^+ ions into organelle lumen, mediated by vacuolar ATPase, with consumption of ATP (Günther et al., 1998) (Figure). Mutations in CLCN5 gene, encoding ClC-5, are responsible for Dent's disease, a rare X-linked disease, characterized by proteinuria and kidney stones, due to alteration of receptor-mediated endocytosis mechanisms in apical proximal tubule of the nephron (Piwon et al., 2000).

One study showed that ClC-5 is expressed in mouse thyroid, where mRNA levels are about 40% of kidney levels and protein was immunolocalized on thyrocyte apical pole (Van den Hove et al., 2006). Using knockout mice ClC-5, channel loss was demonstrated not to inhibit apical endocytosis (as occurs in the kidney) of thyroglobulin labeled with ^{125}I, but induces euthyroid goitre (with normal levels of TSH and T_4 in the serum) to due to slowing iodide efflux apical and organification, associated to pendrin expression decrease, with mRNA and protein levels reduced by 60% (Van den Hove et al., 2006) . In light of these data, three hypotheses have been advanced about ClC-5 role in the thyroid gland and interaction with pendrin: the channel may act as an alternative apical iodide channel, although it has greater affinity for chloride, could be involved in recycling of chloride in follicular lumen, to support the antiport mediated by I^-/Cl^- pendrin, finally, could act indirectly, by modulating pendrin gene expression. However, regardless of exact action mechanism, these data suggest importance of ClC-5 in chlorine and iodine homeostasis in the thyroid gland.

1.3 MALIGNANT TUMOURS OF THYROID GLAND

Thyroid cancers are rare tumours and represent, in fact, only about 1% of all malignancies. Thyroid cancers primarily affect adults and females and can be

hereditary or sporadic. Among the predisposing environmental factors, the main is represented by exposure to ionizing radiation.

There are four main subtypes of thyroid carcinoma: three well-differentiated, i.e. papillary, follicular and medullary, and a highly undifferentiated anaplastic . In most cases these are well-differentiated carcinomas, most common is papillary carcinoma, which represents about 80% of all cases of thyroid cancer, followed by the follicular (about 15% of cases) and bone marrow (about 5%). Anaplastic carcinoma is very rare. All carcinomas of thyroid follicular epithelium originate with the exception of medullary carcinoma, which is derived from the C cells.

Papillary carcinomas arise at any age, but especially between 20 and 40 years, and are more frequently associated with previous exposure to radiation. Microscopic examination of fine needle aspiration biopsies shows papillae, even branched, which possess a stalk fibrovascular covered by one or more layers of cuboidal epithelial cells. Prognosis is generally very good, with a 10-year survival rate of 95% (Dohan et al., 2003).

Follicular carcinomas appear later in life compared to papillary carcinomas (40-50 years) and have a high prevalence in areas with endemic goiter by iodine deficiency. Follicular carcinomas are constituted by small follicles containing colloid, which resemble a normal thyroid. In some cases, follicular differentiation is less evident: there are sheets of cells without colloid. Prognosis depends on tumour extent at the time of diagnosis: the minimally invasive follicular carcinoma is characterized by a 10-year survival greater than 90%.

A variant of papillary and follicular carcinomas is represented by oncocytic tumour, in which neoplastic cells are characterized by an aberrant mitochondrial mass increase of the cell, responsible for appearance of swollen cells ("oncocytic" term is derived from the Greek word onkoustai, which means swell) (Gasparre et al., 2010).

Anaplastic thyroid carcinoma is an undifferentiated tumour, with rapid growth and, unlike differentiated thyroid carcinoma is highly aggressive and lethal, with a mortality rate of almost 100%. It may arise *de novo* or derive from the dedifferentiation of a well-differentiated carcinoma, accumulation of genetic mutations, such as loss of p53. It strikes at an older age than other thyroid cancers (around 65 years) .

1.3.1 RADIOIODIDE IN CANCER THERAPY

For more than sixty years, most of the cases of thyroid carcinoma is treated with total thyroidectomy and subsequent administration of therapeutic doses of radioactive iodine, in particular for elimination of possible micrometastases (which are also able to uptake it). Radioiodide is used not only in therapeutic phase, to destroy the neoplastic cells primitives and/ or metastatic, but also to perform scintigraphic imaging in diagnosis. This is a technique that has been very successful in significantly improving prognosis of patients with thyroid cancer because it is characterized by specific cytotoxicity to cells of the thyroid, with minimal side effects.

A key role both in physiology in the pathogenesis of thyroid cancer is done by the NIS, responsible for the accumulation of iodide, and therefore also of radioiodide in thyroid follicular cells. Efficacy of therapy with radioiodide is reduced when in tumour cells of thyroid gland NIS expression is suppressed and insufficient, for example because of cellular dedifferentiation increase or TSH receptor expression decrease (Spitzweg and Morris, 2002). "Hot" thyroid nodules are intensely stained with scintigraphy, because these nodules accumulate radioiodide and have increased expression of NIS, the "cold", instead, express low levels of NIS and radioiodide uptaken slightly. Most of thyroid carcinomas, even those differentiated, behave as cold hypofunctional nodules and many studies have shown that in these tumours levels of expression NIS, both as mRNA and as a protein, are much lower, in some cases absent, compared to normal thyroid tissue. In contrast to these data, some studies have found high levels of NIS expression in a high percentage (up to 70%) of tumour samples analyzed (Saito et al., 1998; Dohan et al., 2001): in these tumours NIS was localized both on plasma membrane (in a non-polarized) that in intracellular compartments, suggesting that malignant transformation may result in alteration of NIS correct positioning or retention mechanisms in plasma membrane.

Although most of thyroid tumours and their metastases respond effectively to the ablation, about 30% of patients with malignant thyroid tumours are resistant to this therapy. To increase effectiveness of radiotherapy in patients with ^{131}I-resistant, strategies should be carried out to restore a sufficient NIS activity in primary tumour

and metastasis by stimulating transporter expression or promoting its correct localization in plasma membrane.

Decreased expression and/ or functionality of NIS only partly explain low capacity of radioiodide uptake generally observed in thyroid tumour tissue. A role is played also by iodide efflux channels, which promote the escape of the radioactive isotope accumulated through NIS and cause failure of therapy with radioiodide. Another strategy to increase the effectiveness of therapy with ^{131}I, therefore, could be the inhibition of activity of outflow channels. Lithium carbonate, used for the treatment of mood disorders, potentiates ^{131}I therapy due to its inhibitory effect on iodide release by neoplastic cells (Koong et al., 1999).

Since NIS is expressed physiologically even in extrathyroidal tissues, radioiodide could be used for diagnosis and treatment of these tumours. For example, with regard to breast cancer, NIS is expressed in epithelial cells of mammary gland tumour (both in plasma membrane nda inside the cells) in more than 80% of cases, while in the healthy gland only during terminal stage of pregnancy and during lactation (Tazebay et al., 2000). Applicability of radioiodide therapy in breast carcinomas represent a major breakthrough in treatment of malignant cancer more deadly in women.

In the light of its potential diagnostic and therapeutic and thanks to gene therapy, NIS expression may be induced in tumour cells non-thyroidal, in order to make even the primitive tumours not susceptible to destruction of thyroid gland with radioiodide (Spitzweg et al. 2002). Several attempts of gene transfer were performed on human and mouse cell lines of various tumours, demonstrating induction of iodide accumulation and cytotoxic effect of selective radioiodide accumulation (Boland et al., 2000; Mandell et al., 1999). *In vivo* studies have yielded good results: human tumour xenografts in nude mice and expressing NIS are able to accumulate radioiodide (Boland et al., 2000). Demonstrated ability of NIS gene transfer to induce activity of iodide uptake in tumour cells, therapeutic efficacy remains to be confirmed *in vivo*. Spitzweg et al., 2000, showed an average reduction of more than 90% of tumour volume by NIS expression in a prostate tumour line xeno-grafted in nude mice. Results obtained so far are very promising but remain to be solved typical problems of gene therapy, in particular identification of transduction systems more efficient and safer, allowing a systemic administration of vector and a tumour-specific regulation of gene expression.

1.4 CHLORIDE TRANSPORT

Between anions with high physiological relevance, chloride, iodide, bicarbonate and thiocyanate pseudohalide can be numbered. Chloride (Cl^-) is involved in processes as fluid epithelial secretion and cell volume regulation, iodide (I^-) in thyroid hormone synthesis, bicarbonate (HCO_3^-) in pH regulation, thiocyanate (SCN^-) in epithelial sterility. Homeostasis depends also on proper anion flow, activity in which numerous transporters and channels are involved, more or less specific for each anion.

1.4.1 CHLORIDE CHANNELS

Cl^- channels are expressed in epithelial tissues mostly, where exert functions such as cell volume regulation and fluid secretion. Cl^- channels are fundamental also in neuro-excitation and in smooth muscle contraction and involved in endosomal, lysosomal and Golgi acidification (Jentsch et al., 2002).

Cl^- channels allow flow of chloride but also other halides in a less specific manner, such as bicarbonate (HCO_3^-)and thiocyanate (SCN^-) (Verkman et al., 2009).

Many mutations were found and characterized in genes codifying for Cl^- channels; some of these can determine diseases such as cystic fibrosis (mortal genetic disease most diffused among Caucasian), macular degeneration, kidney lithiasis, renal loss of salt and hyperekplexia.

Defective transport can provoke disorders such as secretory diarrhea, polycystic kidney disease, osteoporosis and hypertension, whose therapy is based on Cl^- channels modulators, some already employed, some others screened in preclinical and clinical studies.

Cl^- channels are divided into five categories:

- ❖ Volume-regulated chloride channels;
- ❖ CFTR (*Cystic Fibrosis Transmembrane Conductance Regulator*), activated by cAMP-dependent phosphorylation and binding of ATP to nucleotide-binding-domain (NBD);
- ❖ ClC (*Voltage-gated Chloride*), depending on membrane potential variations; one of these, ClC-1, is involved in Cl^- conductance and repolarization after

action potential in skeletal muscle and some mutations of it were associated with myotonia;

❖ GABA/Gly receptors, ligand-dependent Cl⁻ channels (GABA and glycin-activated), situated in brain inhibitory synapses (GABA receptors, bound also by benzodiazepines and barbiturates, modulator used as drugs currently) and spinal cord especially (glycin receptors, activated also by β-alanine and taurine, responsible of neuronal hyperpolarization and consequent lasting inhibition); GABA/Gly receptor mutations were associated with epilepsy and hyperekplexia respectively;

❖ CaCC (Calcium-activated Chloride Channel), Cl⁻ channels activated by high intracellular Ca^{2+} concentrations, whose molecular identity and activation mechanism are unknown so far.

1.4.2 CALCIUM-ACTIVATED CHLORIDE CHANNELS

 CaCC function is mediated by calcium-activated chloride channels, highly expressed in mammalian cells, where exert a role in many physiological processes such as fluid transepithelial secretion, fertilization of the egg cell, smooth muscle contraction, heart muscle and neuron excitation, visual and olfactory signal transduction (Hartzell et al., 2005).

CaCC shared features are mediated stimulation, slow and reversible activation after membrane depolarization and a typical anion permeability order: $NO_3^- > I^- > Br^- > Cl^- > F^-$. So far, molecular identity of this conductance is unclear; protein involved could be Cl^- channels or Cl^- channels components/regulators. Among CaCC candidates, two protein families were considered mainly: bestrofins and anoctamins. Studies on bestrofins revealed some discordances, such as lack of detectable effects in bestrofin-1 *knock-out* mice in calcium-activated chloride currents and in tissues which express it (retinal pigment epithelium mostly) and generation of currents with features different from classical CaCC, when expressed exogenously. Anoctamins remains the most likely CaCC candidate, especially because of anoctamin-1/TMEM16A biophysical and pharmacological properties coherent with CaCC (Kunzelmann et al., 2009).

Sensory, chemical or electrical stimuli can activate transduction pathway leading to CaCC activation: Gq protein coupled receptors stimulate phospholipase C enzyme for inositol 1,4,5-triphosphate (IP_3) synthesis, which mediates intracellular signalling (Yang et al., 2008).

Intracellular calcium concentration increase can be provoked by IP_3 level increase, which leads to cytoplasmic calcium release from intracellular stores, and by calcium influx from extracellular compartment via voltage-gated Ca^{2+} channels. Intracellular calcium increase causes membrane depolarization via CaCC activations and hyperpolarization of Ca^{2+} dependent potassium (K^+) channels (fig.). Transduction pathway leads to CaCC activation by Ca^{2+} direct action, i.e. in salivary glands epithelium, or involves Ca^{2+}-calmodulin-dependent kinase type II (CaMKII) i.e. in intestine epithelium (fig.   ). CaCC can be activated by ATP through its binding to P_2Y_2 purinergic receptor, and carbachol, agonist active on acetylcholine muscarinic receptors. Also Ca^{2+} ionophores as ionomycin can active CaCC increasing membrane permeability to Ca^{2+} .

1.4.3 ANOCTAMINS

1.4.3.1 General features

Anoctamin family consists of ten members in mammalians known so far, called ANO/TMEM16 (ANO1-10, TMEM16A-K). These proteins are highly evolutionarily conserved: particularly, their predicted structure is characterized by eight transmembrane domains and both carboxy- and amino-terminals in cytosol (fig.). Anoctamin name results from fusion between "*an*ion", because anoctamins are involved in anion transport, and "*oct*" because of their eight transmembrane domains. Between TMEM16A and TMEM16B sequence identity is close to 60% but less for the other members, up to 20-30% for TMEM16F, G, H, J, K (Galietta, 2009). Sequence homology arrives to almost 90% for transmembrane domains. A very interesting property is their little homology with other ionic channels families, that places them in a new family.

Anoctamins have a characteristic expression pattern in tissues, and every tissue expresses its own anoctamin set. Anoctamins 1, 5, 6, 7, 8, 9, 10 are expressed in epithelial tissues mostly, anoctamins 2, 3, 4 in nervous system. Their exogenous expression was considered in several studies: one of these (Schreiber et al., 2009) found that all anoctamins are localized in plasmatic membrane when expressed in FRT cell line (from rat normal thyroid epithelium, not expressing thyroid differentiation markers but highly polarized).

As far as it regards functional role, anoctamins are little known; TMEM16A, TMEM16B function is known (calcium-activated chloride channel or CaCC); also TMEM16H and TMEM16F have CaCC activity (the latter, in particular, is included in "scramblase complex" of platelets, Suzuki J, Nagata S., 2011). Likely also other members of family are involved in anion transport, since they share sequence homology, with functional properties still to be defined.

1.4.3.1 Anoctamin-1/ TMEM16A

Anoctamin-1/TMEM16A gene is located on q-arm of human 11 chromosome. It was cloned by mouse retina originally. Human protein shares high homology with mouse ortholog (91%). TMEM16A exerts a role in CaCC activity in epithelium and smooth muscle contraction. Its properties and predicted expression in virtually all tissues, as CaCC, suggested it could be a potential candidate.

CaCC activity was known and studied for a long time but its molecular identity not so clear. Recently three different independent laboratories identify TMEM16A as CaCC molecular mediator with their own strategy:

- ❖ search for transmembrane proteins with multiple transmembrane domains and isoforms without any known function in data-banks (Young et al., 2008);
- ❖ genomic functional studies after an experimental evidence: interleukin-4 (IL-4) increased calcium-activated chloride secretion in human bronchial epithelial cells, then IL-4 up-regulated genes codifying orphan membrane protein were identified with expression mRNA microarray (Caputo et al., 2008);
- ❖ expression cloning with amphibian Axolotl oocytes, without CaCC endogenous activity (Schroeder et al., 2008).

Besides, silencing provoked blockade of a typical CaCC-dependent function, salivary glands secretion inhibition *in vivo* (Yang et al., 2008).
TMEM16A-*knock-out* neonatal mice dead, likely because of high tracheomalacia, and show electrolytic cell transport defects similar to cystic fibrosis, such as strongly reduced CaCC in airways, mucus accumulation in lumen and reduced ciliary motility (Rock et al., 2008; Rock et al., 2009).
Taken together, all these evidences strongly support hypothesis on TMEM16A as a CaCC, fundamental in airway epithelium physiology. Likely high mortality of *knock-out* mice could be due to a functional default in multiple organs, since TMEM16A is highly expressed in secretory epithelial tissues as pancreas, prostate, salivary glands, thyroid, colon (Schreiber et al., 2009). Tracheal cartilage anomalies are not known but

could be due to loss of normal tissue architecture, provoked by mucus accumulation and other effects of TMEM16A lack (Rock et al., 2008).

A notable evidence is a CaCC residual activity in TMEM16A *knock-out* mice, which suggests involvement of other proteins, putatively other members of anoctamin family, in CaCC.

Differential maturation of anoctamin-1 transcript leads to various isoforms due to presence or absence of four segments (Caputo et al., 2008):

- ❖ "a" segment, consisting of 116 aminoacid residues, localized at amino-terminus;
- ❖ "b" segment, consisting of 22 aminoacid residues, localized before of first transmembrane domain;
- ❖ "c" and "d" segment, consisting of 4 and 26 aminoacid residues respectively, localized inside the first intracellular loop, that connects the second transmembrane domain to the third .

TMEM16A(abcd), complete protein including all four peptide segments, consists of 1008 aminoacid residues. TMEM16A(0), is the basic isoform and consists of 840 aminoacid residues, can transport anions but without voltage-dependent activation (Ferrera et al., 2010).

According with recent hypothesis, process of alternative *splicing* could regulate channel biophysical and pharmacological properties, as voltage-dependence and calcium sensitivity.

Some predictions suggest presence of a pore forming structure: region between the fifth and the sixth transmembrane segment should form a re-entrant loop in plasmatic membrane, not completely extracellular. This feature was showed by a mutational study, through identification of three highly conserved charged residues, whose mutations provoked alterations in protein ionic properties.

So far, is not clear calcium-dependent activation of TMEM16A, which does not contain domains with direct binding sites for calcium or calmodulin (such as E-F hand domain and others). This fact suggests existence of non canonical domains or sites for other mediator, such as PKA, PKC e CaMK kinases, whose consensus sequence were found in TMEM16A cytosolic region (Kunzelmann et al., 2009).

Among TMEM16A inhibitors can be numbered niflumic acid, acid 5-nitro-2-(3-fenilpropilamino) benzoic acid (or NPPB) or other classic CaCC inhibitors (Hartzell et al., 2005), active at uM concentrations.

Anoctamin-1 stimulates the highest basal anionic conductance, ATP-dependent rapid activation among tested anoctamins, and, notably, can be activated by ionomycin in contrast to other members (Schreiber et al., 2009).

High cytosolic calcium concentrations are required for anoctamin-1 ($EC_{50} = 0.7$ μM), that is inhibited by extracellular calcium removal. Anoctamin-1 activity is maximum with 10uM intracellular calcium but inhibited by higher concentrations.

Anoctamin-1 appears to be activated by an increase of intracellular Ca^{2+} (Galietta, 2009), but exact mechanism is not know yet, as with other CACC. Certain assumptions are activation mediated by calmodulin and Ca^{2+}-dependent phosphorylation (Galietta, 2009).

A likely mechanism of activation is given by presence of ATP extracellular receptor agonist P2, which not only produces an increase in IP_3 and a robust mobilization of Ca^{2+} from intracellular stores, but also promotes calcium influx, arachidonic acid (AA) release and I^- efflux FRTL-5 cells (Smallridge and Gist, 1994).

Recently, a study showed the possible mechanism of TMEM16A and bestrofin-1 (a Ca^{2+}-activated Cl^-/ I^- channel) operation, following intracellular Ca^{2+}- increase due to ATP binding to its receptor P2Y (Kunzelmann et al., 2009). Resulting stimulation of G protein (Gq/11) and of phospholipase C (PLC) increases the IP_3, inducing Ca^{2+} release from endoplasmic reticulum stores and bestrofin-1 activation, which in turn facilitates the release (Figure). Bestrofin-1 activity is regulated by PP2A and PKA2 kinases. Intracellular calcium release stimulates TMEM16A activation (Kunzelmann et al., 2009).

Furthermore, CACC activity was studied in CFPAC cells and CFBE41o-1-(cell line of human tracheal epithelium, homozygous for ΔF508 CFTR mutation) transfected with the siRNA specific, with a Yellow Fluorescent Protein(YFP)-based assay halide-

sensitive (Caputo et al., 2008). The cells were stimulated with UTP (Figure) in order to produce intracellular calcium increase; fluorescence decrease was caused by a high influx of I⁻ through CACC. Cells transfected with siRNA against TMEM16A mRNA showed a 60% reduction of the influence of iodide Ca^{2+}-dependent compared to cells treated with siRNA control or against other targets (Caputo et al., 2008).

In some studies (Caputo et al., 2008; Hartzell et al., 2009), it was demonstrated that flow-dependent anion ANO1 is highly sensitive to NFA and NPPB, which typically inhibit CACC, but is not affected by inhibitors such as CFTRinh-172 and DPC. Two recent studies (Namkung et al., 2010th; Namkung et al., 2010b) have identified other inhibitors of ANO1 as tannic acid (TA), a compound belonging polyphenol family, contained in a wide range of natural products, such as green tea and red wine. By means of electrophysiological analysis (short-circuit analysis) in FRT cells, it was demonstrated that tannic acid (100μM) inhibits (selective) to 95% of TMEM16A Cl⁻ conductance of stimulated by ionomycin (ionophore that increases Ca^{2+} permeability of membranes) which, at the same concentration, has only a slight effect on CFTR Cl⁻ conductance (Namkung et al., 2010b).

Since its involvement in many processes, TMEM16A and the other anoctamins could be employed as a new class of pharmacological targets for several human diseases, i.e. to compensate chloride defective transport in cystic fibrosis, and to regulate smooth muscle contraction in asthma, hypertension and gastrointestinal motility disorders.

An interesting evidence of anoctamin-1 is its increased expression in several human tumours, as gastrointestinal stromal tumour (or GIST). TMEM16 is called also DOG1 because "Discovered On GIST" (Espinosa et al., 2008). TMEM16A shows higher expression in many epithelial tumours, in fact another name is ORAOV2 (ORAl cancer OVerexpressed 2).

Anoctamin-1 is located inside a chromosomal region containing several oncogenes, as cyclin D1, this could explain its increased expression in cancer cells. So far, TMEM16A was used as a tumour biomarker, i.e. in human coloncarcinoma and could be still used, not only for diagnosis and follow-up, but also for as a target of therapy, if chloride conductance were showed to be connected with tumourigenesis.

1.4.3.2 Anoctamin-2/ TMEM16B

Anoctamin-2/TMEM16B is expressed on plasmatic membrane of nervous and epithelial cells, as eye cells, where its transcript has the highest expression (Schreiber et al., 2009). TMEM16B seems to show a CaCC activity in sensorial transduction, i.e. in ciliated olfactory cells (Stephan et al., 2009) and in photoreceptors (Stöhr et al., 2009). As TMEM16A, also TMEM16B was expressed in a heterologous system to discover its effects, Axolotl oocytes (Schroeder et al., 2008) and HEK (Human Embryonic Kidney) cell lines (Pifferi et al., 2009). TMEM16B resulted to produce CaCC activity but with some properties, such as more rapid membrane depolarization-dependent activation, less calcium sensitivity, anion permeability order, $SCN^- > I^- > NO^{3-} > Br^- > Cl^-$, less membrane potential-dependent calcium affinity (property different from TMEM16A (Galietta, 2009). Comparative studies of these two anoctamins could lead to understanding structure-function relationships with more details for the whole family.

Mouse anoctamin-2 is expressed in neural tube and dorsal root ganglia during nervous system development (Harfe and Rock, 2008).

Among related diseases, it is notable founding of deletions of von Willebrand e TMEM16B genes, located on p-arm of chromosome 12 in some patients with von Willebrand type 3 disease, which provokes impaired coagulation (Schneppenheim et al., 2007); one TMEM16B polymorphism related to panic disorder was found in a genome –wide scan study (Otowa et al., 2009).

1.4.3.3 Anoctamin-3/ TMEM16C

Also anoctamin-3/TMEM16C is expressed mostly in nervous system, in cerebral and cerebellar cells (Schreiber et al., 2009). Human TMEM16C is located on p-arm of 11 chromosome. So far, no physiological information have been described about this protein.

1.4.3.4 Anoctamin -4/ TMEM16D

Anoctamin-4/TMEM16D is codified by a gene localized on q-arm of chromosome 12. Mouse protein is expressed in nervous tissue, particularly in spinal cord and brainstem (Schreiber et al., 2009). Rat TMEM16D mRNA was found in pulmonary artery smooth muscle cells at low levels (Manoury et al., 2010). So far, no physiological information have been described neither about this protein.

1.4.3.5 Anoctamin-5/ TMEM16E

Anoctamin-5/TMEM16E is codified by a gene localized on q-arm of chromosome 11, codified protein consists of 913 aminoacid residues (Katoh and Katoh, 2004a). Mouse protein showed an epithelial expression (thyroid particularly), in skeleton muscle, in cartilage and nervous system (Schreiber et al., 2009). Another name is GDD1 because its gene is mutated in "GnathoDiaphyseal Dysplasia" in a rare human genetic disease likely with impaired bone calcification (Tsutsumi et al., 2004). Protein seemed to be involved in embryonic/ fetal development of mouse skeletal muscle system (Mizuta et al., 2007). Its heterologous expression in FRT cell line led to a small CaCC (Schreiber et al., 2009).

1.4.3.6 Anoctamin -6/TMEM16F

Anoctamin-6/TMEM16F is codified by a gene localized on q-arm of chromosome 12. Its expression was found ubiquitously, especially in epithelium (Schreiber et al., 2009), but also in embryonic stem cells and foetal liver (Katoh and Katoh, 2004a) and in smooth muscle cells of rat pulmonary arteries (Manoury et al., 2010). Heterologous expression in FRT cell line revealed ATP-stimulated chloride conductance, coherent with CaCC activity, with patch-clamp technique (Schreiber et al., 2009). In FRT cells also its endogenous expression was found, likely responsible for their small chloride conductance. High intracellular calcium concentration is requested for its activation,

as observed with TMEM16A, but is not influenced by niflumic acid (Schreiber et al., 2009).

As far as it regards relates diseases, TMEM16F gene mutations were found in Scott's syndrome (one patient), characterized by loss of calcium-dependent phosphatidylserine membrane exposition by activated platelets and consequent impaired procoagulant activity (formation of scramblase complex) (Suzuki et al., 2010).

Human chronic myeloid leukemia and intestinal cancer showed TMEM16F expression (Katoh and Katoh, 2004a).

TMEM16F was confirmed to provoke phospholipid scrambling in platelets (Suzuki J, Nagata S., 2011).

1.4.3.7   Anoctamin -7/TMEM16G

Anoctamin-7/ TMEM16G is codified by a gene localized on q-arm of chromosome 2and contains 25 exons (Katoh and Katoh, 2004b). Codified protein consists of 932 aminoacid residues and shows two isoforms, ANO7S, short, and ANO7L, long. Its expression was found especially in epithelial tissues in mice, such as stomach (Schreiber et al., 2009).

Heterologous expression in FRT cell line revealed CaCC activity (Schreiber et al., 2009).

Another name is NGEP (New Gene Expressed in Prostate), because of its expression in both normal and tumour human prostate (Bera et al., 2004).

1.4.3.8   Anoctamin-8/TMEM16H

Human anoctamin-8/TMEM16H is codified by a gene localized on p-arm of chromosome 19 and contains 18 exons; presence or absence of intron 17, due to alternative *splicing* of its transcript, leads to expression of two isoforms (Katoh and Katoh, 2004b). Between the fifth and the sixth transmembrane domain there is a longer region and rich in negative charges due to an additional segment containing 20

glutamate and aspartate residues, carboxy-terminus is rich in prolines (Galietta, 2009), features that make TMEM16H different from other anoctamins.

Endogenous expression in FRT cell line produced a small ATP-stimulated CaCC activity (Schreiber et al., 2009).

Its expression was found in stem embryonic cells and foetal brain (Katoh and Katoh, 2005).

1.4.3.9 Anoctamin-9/TMEM16J

Human anoctamin-9/ TMEM16J is codified by a gene localized on p-arm of chromosome 11.

Heterologous expression in FRT cell line blocked both basal chloride conductance and CaCC activity and, interestingly, inhibited anoctamin-1 activity when co-expressed (Schreiber et al., 2009).

Its expression was found mostly in mouse epithelial tissues such as thyroid, and cartilage (Schreiber et al., 2009).

1.4.3.10 Anoctamin-10/TMEM16K

Human anoctamin-10/ TMEM16K is codified by a gene localized on p-arm of chromosome 3.

Endogenous expression in FRT cell line produced CaCC , showed with patch-clamping studies and blocked basal anoctamin-6 chloride conductance and TMEM16A CaCC activity when co-expressed (Schreiber et al., 2009).

Niflumic acid slightly inhibited anoctamin-10 currents and CaCC activation required cytosolic calcium concentration smaller than anoctamins -1 and -6 (EC50% = 0.2 μM).

Anoctamin-10 gene mutations were found in patients carrying autosomal recessive cerebellar ataxia (Vermeer et al., 2010).

1.5 FLUORESCENT BIOSENSORS

Current methods used for study of cellular iodide transport are numerous; among these, radiotracers can monitor ion flows across cell membranes and electrophysiological techniques can measure ionic currents induced by iodide. Fluorescent indicators of halide (iodide and chloride) can also be used for this purpose. Among these, chemical compounds such as quinolinium (Galietta et al., 2001) have, however, some disadvantages, i.e. require pre-incubation and washing of cells, have an imperfect cell retention and it is not possible to identify their specific subcellular localization (Galietta et al., 2001).

Troubles described were solved with fluorescent indicators halide sensitive, derived from green fluorescent protein (GFP) (Mansoura et al., 1999), endogenously expressed in Aequorea victoria jellyfish (Figure) , pH but not halide-sensitive.

These intracellular chloride and iodide biosensors, GFP variants, can be stably expressed by cells, do not require pre-loading or washing in cells, are perfectly held inside cells and have better optical properties and photostability compared to chemical indicators (Jayaraman et al. , 2000).

The EYFP (Enhanced Yellow Fluorescent Protein) variant contains four different amino acid substitutions that shift the fluorescence from green (509 nm) to yellow-green (527 nm). Although EYFP's fluorescence excitation maximum is 513 nm, it can be efficiently excited at 488 nm, the standard laser line for an argon-ion laser.

GFP variant YFP (Yellow Fluorescent Protein) has four point mutations (S65G, V68L, S72A, T203Y) and excitation spectra and emission shifted towards the red compared to GFP (Mansoura et al., 1999; Elsliger et al. , 1999) .

Cells expressing YFP coding sequence show fluorescence distributed in cytoplasm and nucleus in a uniform manner.

YFP fluorescence is pH sensitive can bind halides and pseudohalides (Elsliger et al., 1999; Wachter and Remington, 1999). Process takes place provoking pKa changes (Galietta et al., 2001b) (-log10Ka), where Ka is acid dissociation constant, index of dissociation degree of an acid. If pKa of YFP chromophore undergoes changes, absorption of radiation capability can be mutated (Galietta et al., 2001b). Higher halide concentration leads to pKa increase and YFP fluorescence decrease, while increased pH (with chromophore deprotonation and pKa reduction), leads to fluorescence increase. These changes in YFP fluorescence, in response to changes of halide concentration or pH, occur within a few milliseconds.

YFP has a binding site distinct halide, but near the chromophore, which is formed by three adjacent amino acids: glycine 65 (serine in GFP), tyrosine 66, glycine 67 (Wachter et al., 2000.

YFP-H148Q variant is characterized by substitution of histidine residue in position 148 with a glutamine. Compared to YFP has a rather low chloride sensitivity, with a Kd bigger than 100 mM (at that concentration of chloride, YFP fluorescence is reduced by 50%) (Galietta et al., 2001b). This form of YFP has a wider cavity at the level of chromophore, structure that explains its high affinity for an ion voluminous as I^-, with a K_d of 21 mM (Galietta et al., 2001b; Wachter et al., 2000).

Randomly changing the six hydrophobic residues close to halide binding site, to change polarity and/ or size of this site, YFP-H148Q variants were obtained and selected with increased affinity for iodide and chloride, respectively YFP -I152L (K_d for I^-: 2 mM) and YFP-V163S (K_d for Cl^-: 40 mM) (Galietta et al., 2001b). These YFP mutants exhibit a specific sequence of sensitivity to anions: for YFP-I152L $I^- > NO^{3-} > Br^- > Cl^-$, for YFP-V163S $Cl^- > NO^{3-} > I^- > Br^-$ (Galietta et al., 2001b) (Fig.). Probably, difference is caused by environment: halide binding pocket resulted more hydrophilic in YFP-V163S by mutation of valine in position 163 with a serine (chloride binds more strongly to the nearby water molecules) (Galietta et al ., 2001b).

YFP-V163S is ideal for measuring Cl^- concentration in subcellular organelles, in which Cl^- concentration is approximately 25-40 mM, and then close to its K_d for Cl^- (Galietta et al., 2001b).

YFP-I152L is suitable for studies on the cellular transport of I-, in particular in thyroid gland, which uses iodide for thyroid hormones synthesis.

CHAPTER 2

AIM

The aim of this project is the identification of new channels involved in iodide efflux in thyroid follicular cells. According to the working hypothesis of the project, TMEM16A, a Ca^{2+}-activated chloride channel (CaCC) which regulates chloride homeostasis, could also play a role in the transport of iodide in thyroid gland. Thus, the aim of the research is the characterization of TMEM16A expression and function in the thyroid gland.

Specific aims:

- ❖ Determination of TMEM16A mRNA expression in thyroid cells (human normal or tumor thyroid gland and normal rat thyroid FRTL-5 cells)

- ❖ Identification of *splicing* TMEM16A mRNA isoforms expressed in FRTL-5 cells

- ❖ Identification of members of anoctamin family mRNA expressed in FRTL-5 cells

- ❖ Functional analysis of TMEM16A in FRTL-5 cells, verifying that its activity is compatible with described features, such as Ca^{2+} dependence and purine nucleotide-mediated activation (such as ATP), membrane voltage-dependence (induced by depolarization)

- ❖ Molecular analysis of TMEM16A mRNA and functional analysis of iodide efflux in a recombinant system

❖ Functional analysis of iodide efflux properties in FRTL-5 cells, evaluating the effect of intracellular Ca^{2+}, depolarization, agonists/antagonists of purinergic receptors, specific CaCC inhibitors

❖ Molecular analysis of TMEM16A mRNA and functional analysis of iodide efflux in FRTL-5 cells, evaluating the effects of TMEM16A RNA silencing

❖ Molecular analysis of hTMEM16A protein in a recombinant system using a proteomic approach

CHAPTER   3

MATERIALS AND METHODS

3.1 CELL CULTURE

3.1.1 FRTL-5 CELLS

The FRTL-5 cell line is derived from normal thyroid epithelium of Fisher strain albino rat (Fig 3.1). FRTL-5 cells grow in adhesion to substrate, are not polarized but are highly differentiated with expression of thyroid specific markers such as NIS, pendrin, TSH receptor, TPO, and TG. FRTL-5 cells are used as the cell model of choice for studies on the thyroid gland.
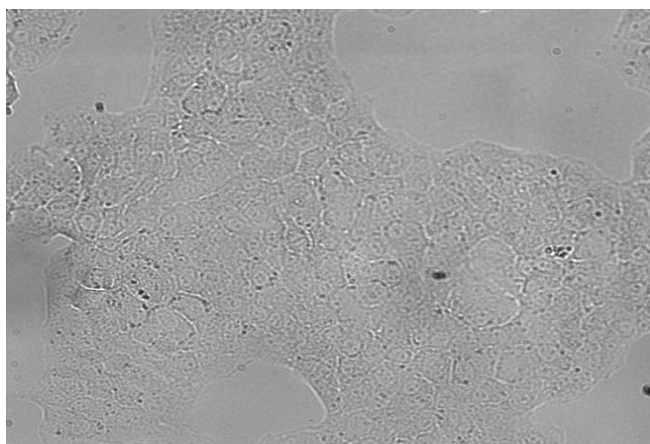
Fig. 3.1 FRTL-5 cells. Image acquired under transmitted light, 20X objective, Zeiss Axiovert 200 microscope.

3.1.2 FRTL-5 CELLS WITH YFP-H148Q/I152L STABLE EXPRESSION

Analysis of iodide fluxes in FRTL-5 cells requires the expression of a suitable biosensor. Stable clones of FRTL-5 expressing YFP-H148Q/I152L were previously developed in our laboratory (details in section 3.2.8) (fig. 3.2).
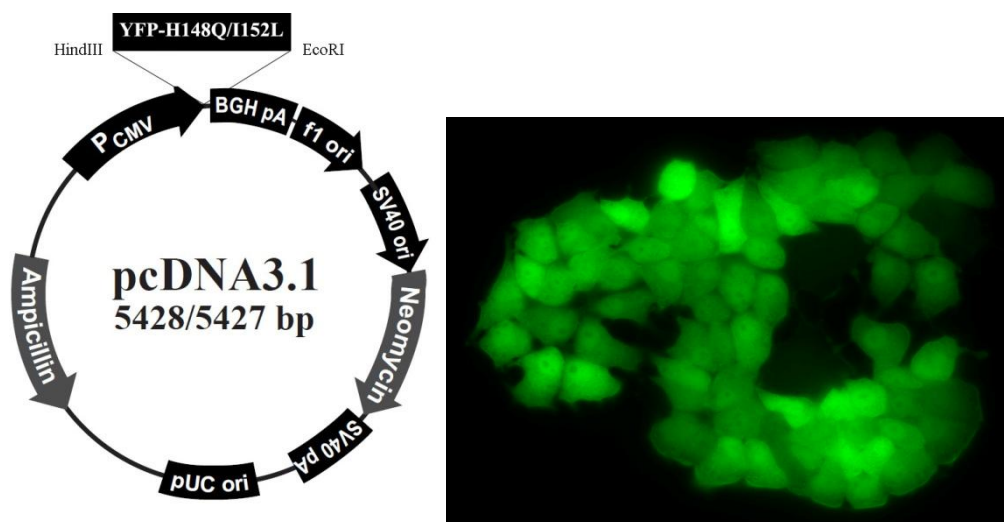
Fig. 3.2. Left: pcDNA3.1-YFP H148Q/I152L plasmid (Invitrogen®). Right: Fluorescence image of FRTL-5 cells stably expressing YFP H148Q/I152L.

3.1.3 CULTURE MEDIUM

FRTL-5 cells were cultured in 6H5 Coon's medium (Sigma-Aldrich®), specifically designed for the culture of differentiated thyroid cells (Ambesi-Impiombato et al., 1980). Cells were plated and maintained in T_{25} and T_{75} flasks, at constant temperature and CO_2 (37°C and 5% CO_2 in incubator).

When FRTL-5 were needed to suppress NIS transporter expression, were grown in TSH-free COON'S medium, also called 5H5, for at least one week.

F-12 COON'S MODIFICATION medium powder (Sigma-Aldrich®) was dissolved in milliQ water under continuous stirring. $NaHCO_3$ 30mM was added as a buffer agent. Medium pH was adjusted up to 7,3 with 1M HCl. Under sterility conditions the following additions were made:

❖ serum NCS 5% (Newborn calf serum, Sigma-Aldrich®);

- ❖ penicillin 100 U/ml (Euroclone®);

- ❖ streptomycin 100 µg/ml (Euroclone®);

- ❖ apotransferrin 5 µg/ml (Sigma-Aldrich®);

- ❖ hydrocortison 10 nM (Sigma-Aldrich®);

- ❖ somatostatin 10 ng/ml (Sigma-Aldrich®);

- ❖ GHL (glycine-L-histidine-L-lysine acetate) 10 ng/ml (Sigma-Aldrich®);

- ❖ TSH 1 mU/ml (Sigma-Aldrich®);

- ❖ insulin 1 µg/ml (Sigma-Aldrich®);

Sterilization was made with filtration (Millipore® 0,22 um filters), it usually brought medium pH up to 7.4.

3.1.4 FRTL-5 PASSAGE

Culture medium was changed almost every 2-3 days. FRTL-5 cells were passed when they reached 70%-80% confluence. Cells were washed with Ca2+-free PBS and incubated with CTC mix for 30':

- ❖ 50 U/ml collagenase (Sigma-Aldrich®);
- ❖ 500 U/ml trypsine (Sigma-Aldrich®);
- ❖ 2% chicken serum dialysed in HBSS (Hanks' buffered salt solution Ca^{2+} and Mg^{2+} free).

This detachment medium has been specifically designed for FRTL-5 cells (Ambesi...). In particular, collagenase is included to facilitate digestion of the extracellular matrix synthesized by thyroid cells. Chicken serum (which is devoid of trypsin inhibitory activity) is used to maintain viability during cell detachment. Cells were resuspended in 6H5 medium, so serum contained could block protease effects, and centrifuged at 300 g for 5'. After removal of supernatant, FRTL-5 were resuspended in 6H5 medium and plated with an usual dilution 1:4.

3.1.5 CELL FREEZING AND THAWING

FRTL-5 were washed with Ca^{2+}-free PBS and detached with CTC mix, centrifuged at 300 g for 5' and counted with Burker's chamber.

Cells (1×10^6 cells/ml) were cryopreserved in a solution containing 6H5 medium (50%) and NCS (40%), and DMSO (10%). using freezing containers (Mr. Frosty Nalgene$^®$) containing isopropanol at -80°C to allow a slow and successful freezing (1 °C/min). For long-term preservation, cryovials were maintained in liquid nitrogen.

Thawing was performed by rapidly immersing vials in a 37°C bath. After cleaning the vial with 70% ethanol in deionized water, cell suspension was transferred into tubes with 20ml COON'S medium and centrifuged to remove DMSO, toxic at RT. Pellet was resuspended in 5ml 6H5 medium and plated into T_{25} flasks.

3.1.6 FRTL-5 CULTURE FOR FUNCTIONAL STUDIES

Functional experiments required growth of FRTL-5 cells on round 25mm diameter coverslips. Coverslips were first cleaned by soaking overnight in 70% ethanol and 1% HCl, and sterilized by UV in 6-well plates. FRTL-5 cells were plated at a density of $0,8\times10^5$ cells/well and grown for 1 week before *in vivo* functional experiments.

3.1.7 CHO CELL LINES

CHO cell lines are from a biopsy of an ovary of an adult Chinese hamster. CHO K1 cell line used in our studies was a subclone from the parental CHO cell line (Fig 3.3). These cells grow in a monolayer.
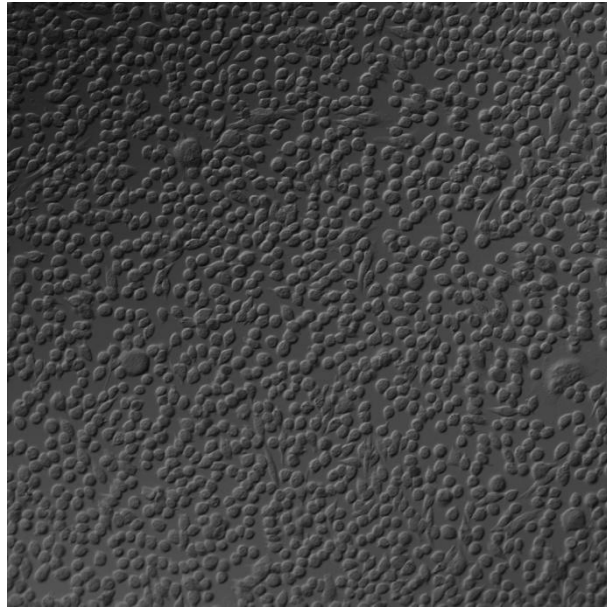
Fig. 3.3 CHO K1 cells. Image acquired under transmitted light with an FluoView 1000 confocal microscope, 20X objective (Olympus, Tokyo, Japan).

3.1.8 CHO CELLS WITH YFP-H148Q/I152L AND hNIS STABLE EXPRESSION

Analysis of iodide efflux in CHO K1 cells required expression of a suitable biosensor. Thus, stable clones of CHO K1 expressing YFP-H148Q/I152L and hNIS proteins were obtained in our laboratory previously (details in section 3.2.8), suitable for functional *in vivo* experiments on iodide flow (fig.3.4).
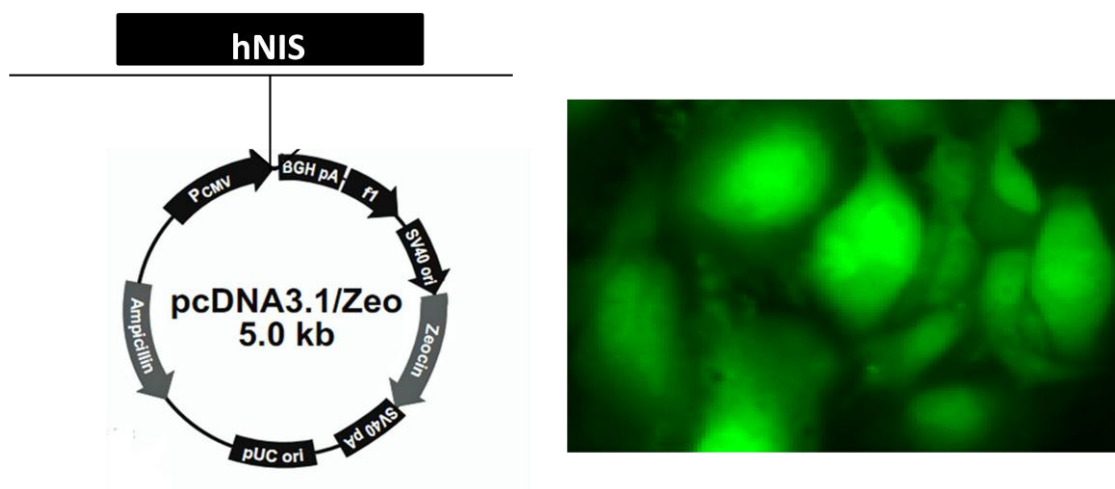
Fig. 3.4. Left: pcDNA3hNIS Zeo (Invitrogen®) with MCS region. Right: CHO K1 cells stably expressing YFP H148Q/I152L. Image acquired with inverted optical microscope Zeiss™ Axiovert 200, through an oil immersion 40X objective. YFP fluorescence was observed at these wavelength (λ): excitation 500 ± 12.5 nm and emission 545 ± 17.5 nm; specific filters set used was XF104-2, OMEGA® optical.

3.1.9 CULTURE MEDIUM

CHO K1 cells required proline in their medium for growth, so proline-containing HAM's nutrient mixture F12 medium or DMEM-F12 1:1 mixture (Sigma-Aldrich®) were used. Cells were plated and maintained in T_{25} ,T_{75} flasks or 100mm dishes, at constant temperature and CO_2 (37°C and 5% CO_2 in incubator).

Under sterility conditions the following additions were made:

- ❖ serum FBS 10% (Fetal bovine serum, Sigma-Aldrich®);

- ❖ penicilline 100 U/ml (Euroclone®);

- ❖ streptomicine 100 µg/ml (Euroclone®);

3.1.10 CHO PASSAGE

Culture medium was changed almost every 2-3 days. CHO K1 cells were passed when they reached 90% confluence. Old medium was removed and 3 washes with Ca^{2+}-free PBS were made, to eliminate FBS residues, containing trypsin inhibitors. for some minutes cells were incubated in PBS:

- ❖ KCl 2,7 mM;

- ❖ KH2PO4 1,8 mM;

- ❖ NaCl 137 mM;

❖ Na2HPO4 1 mM;

Containing:

   ❖ 0.25% (w/V) trypsin

   ❖ 0.04% (w/V) EDTA (Sigma-Aldrich®), bivalent ion chelating agent, involved
   in intercellular junctions.

Cells were resuspended in F12 medium, so serum contained could block protease effects, and centrifuged at 300 g for 5'. After removal of supernatant, CHO K1 were resuspended in F12 medium and plated with an usual dilution 1:20/1:50, depending on experiments.

3.1.11 CELL FREEZING AND THAWING

CHO K1 were washed with Ca^{2+}-free PBS and detached with trypsin solution, centrifuged at 300 g for 5' and counted with Burker's chamber.

Cell *pellet* was resuspended in a solution containing FBS (90%), then cryopreserving agent DMSO (10%) was added after, to avoid its toxic effects as much as possible. Next steps were the same as FRTL-5.

Thawing was performed immersing vials in a 37°C bath (rapidly, for 1'). After cleaning vial with 70% ethanol in deionized water, cell suspension was transferred into tubes with 20ml F12 medium and centrifuged to remove DMSO, toxic at RT. Pellet was resuspended in 5ml F12 medium and plated into T_{75} flasks or 100mm dishes.

3.1.12 CHO CULTURE FOR FUNCTIONAL AND PROTEIN STUDIES

For functional experiments CHO K1 were grown in 6 well plate with coverslips as described before.

For proteomic experiments CHO K1 cells were plated on 100mm Petri dishes (4,5 10^5 cells/dish) and grown for 2-3 days up to 95% confluence before performing every assay.

3.2 MOLECULAR ANALYSIS

Exogenous expression was induced with cDNA transfection. Anoctamin transcripts were detected by RT-PCR, Real Time RT-PCR (quantitative). Transcript silencing was performed by small-RNA-interference (siRNA). TMEM16A-EYFP fusion protein were obtained by expression cloning. Protein was analyzed with proteomic assays and detected by fluorescence staining or Western Blot.

3.2.1 CELL OR TISSUE COLLECTION

Cells were detached as previously described, resuspended in PBS and centrifuged at 300 g for 5'(3X), with a final wash in microtubes at 600g. After removal of the supernatant, *pellets* were kept at -80°C. Tissue samples were collected from biopsies and kept at -80°C or in liquid nitrogen. Before extraction, cell pellets were thawed, tissue samples were homogenized with a specific pestle and chopped on ice.

3.2.2 RNA EXTRACTION

Total RNA from cells or tissues was extracted with TRIZOL® (SIGMA) or TRI REAGENT® (Ambion) according to manufacturer's instructions. The method is a modification of the phenol chloroform method, developed by Chomczynski and Sacchi , 1987 which isolates aqueous phase containing RNA .

3.2.3 DNASE TREATMENT

To remove contaminant genomic DNA which could cause nonspecific signals in RT-PCR, extracted RNA was processed with DNAse I enzyme. After extraction, RNA samples were diluted in:

❖ reaction buffer;

❖ DNasi I (Applied Biosystems®) 0.1 U/μl.

After 15' incubation, DNAse was inactivated with stop solution for 10' at 70°C.

3.2.4 RNA QUANTIFICATION

RNA was quantified spectrophotometrically, by measuring RNA absorbance at 260 nm wavelength (value of maximum absorbance) according to the Lambert-Beer law:

260 nm absorbance · dilution factor · 40 μg/ml.

Sample purity was checked according to the ratio between signals at 260/280 nm (proteins have maximum absorbance at 280 nm) and at 260/230 nm (solvents such as ethanol have maximum absorbance at 230 nm).

RNA quality was checked by electrophoretical migration on 1% agarose gel.

3.2.5 RETROTRANSCRIPTION (RT)

RNA-complementary DNA (cDNA) was obtained by retrotranscription, catalyzed by a recombinant reverse transcriptase, with RNA-dependent DNA-polymerase activity. Random hexamers were usually employed as primers for cDNA synthesis.

Reagents (Applied Biosystems®):

- ❖ RT TaqMan 10x buffer;

- ❖ $MgCl_2$ 5.5 mM;

- ❖ dNTP mix (deoxyribonucleoside triphosphate), 125 μM each;

- ❖ RNase inhibitor 0.4 U/μl;

- ❖ random hexamers 2.5 μM;

- ❖ MultiScribe Reverse Transcriptase, recombinant enzyme from Moloney Mouse Leukemia Virus) 1.25 U/μl;

- ❖ milliQ water up to proper reaction volume.

Usually 1 ug RNA/25 ul reaction volume was used.

To check the cDNA purity of samples, two samples/ experimental set were processed without enzyme in order to check for contaminant genomic DNA residues (RT-samples).

To remove intramolecular pairings, RNA was denatured at 60°C for 10'.

RT reaction steps:

- ❖ 25°C 10' priming;

- ❖ 48°C 30' enzyme binding and elongation;

- ❖ 95°C 5' enzyme inactivation;

cDNA samples were stored at -20°C, RNA samples at -80°C.

3.2.6 RT-PCR

PCR (Polymerase Chain Reaction) was used to amplify DNA sequences *in vitro*. We used RT-PCR (cDNA as input DNA).

RT-PCR reagent mix (Applied Biosystems®):

- ❖ 10x reaction buffer;
- ❖ $MgCl_2$ (2, 3, 4 or 5.5 mM, depending on primers used);
- ❖ dNTP mix with

o   dATP 200 μM;

o   dGTP 200 μM;

o   dCTP 200 μM;

o   dUTP 400 μM;

- ❖ forward primer 200 nM;

- ❖ reverse primer 200 nM;

- ❖ AmpliTaq Gold DNA polymerase 0.025 U/μl;

- ❖ uracil-N-glycosylase (UNG) 0.01 U/μl;

- ❖ milliQ water up to proper reaction volume

UNG enzyme removes uracil residues from DNA, to prevent carry-over contamination due to DNA from previous reactions (uracil-containing). Contaminant

DNA is degraded by UNG at 50°C (PCR first step). UNG is inactivated at 95°C before amplification.

Usually 1 ul cDNA/25 ul reaction volume was used.

PCR reaction steps:

- ❖ 50°C 2' UNG reaction;

- ❖ 95°C 10' cDNA melting and UNG inactivation;

- ❖ 35 cycles

o   95°C 15" DNA melting;

o   60°C, 62°C o 64°C 30" (annealing temperature, depending on primers used)

o   72°C 30" elongation

- ❖ 72°C 7' final elongation.

Final conditions used were:

TMEM16A	2/3 mM	60°C
TMEM16C	3 mM	60°C
TMEM16D	5.5 mM	60°C
TMEM16E	3 mM	60°C
TMEM16F	2/3 mM	60°C
TMEM16G	3 mM	64°C
TMEM16H	3 mM / 4 mM	60°C / 64°C
TMEM16K	all	60°C

For the other primers the final conditions used were 5.5 mM $Mg^{2+}Cl^-$ and 60°C annealing temperature.

3.2.6.1 PRIMERS

- ❖ human GAPDH (housekeeping gene):
  - o Forward primer: 5'-CTCTCTGCTCCTCCTGTTCGAC-3'
  - o Reverse primer: 5'-TGAGCGATGTGGCTCGGCT-3'
  - o 69 bp amplicon

- ❖ human β-actin II (housekeeping gene):
  - o Forward primer: 5'-CCTGGCACCCAGCACAAT-3'
  - o Reverse primer: 5'-GGGCCGGACTCGTCATACT-3'
  - o 144 bp amplicon

- ❖ rat β-actin (housekeeping gene):
  - o Forward primer: 5'-CGCCGGTCCACACCCGCCAC-3'
  - o Reverse primer: 5'-CCGCGAAGCCGGCCTTGCACA-3'
  - o 96 bp amplicon

- ❖ human NIS:
  - o Forward primer: 5'-TACGTGGCTTGCCGCACAGAGAAG-3'
  - o Reverse primer: 5'-CATGACGATGCCACAGCAGGC-3'
  - o 105 bp amplicon

- ❖ rat NIS:
  - o Forward primer: 5'-TATGTCGCCTGCCACACAGAG-3'
  - o Reverse primer: 5'-CATGACAATGCCACAGCAAG-3'
  - o 105 bp amplicon

- ❖ human TMEM16A:

- o Forward primer: 5'-TGAAACTGAAGATGCCGACGAAGAA-3'

- o Reverse primer: 5'-CTTTGGGCTGGATGGGATCTGTGAT-3'

- o 111 bp amplicon

❖ rat TMEM16A (QRT-PCR):

- o Forward primer: 5'-ACAACATCACCATGTGTCCT-3'

- o Reverse primer: 5'-AGCCCAGAGGGCCATAAACAC-3'

- o 140 bp amplicon

❖ rat TMEM16A "a" segment:

- o Forward primer: 5'-CACAAGAGAGCCTCGGGTAG-3'

- o Reverse primer: 5'-ATCTTCACAAACCCGACACC-3'

- o 267 bp amplicon

❖ rat TMEM16A "b" segment:

- o Forward primer: 5'-CAAAACCCGGAGCACAATAG-3'

- o Reverse primer: 5'-CAGGAGTTTCCTGTCGTTGA-3'

- o 241/175 bp amplicon

❖ rat TMEM16A "c" segment:

- o Forward primer: 5'-CTCTGGGCTGCCACCTTC-3'

- o Reverse primer: 5'-TGGCTTCATACTCTGCTCTGG-3'

- o 130/118 bp amplicon

❖ rat TMEM16A "d" segment:

- o Forward primer: 5'-TCCCAGAGCAGAGTATGAAGC-3'

- o Reverse primer: 5'-AGATGGGGAGGAGTTCATGG-3'

- o 305/230 bp amplicon

❖ rat TMEM16A:

- o Forward primer: 5'-TCCAAAGACTTCTGGGCTGT-3'

- Reverse primer: 5'-TACTCGTAGCTGGGGACTGG-3'

- 305 bp amplicon

❖ rat TMEM16B:

- Forward primer: 5'-CCAGGGAAGCAGAGTTCTTG-3'

- Reverse primer: 5'-TGTTGTTGGCTCGAGAACAG-3'

- 297 bp amplicon

❖ rat TMEM16C:

- Forward primer: 5'-TCGGACTGCTACACTGGCCCT-3'

- Reverse primer: 5'-CAGCGTGCCCAGCGCTCATA-3'

- 290 bp amplicon

❖ rat TMEM16D:

- Forward primer: 5'-TGGCTTCGAGGGCCAAGGACA-3'

- Reverse primer: 5'-TGAGGCGGGTCCCGGTAGTC-3'

- 319 bp amplicon

❖ rat TMEM16E:

- Forward primer: 5'-ACGGCCAAAGTACCCACCCCT-3'

- Reverse primer: 5'-ACTGGCCATCATGGAGCGGG-3'

- 293 bp amplicon

❖ rat TMEM16F:

- Forward primer: 5'-AGCCATCCTGGCCGTGGTGA-3'

- Reverse primer: 5'-GCCCGGGTGGGTTTCGGAAG-3'

- 304 bp amplicon

❖ rat TMEM16G:

- Forward primer: 5'-TGGCGCCGCTTTTTGCCCTA-3'

- Reverse primer: 5'-GCAAGTGCGGTTGTGTGCCG-3'

- o 302 bp amplicon

❖ rat TMEM16H:

- o Forward primer: 5'-AAGTTCGCCACCACCGCCAC-3'

- o Reverse primer: 5'-TGATGCCTCGTGCAGCCAGC-3'

- o 324 bp amplicon

❖ rat TMEM16J:

- o Forward primer: 5'-GGCTGGCCTGTGGAAGCTGG-3'

- o Reverse primer: 5'-GCCAACAGGGGTGCGAGTGG-3'

- o 327 bp amplicon

❖ rat TMEM16K:

- o Forward primer: 5'-GGCTACCCGCAGGCCAAATTG-3'

- o Reverse primer: 5'-CCCACACGAACAGGTAGTAGGGC-3'

- o 280 bp amplicon

Primers for the anoctamin family and TMEM16A/ANO1 isoforms have been published (Manoury et al., 2010). Other primers were designed with PRIMER BLAST software, taking sequences published on the NCBI database as reference (http://www.ncbi.nlm.nih.gov). Sequences were aligned with BLAST software (http://www.ncbi.nlm.nih.gov/BLAST) to check for any predicted pairing with non specific sequences or to test cross-pairings.

For each primer couple, reactions were optimized by testing different conditions such as Mg^{2+} concentration and annealing temperature.

3.2.7 REAL TIME PCR (QUANTITATIVE, QRT-PCR)

Levels of transcript expression were quantified with quantitative RT-PCR, also called Real Time PCR, since amplicon signals can be detected and followed "real time".

This technique allows absolute or relative quantification of cDNA expression, compared to a reference gene.

SYBR Green I was used as a probe, whose fluorescence at 530nm increases more than 200 fold when bound to the DNA minor groove. Fluorescence is proportional to DNA copy number synthesized during amplification reaction, according to cDNA input concentration.

Since SYBR Green I is a non specific probe a melting curve was obtained at the end of the reaction, in order to detect any signal due to non specific amplicon (i.e. primer dimers). The double strand DNA melting temperature (Tm), specific for each amplicon, is determined by gradually increasing the temperature above the primer Tm. Fluorescence is rapidly quenched at the melting point, since the probe is not able to bind DNA. Detection of overlapped melting peaks is good purity index, whereas different peaks indicate nonspecific amplicons.

QRT-PCR was performed in accordance with manufacturer's instructions (Applied Biosystems®), with a specific kit.

Reaction mix:

- ❖ Fast SYBR® Green Master Mix;
- ❖ forward primer 0.5 μM;
- ❖ reverse primer 0.5 μM;
- ❖ milliQ water up to proper reaction volume

Usually 2 ul cDNA/20 ul reaction volume was used.

QRT-PCR stages:

- ❖ 95°C 20" cDNA denaturation;
- ❖ 40 cycles:
- o 95°C 3" cDNA denaturation;
- o 60°C 30" annealing and elongation

The threshold cycle is the number of cycles necessary to reach a fluorescence signal significantly higher than background, at the beginning of the exponential phase of amplification. At this stage DNA is quantified, since the fluorescence signal is not influenced by other reagents, which are limiting in the plateau phase, but is directly proportional to the number (n) of cycles. By convention the CT value is defined as 10 times standard deviation of the fluorescence signal during the first 15 cycles.

Analysis was performed using 7500 Fast Real-Time PCR System software (Applied Biosystems®). Average Ct between duplicate samples was calculated.

The threshold cycle comparison method was employed for analysis (Livak and Schmittgen, 2001), to determine gene differences in expression of control samples (calibrator) and treated samples. Differences among input cDNA quantity or quality were corrected with a comparison between the target gene and a reference housekeeping gene (normalizer), whose expression is stable under different conditions.

Threshold cycle (CT) indicates the fractional cycle number at which the XN,q amount of amplified target reaches a fixed threshold (Livak and Schmittgen, 2001). According to this method ($\Delta\Delta$CT or Fit Point), target gene ΔCT was calculated both in control sample, ΔCT (C), and in treated sample, (ΔCT (T):
ΔCT target gene = CT target gene − CT normaliser gene.

Then $\Delta\Delta$CT was calculated for every sample: $\Delta\Delta$CT (T) = ΔCT (T) - ΔCT (C). Finally, target gene expression levels in treated samples compared to control was calculated with the following function: $2^{-\Delta\Delta CT\ (T)}$.

To check the applicability of this method it was first necessary to calculate and compare primer efficiencies, since, according to the $\Delta\Delta$CT method, amplification primer efficiency must be the same and maximum (E = 1). Calibration curves were performed with different input DNA concentrations (serial dilutions) amplified in the same reaction. Calibration curves were obtained by linear regression of CP (crossing point) values depending on input cDNA concentration, using GraphPad software.

Efficiency was calculated with the following formula: E = 10-1/slope − 1 (Pfaffl., When calibration curve slope is -3.3, efficiency is maximum.

According with this analysis primer efficiencies were not significantly different and close to 1 (fig. 3.5) . Therefore, the ΔΔCT method could be used.

TMEM16A r2=0.85, slope = -3.32
NIS r2=0.85, slope = -3.21
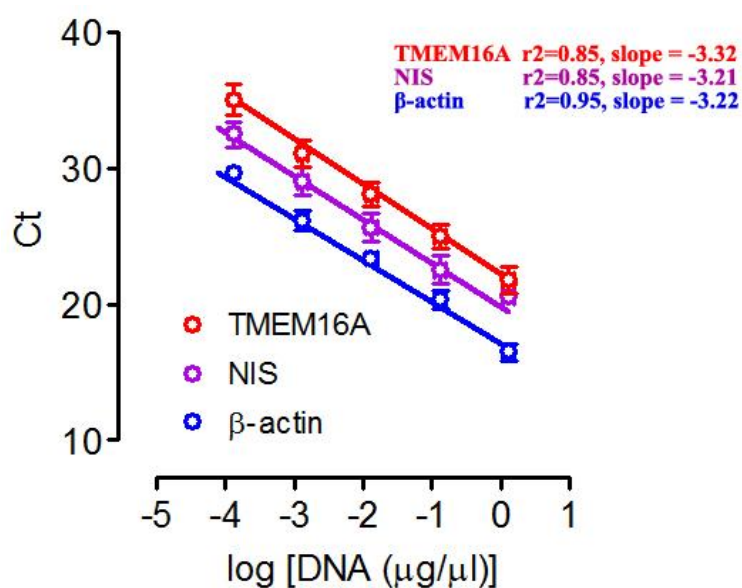β-actin r2=0.95, slope = -3.22

Fig. 3.5. Calibration curves for QRT-PCR primers: TMEM16A, NIS, β actin. Correlation coefficients (r^2) and angular coefficients (slope) of each curve are shown. Ct: Cycle-threshold, DNA input concentration ug/ul in logarithmic scale.

PCR products were observed with electrophoretical migration on 2% agarose gel. Solution used was Tris Borate EDTA (TBE):

❖ 1.09 % (w/V) Tris-amino-metano base;

❖ 0.557 % (w/V) boric acid;

❖ 0.074 % (w/V) EDTA bisodium as bivalent ion chelating agent to inhibit nuclease activity.

Gel staining was performed with 0.5 μg/ml ethidium bromide, whose fluorescence is 20 fold more when bound to double strand DNA. Emitted light was detected with a UV transilluminator.

The loading buffer for samples contained:

- ❖ bromophenol blue

- ❖ glycerol

Electrophoretical run was done at 150 V.

3.2.8 TRANSFECTION

Exogenous genetic material can be targeted into cells in different ways. The present study used transfection, a system which uses artificial constructs to deliver a DNA/RNA to eukaryotic cells and allow its expression.

Transient transfection was used to induce target cDNA expression and to knock-down target mRNA expression, in order to determine their functional effect on iodide transport in cells studied.

Selection of stable clones after transfection was used to obtain cell models that are homogeneous and suitable for continuous functional assays on iodide transport.

When necessary, empty vectors were used as a control in transient transfection.

Employed *in vitro* transfection techniques:

a) Lipofection (with Lipofectamine 2000®, Invitrogen), for DNA transient/stable expression or RNA interfering delivery;

b) Polifection (with PEI, polyethyleneimine, Sigma), for DNA transient expression;

c) Superfect (Quiagen®), for RNA interfering delivery;

d) Peptide-based system (with N-TER™, Sigma), for RNA interfering delivery.

a) Lipofection uses cationic lipids, which contain positively charged head group and one or two hydrocarbon chains. Lipid groups mediate entry of construct into cells,

charged head groups regulate interaction between lipid and phosphate backbone of the nucleic acid, producing DNA condensation. A neutral co-lipid or helper lipid is often inserted to form a unilamellar liposomal structure with a positive surface charge in water. Positively charged head group can also help the interaction of nucleic acids and cell membrane, so that liposome and nucleic acids ("transfection complex") can fuse with the negatively charged cell membrane. The transfection complex is then thought to undergo endocytosis: a membrane bound/intracellular vesicle includes liposome and nucleic acid. Once inside the cell, the complex avoids the endosomal pathway, and enters the nucleus.

Plasmids used:

❖ **pcDNA3 hNIS** (S. Jhiang, Ohio State University)

❖ **pcDNA3.1 YFP-H148Q/I152L** (L. J. V. Galietta, Laboratory of Molecular Genetics, Istituto Giannina Gaslini, Genova)

❖ **pcDNA3.1 hTMEM16A** (L. J. V. Galietta, Laboratory of Molecular Genetics, Istituto Giannina Gaslini, Genova)

Cells were typically grown in 6 well plates and were transfected when 90% confluence was reached.

To obtain stable clones expressing YFP-H148Q/I152L, FRTL-5 were grown in 24 well-plates and transfected with pcDNA3.1-YFPH148Q/I152L (0.8ug/well). Lipofectamine 2000 (Invitrogen ®) was used as transfection agent, with 4ul liposome: ug DNA ratio (Rhoden et al. 2007). FRTL-5 cell clones with stable YFP expression (FRTL-5 YFPH148Q/I152L, fig. 3.2, right) were selected by proliferation in an medium containing antibiotic (G418 or Geneticin, 500 ug/ml) for two-three weeks, followed by limit dilutions of survived cells to obtain clonal populations (Rhoden et al., 2007).

To obtain stable clones expressing YFPH148Q/I152L and hNIS, CHO K1 were grown in 6 well-plates and transfected with pcDNA3.1-YFPH148Q/I152L (2 ug/well) and pcDNA3.1/Zeo-hNIS (2 ug / well) with Lipofectamine 2000 (Invitrogen ®) (ratio: 4µl Lipofectamine: 2µg DNA). Initially CHO-K1 cells were transfected with

pcDNA3.1-YFPH148Q/I152L, then underwent several rounds of selection with G418 antibiotic (200-400 ug/ ml). YFPH148Q/I152L expression was monitored by fluorescence microscopy. A cell population with high stable fluorescence was used for subsequent transfection with pcDNA3.1/Zeo-hNIS. After the second transfection, cells were maintained in culture medium with G418 100 ug/ ml, to maintain selection for pcDNA3.1-YFP-H148Q/I152L, and Zeocina 100 ug/ ml to select the cells transfected with pcDNA3.1/ Zeo-hNIS. Selected cells were plated in 96-well plates at a limiting dilution to obtain a single cell/well. Clonal populations expressing both YFPH148Q/I152L and hNIS were obtained and tested for functional studies on iodide uptake.

TMEM16A expression was induced with ratio 3μl Lipofectamine 2000: 1μg DNA, according to manufacturer's instructions. Particularly, stably expressing YFP-H148Q/I152L and hNIS CHO-K1 cells were transfected to induce transient expression of human TMEM16A, with pcDNA3.1-hTMEM16A (2μg/ well 6WP), and Lipofectamine 2000, with ratio 4 ul Lipofectamine: 2 ug DNA.

b) Polyfection methods are based on cationic polymers. Polyethyleneimine (PEI) was the second polymeric transfection agent discovered (Vancha et al., 2004), after poly-l-lysine. Its secondary amines can condense DNA into positively charged particles, which can interact with anionic cell surface residues and undergo endocytosis. Inside the cell, amines are protonated, counter-ion influx and the osmotic potential is lowered, leading to osmotic swelling and consequent release of polymer-DNA complexes (polyplex) from vesicles into the cytoplasm. DNA can diffuse to the nucleus if polyplex becomes less condensed (Rudolph et al., 2000; Akinc et al., 2004).

For proteomic experiments CHO K1 cells were passed 1-2 days before transfection at $4,5*10^5$ /100mm dish. The ratio of PEI nanoparticles (Sigma®): DNA was 3ul: 1ug.

Transfection was performed according to manufacturer's instruction, exposing cells to construct overnight.

Plasmids used:

- ❖ **pEYFP-N1** (Dr. Diego Alvarez De La Rosa Rodríguez, Pharmacology Unit, Canary University Hospital, La Laguna University, Tenerife)

❖ **pEYFP-N1-hTMEM16A**

❖ **pcDNA3.1-neo hTMEM16A** (L. J. V. Galietta, Laboratory of Molecular Genetics, Istituto Giannina Gaslini, Genova)

c) SuperFect Transfection Reagent is a specifically designed activated dendrimer . SuperFect Reagent architecture is spherical, and contains branches radiating from a central core with terminal charged amino groups. SuperFect Reagent optimizes entry of DNA into the cell assemblying DNA into compact structures. SuperFect–DNA complexes are positively-charged, therefore capable of binding to negatively charged receptors (i.e, sialylated membrane glycoproteins) on surface of eukaryotic cells. After its access into cytosol, SuperFect Reagent buffers lysosome after its fusion with endosome, inhibiting pH-dependent lysosomal nucleases and stabilizing SuperFect–DNA complexes.

The protocol is described in section 3.2.9.

d) N-TER™ (Sigma) Nanoparticle siRNA Transfection System is a peptide-based system. N-TER Peptide can bind siRNAs non-covalently, forming a nanoparticle, which can interact with cell membrane surface lipids. The complex can diffuse through cell membrane and deliver siRNA directly to the cytoplasm, avoiding endosomal pathway and consequent likely degradation of compartmentalization.

This system was designed specifically to deliver siRNAs into cells and induce RNA interference.

The protocol is described in section 3.2.9.

3.2.9 SMALL INTERFERENCE RNA (siRNA)

RNA interference (RNAi) is a cytosolic RNA-dependent mechanism of silencing produced by double strand RNA molecules (dsRNA). dsRNA are exogenous in human cells and recognized by Dicer enzyme (Lewin, 2004). *In vitro* this enzyme was demonstrated to cut dsRNA with a ATP-dependent process, producing breaks in each 3' –end and, accordingly, small RNA molecules, "siRNA" (short interfering RNA) of 21-23 bps, with short 3'ends protruding 2 bps (Lewin, 2004).

A more successful system is delivery of synthetic siRNA specific for target mRNA into cells artificially. siRNA are included in a protein complex, "RISC" (RNA-induced silencing complex), which breaks siRNA duplex with formation of free single strand RNA fragments. RISC complex leads binding between siRNA and complementary mRNA, which is degradated and knocked-down. Result is post-transcriptional silencing (Hannon and Rossi, 2004) (fig. 3.6).
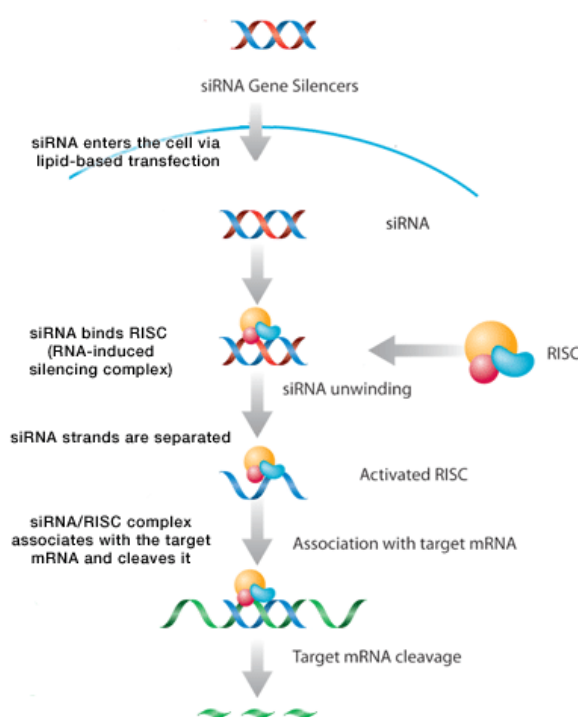

Fig. 3.6. RNA interference mechanism (image from www. scbt.com).

FRTL-5 cells were transfected with siRNA to induce TMEM16A silencing, employing Lipofectamine 2000 (Invitrogen®), Superfect (Quiagen®), N-TER nanoparticle SiRNA transfection system (Sigma®), and with the following siRNA against rTMEM16A mRNA (all from Sigma Aldrich ®):

❖ SASI_Rn02_00230075;
❖ SASI_Rn02_00230076;
❖ SASI_Rn02_00230077 ;

❖ universal negative control siRNA (Sigma Aldrich ®) ("scrambled" siRNA, which recognize no RNA sequence)

Lipofectamine was used at the ratio of 1µl (Lipofectamine): 20pmol (siRNA), with 25/50 pmoles of siRNA, corresponding to concentrations of 50/100 nM.

Superfect was used at the ratio of 1.32 ul (Superfect, 3µg/µl): 20 pmoles (siRNA), with 25/50 pmoles of siRNA, corresponding to concentrations of 50/100 nM.

N-TER nanoparticle siRNA transfection system was used with recommended volumes, 8% v/v, and 50/100 nM siRNA were added. Cells were exposed to constructs in +/- serum medium, according to manufacturer's instructions, for 24 h.

Finally, after each kind of transfection experiment, cells expressing YFP-H148Q/I152L were observed after 2-3 days with an inverted microscope (Zeiss Axiovert 200) equipped with a XBO Xenon 75 W lamp, XF104-2 YFP filter set of YFP excitation wavelengths (500 ± 12,5 nm) and emission wavelengths (545 ± 17,5 nm) (Omega Optical).

Fluorescence signal was used as a index of successful DNA transfection or mRNA silencing, depending on effects produced by constructs delivered into cells.

3.2.10 EXPRESSION CLONING

Expression cloning of hTMEM16A coding sequence was performed to study protein expression in a recombinant system (CHO K1), using a COOH-terminal-tag.

The original expression vector (pcDNA3.1) contained the coding sequence of human TMEM16A (kindly donated by Dr. J. Galietta, Laboratorio di Genetica Molecolare, Istituto Giannina Gaslini, and Centro di Biotecnologie Avanzate, Genova, Italy)

(empty vector in fig. 3.7, Invitrogen®). Dideoxy-nucleotide sequencing was performed in our laboratory previously.
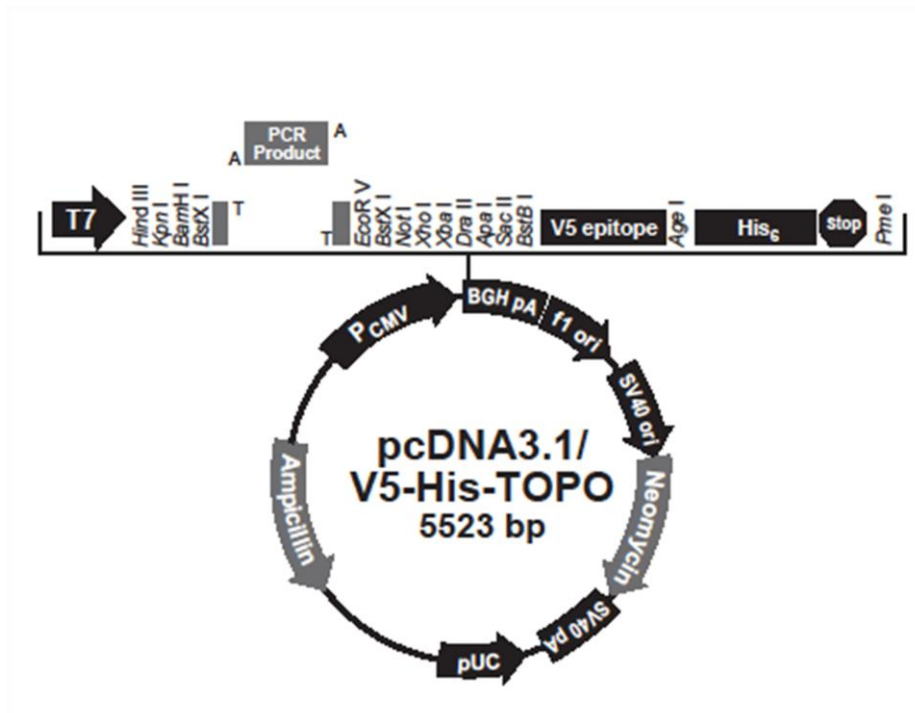

Fig. 3.7. pcDNA 3.1/V5-His-TOPO empty vector (Invitrogen®) with MCS region.

Human TMEM16A cDNA (NCBI Reference Sequence: NM_018043.5) was subcloned into pEYFP-N1 plasmid, containing EYFP (Enhanced Yellow Fluorescent Protein) coding sequence (kindly donated by Dr. Diego Alvarez De La Rosa, Departamentos de Fisiología y Farmacología, Instituto de Tecnologías Biomédicas, Facultad de Medicina, Universidad de La Laguna, La Laguna, Spain) (CLONTECH Laboratories, Inc.)(fig. 3.8).
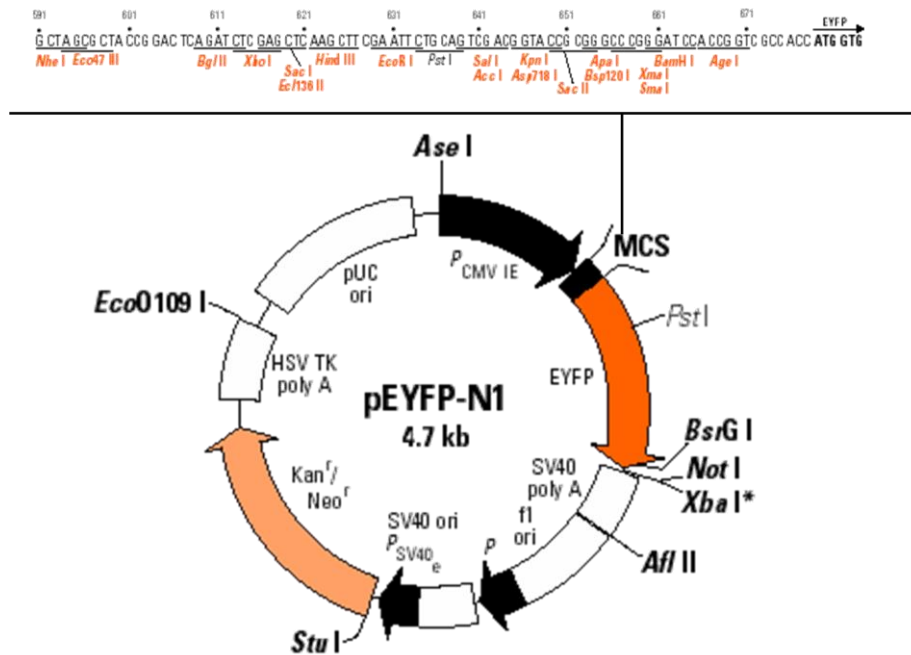
Fig. 3.8. pEYFP-N1 empty vector (CLONTECH Laboratories, Inc.) with MCS region.

Enhanced Yellow Fluorescent Protein (EYFP) was in-frame fused to COOH-terminus of hTMEM16A in pEYFP-N1 vector, to limit any possible functional alteration (more probable with EYFP-*tagging* at long hTMEM16A NH_2-terminus).

First of all, a PCR reaction was performed with primers specific for hTMEM16A, containing restriction sites for NheI and BamHI enzymes (in bold) using a proofreading DNA polymerase cocktail (Expand-High Fidelity PCR System kit, Roche-Applied Science®), according to manufacturer's instructions.

Forward primer: 5'-GCA**GCTAGC**GCCACCATGAGGGTCAACGAGAAGTAC-3'

Reverse primer: 5'-CGGTGGATCCCGCAGGACGCCCCCGTGGTA-3'

Reverse primer (sense sequence):

5'-TACCACGGGGGCGTCCTGCG**GGATCC**ACCG-3'

Amplicon: 2955 bp.

PCR product size and quality were assessed by agarose gel electrophoresis (1% agarose gel, ethidium bromide staining) and construct was extracted and purified with a commercially available kit (Illustra GFX PCR DNA & Gel Band Purification Kit - GE Healthcare), according to manufacturer's instructions.

After linearization with the appropriate restriction enzymes (Nhe1 and BamH1), constructs were dephosphorylated with APex™ Heat-Labile Alkaline Phosphatase (Epicentre®), to avoid vector recircularization, and finally purified. All purification steps were needed to remove salts, inhibitors of next treatments.

Ligation between the constructs was performed with Fast-Link ™ DNA Ligation Kits ® (Epicentre) according to manufacturer's instructions. Bacterial suspensions of DH5-α Escherichia coli strain (electrocompetent) were transformed with the resulting construct by heat-shock. As a comparison (negative control), another aliquot of bacterial suspension was transformed with linearized plasmid only. Transformed bacteria were plated into selection LB-BROTH medium with 10ug/ml kanamycin (proper antibiotic whose resistance is encoded by pEYP-N1 vector) and grown at incubator (37°C, 5% CO_2). Plates seeded with both of the constructs or vector only were compared, counting number of grown colonies in each plate, as an estimate of relative probability to have successful transformation. Mini-preparations of constructs to be screened were made with DNA Mini-Prep kit ILLUSTRA Spin Kit ® (GE-HEALTHCARE) and tested by agarose gel electrophoresis. Only one construct, with the most consistent molecular weight, according to theoretical of insert-containing vector (pEYFP-N1-hTMEM16A), was chosen to produce MIDI-preparations of plasmid DNA, from respective bacterial suspensions, using DNA Midi-Prep kit ILLUSTRA Spin Kit ® (GE-HEALTHCARE). Vectors were resuspended in water and quantified by absorption spectroscopy with a Nanodrop instrument (Thermo-Scientific).

The chosen construct was employed for transfection of CHO K1 cell cultures, to confirm expression of fusion protein, through observation of fluorescence before next studies. Images were acquired with a FluoView 1000 confocal microscope (Olympus, Tokyo, Japan). Transfection details are described in section 3.2.8.

3.2.11 BIDIMENSIONAL SDS PAGE AND WESTERN BLOT

Proteomics is an approach recently established for large-scale study of protein structures and functions "Proteome" is fusion between "protein" and "genome" (Wilkins et al., 1996). Proteome is the whole set of protein products from an organism or system, variable depending on time, stimuli or stresses undergone by a cell or organism.

Among several techniques suitable for proteomic approach, we used 2-Dimensional SDS PAGE, capable of determining expression and post-translational modification of a complex mixture of proteins, by acrylamide gel electrophoresis in "two-dimensions". Proteins are focused first in one direction, and then in another, to separate their modified and unmodified form.

Fusion protein hTMEM16A-EYFP was tested with 2-dimensional SDS Page, to determine the actual protein electrophoretic migration pattern, according its molecular weight and isoelectric point.

Before performing this experimental set, we calculated hTMEM16A protein (NCBI Reference Sequence: NP_060513.5) theoretical molecular weight and isoelectric point with prediction software provided by Massachusetts Institute of Technology (http://scansite.mit.edu/). Particularly, we calculated values for hTMEM16A-EYFP fusion protein and hTMEM16A original protein to choose the suitable pH range for the first dimension and acrylamide concentration for the second gel electrophoresis. hTMEM16A predicted molecular weight was 114.1 kDa, isoelectric point 8.76 in the absence of phosphate groups (Tab. 3.1). hTMEM16A-EYFP predicted molecular weight was 125.4 kDa, isoelectric point 8.59, in absence of phosphate groups (Tab. 3.2).

# Phosphates	Molecular Weight	Isoelectric Point
0	114116,3352	8.76
1	114194,2992	8.67
2	114272,2632	8.57
3	114350,2272	8.45
4	114428,1912	8.31
5	114506,1552	8.14
6	114584,1192	7.92
7	114662,0832	7.69
8	114740,0472	7.48

Tab. 3.1. Molecular weight (Da) and isoelectric point (pH values) prediction for hTMEM16A protein (NCBI Reference Sequence: NP_060513.5) +/- phosphate groups . Calculation performed with software on http://scansite.mit.edu/ webpage (Massachusetts Institute of Technology).

# Phosphates	Molecular Weight	Isoelectric Point
0	125,4359581	8.59
1	125,5139221	8.48
2	125,5918861	8.36
3	125,6698501	8.20
4	125,7478141	8.00
5	125,8257781	7.76
6	125,9037421	7.53
7	125,9817061	7.34
8	126,0596701	7.18

Tab. 3.2. Molecular weight (Da) and isoelectric point (pH values) prediction for hTMEM16A-EYFP fusion protein +/- phosphate groups. Calculation performed with software on http://scansite.mit.edu/ webpage (Massachusetts Institute of Technology).

EYP protein coding sequence in pEYFP-N1 vector (submission in progress on GenBank for corresponding cDNA):

K L E Y N Y N S H N V Y I M A D K Q K N G I K V N F K I R H N I E D G S V Q L
A D H Y Q Q N T P I G D G P V L L P D N H Y L S Y Q S A L S K D P N E K R D H
M V L L E F V T A A G I T L G M D E L Y K

CHO K1 cells were plated on 100mm Petri dishes (4,5 10^5 cells/dish) and grown for 2-3 days before transfection up to 95% confluence. hTMEM16A-EYFP cDNA was delivered to cells with lipofection (Lipofectamin2000 ®, INVITROGEN), at the ratio of 1:3 DNA-lipofectamine, or with PEI, (Polyethylene-imine, SIGMA®) at the ratio of 0,8/1,2ug: 3ul DNA:PEI (1 mg/ml).

One protein sample was tested on each 2-D gel. Membrane fractions from cell *pellets* were collected with a specific kit (Ready Prep Protein Extraction ®, BIORAD); complete cell lysis required sonication. Samples were then purified with Clean-up Ready Prep kit ® (BIORAD). Samples were resuspended in a specific buffer (Destreak ®, GE-HEALTHCARE) containing urea, carrier ampholytes and a reducing agent to solubilise proteins. Samples were quantified using 2-D Quanti-IT kit ® (GE-HEALTHCARE) kit, to control sufficient amounts of protein and not to overload gel.

Each sample (125 ul) was placed in contact with its own gel of the first dimension to be rehydrated. Gel consisted of a non linear gradient strip (ReadyStrip IPG Strip BIORAD), 7cm long, pH range 3-10.

Samples diffused passively during 1h incubation in an electrophoresis cell, then gels were placed in a tray (PROTEAN® IEF System, BIORAD, fig. 3.9), covered by mineral oil (BIORAD) to avoid overwarming. Focusing was performed by applying a constant voltage, initially to allow active diffusion, then protein focusing, according to manufacturer's instructions.
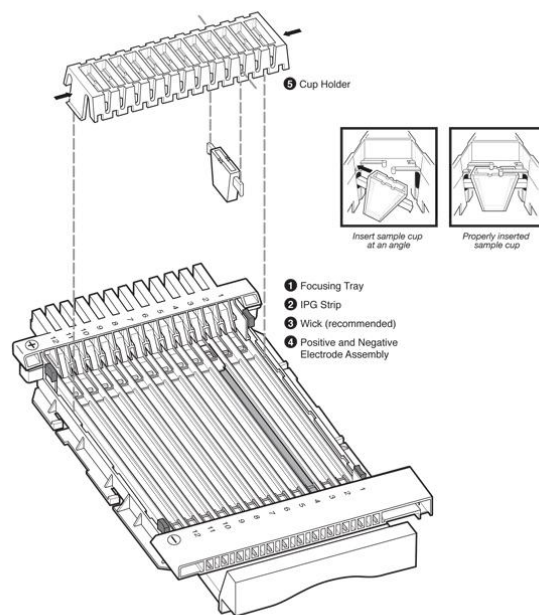
Fig. 3.9. Set-up of electrofocusing tray (PROTEAN® IEF System, BIORAD).

After overnight isoelectrofocusing, the accumulated electric charge was greater than 20,000 V. Strips were incubated in equilibration buffer I for 15', to reduce sulphydryl groups, then in buffer II for 15', to alkylate reduced sulphydryl groups, as described in Ready Strip IPG Instruction Manual (BIORAD), and finally in running buffer for gel electrophoresis.

Each strip was placed on its own acrylamide gel to perform migration according molecular weight (dodecyl sulphate-polyacrylamide gel electrophoresis, SDS-PAGE).

Resolving Gel: 8.5% Acrylamide, 1.5 M TRIS pH 8.8 at 25% v / v, SDS 0.1% w / v, APS 0.05% w / v, TEMED $5 * 10{-4}$% v / v. Gel Run: 160V constant voltage.

Gel transfer to polyvinylidene fluoride (PVDF) membrane was carried out at a constant current of 300 mA. System Mini-Protean ® III (BIORAD) was used for Western blot assay.

Non specific bindings to membranes were prevented with milk 5% solution in TBS (Tris-buffered saline) + Tween20 0,1% (Sigma). Membranes were then incubated with primary antibody anti-GFP 1:000 overnight (J-8 monoclonal, Living Colors® BD Biosciences), a mouse monoclonal (subclass IgG2a) that recognizes all GFP variants, including enhanced and destabilized proteins, fusions to these proteins, and

purified recombinant GFP. After appropriate washes to remove excess antibody, membranes were incubated with anti-mouse secondary antibody conjugated to Horse-Radish-Peroxidase (HRP). At the end of washings, revelation was made with luminol-peroxide system (Immun-Star™ HRP Chemiluminescent Kit BIORAD), protein signal was detected with VersaDoc 4000 MP ® (BIO-RAD) imaging systems.

Detection of whole protein signals was performed also with Sypro-Ruby ® staining (BIO-RAD), a fluorescent probe that binds non-covalently to proteins with a detection limit of the order of 0.25- 1 ng. After 2-D electrophoresis, gels were fixed and incubated with probe and protein signals were checked under UV light. In this case, samples were membrane fractions from CHO K1 cells *wild type* (negative control) or CHO K1 cells transiently expressing hTMEM16A original protein (positive control).

3.3 *IN VIVO* FUNCTIONAL EXPERIMENTS

3.3.1 INSTRUMENTATION

In vivo functional experiments were performed with a perfusion system developed and used in our laboratory for several years (fig. 3.10). Round 25 mm diameter coversplips were used as cell growth substrate. When cells cultured reached confluence, coverslips were removed from 6well-plates and mounted on a perfusion chamber (oval-shaped, to allow a quick laminar flow). Chamber with coverslip was put on a thermo-regulated support (Warner Instrument Corporation™), to maintain temperature in chamber at 36°C-37°C steadily. Cells were observed with an inverted optical microscope Zeiss™ Axiovert 200, equipped with xenon short arc lamp (75W XBO), through an oil immersion 40X objective.
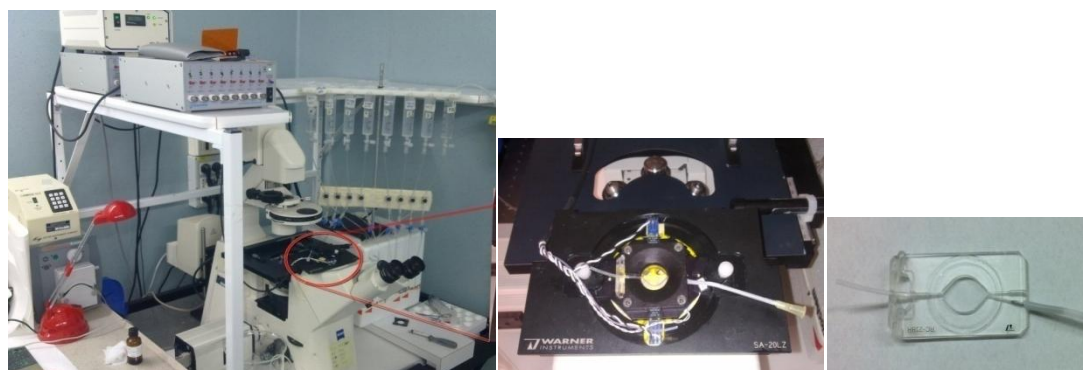
Fig. 3.10. From left to right: inverted optical microscope Zeiss™ Axiovert 200 with perfusion system and CCD camera and shutter 10-C, thermo-regulated support and chamber for coverslips.

Experiments began with continuous perfusion of cells with PBS (10-12 ml/min), to stabilize temperature at 37°C, for at least 5'. Once the region of interest (ROI) had been selected, with software MetaFluor™ (Universal Imaging™, USA/Crisel Instrument™, Italy), image acquisition began. ROI contained at least 20-50 cells. Its average fluorescence was recorded, together with fluorescence of a background region (without cells), which was subtracted to ROI. Every experiment had its own ROI. If necessary, excitation light exposure duration and *binning* (number of image pixels, a resolution parameter) were modified to avoid an excessive effect of *photobleaching* and to obtain optimized fluorescence values. *Photobleaching* is YFP fluorescence decay due to excitation light exposure.

Observation of cells was made real-time. Every image was acquired with a CCD chamber (Coolsnap HQ CCD, Roper Scientific™) and the relative signals were recorded every 2"/5" with MetaFluor™ software.

YFP fluorescence was observed at these wavelength (λ): excitation 500 ± 12.5 nm and emission 545 ± 17.5 nm; specific filters set used was XF104-2, OMEGA® optical.

3.3.2 FUNCTIONAL DATA ANALYSIS

Raw data (absolute fluorescence) derived from experiments were saved with spreadsheet (Microsoft Office Excel). Afterwards data were analyzed with GraphPad Prism™ Software (GraphPad Software, Inc.). Data relative to resting fluorescence (F_0) were analyzed to reduce *photobleaching* effects, which lead to fluorescence decay during experiments. Analysis method provided interpolation of values according to non linear regression with a one-phase exponential decay curve: result was a F_0 theoretical curve for every instant. When cells were exposed to different compounds screened, the obtained fluorescence intensity (F) signals were normalized according to F_0 to obtain a relative fluorescence (RF) for every instant (F/F0). Average fluorescence variation and the associated SEM (Standard Error of the Mean)/*n* experiments were calculated for every experimental set.

To determine the affinity of different purinergic receptor agonists or antagonists concentrations during influx and efflux phase in stimulating iodide fluxes in FRTL-5 cells, data obtained from experiments were analyzed using GraphPad software © and dose-response curve was obtained:

(i). "fitting" of the data recorded was carried in the last phase of I⁻ influx and those obtained during I⁻ efflux, in particular since 30 cycles prior to the phase of efflux. "Fitting" of experimental data was done for each set of concentrations (0.1-100 uM) and was set or on a curve of association to an exponential phase (one-phase exponential association), or on a curve of association exponential two phases (two-phase exponential association). According to obtained data, for each individual experiment, software choose the ideal curve approximation (Fig. 3.11).
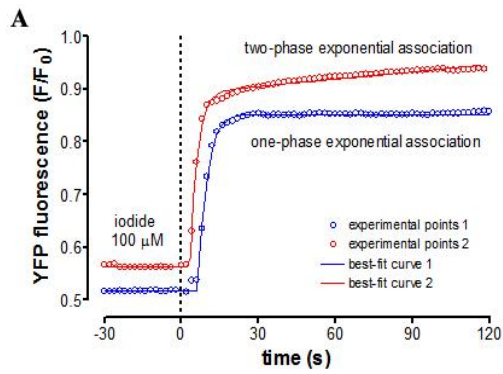
Fig. 3.11. Representative graph of fitting between two single experiments. White dots: single experimental data from single acquisitions and the related best fitting curves.

(ii). Derivative was calculated ($\Delta y / \Delta x$) for individual values on obtained curve. Data obtained from this function represent speed at which fluorescence is increased ($\Delta f / \Delta t$), the flow rate of Γ at any single point, plotted as a function of time (t). Software selected the highest (max $\Delta f / \Delta t$) for each set and for each concentration (Fig. 3.12).
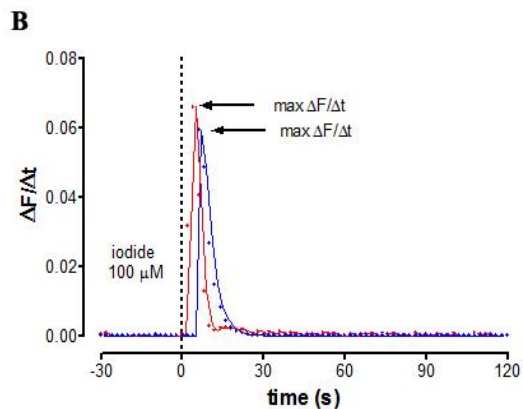
Fig. 3.12. Representative graph. Fluorescence recovery maximum rate ($\Delta f / \Delta t$) (single data as a function of time) related to time t (s^{-1}). Data of two single experiments shown.

(iii) Subsequently, it was set to a graph in which arises in connection with the recovery rate of fluorescence versus time ($\Delta f / \Delta t$) compared to the 3 agonists concentration (shown in logarithmic scale) (fig. 3.13).
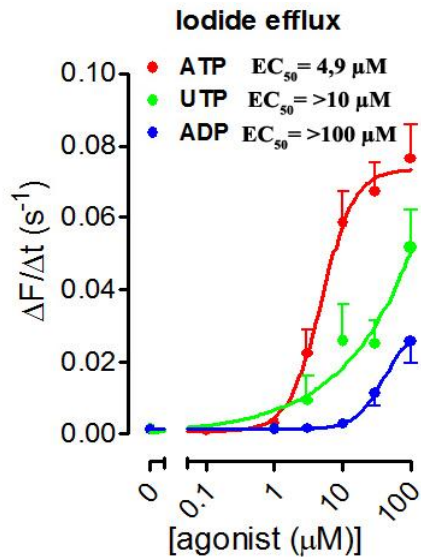
Fig. 3.13. Representative graph (dose-response curve) to calculate agonist affinity with iodide efflux stimulation. Fluorescence recovery maximum rate ($\Delta f / \Delta t$) related to agonist concentration (uM), t (s^{-1}). Logarithmic scale.

Statistical analysis of data relating to maximum fluorescence recovery induced by different agonists/antagonists screened was performed with: T-test means of two groups, ANOVA more than two groups.. ANOVA one-way analysis and subsequently with Dunnett's multiple comparison test which compares each treatment compared to control.

3.3.3 SOLUTIONS

Cells were constantly perfused with a PBS (Phosphate-Buffered Saline) solution at 7.4 pH. Components:

- ❖ NaCl 137 mM;

- ❖ KCl 2,7 mM;

❖ CaCl$_2$ 0,7 mM;

❖ MgCl$_2$ 1,1 mM;

❖ Na$_2$HPO$_4$ 8,1 mM;

❖ KH$_2$PO$_4$ 1,5 mM;

❖ Glucose 10 mM.

Iodide flux experiments required addition of different compounds to PBS, putative agonists, antagonists or inhibitors of iodide efflux. Concentration range of agonists screened was 0.01-100uM.

The effect of depolarization on iodide flux was analyzed perfusing FRTL-5 cells with K$^+$-PBS solution: (tell substitution K instead of Na) influx clor and iodide substituted

❖ NaCl 39,7 mM;

❖ KCl 100 mM;

❖ CaCl$_2$ 0,7 mM;

❖ MgCl$_2$ 1,1 mM;

❖ Na$_2$HPO$_4$ 8,1 mM;

❖ KH$_2$PO$_4$ 1,5 mM;

❖ Glucose 10mM.

Intracellular Ca^{2+} and BAPTA effect on iodide flux, stimulated by ATP and ionomycin, were performed using the following Ca^{2+}-free PBS solution:

❖ NaCl 137 mM;

❖ KCl 2,7 mM;

❖ MgCl$_2$ 1,1 mM;

❖ Na$_2$HPO$_4$ 8,1 mM;

❖ KH$_2$PO$_4$ 1,5 mM;

❖ Glucose 10 mM.

Protocol used for iodide efflux experiments:

❖ cells were perfused with PBS (pH 7.4) for 2' (60 cycles), time usually required to observe a fluorescence stable baseline;

❖ after, cells were perfused with PBS+ NaI 100 µM to let iodide flow into them for 2';

❖ for 8' image acquisition paused, keeping cells in PBS+ NaI 100 µM, to limit *photobleaching* effects;

❖ cells were perfused with PBS/K-PBS+ stimulators or o PBS+ inhibitors (iodide efflux according to concentration gradient) for 2'.

In this kind of studies, images were acquired every 2" maintaining exposition time usually at 50 msec.

Before performing experiments, cells were incubated with BAPTA for some specific experiments, at 25 uM concentration, for 45'. BAPTA is a chelating agent for intracellular Ca^{2+}. BAPTA-AM is acetoxymethyl ester form for BAPTA, is cell membrane permeable. Once inside cells, it is hydrolyzed by cell esterases. Result is active form (BAPTA), which chelates intracellular Ca^{2+} (fig. 3.14).
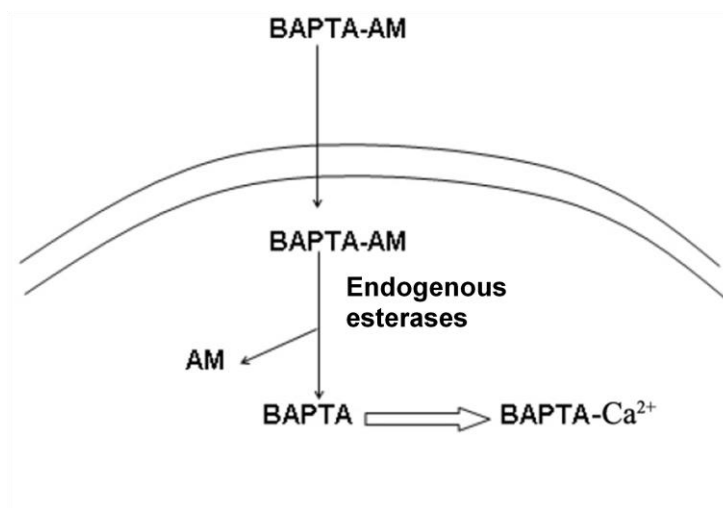
Fig. 3.14. BAPTA-AM action mechanism. Acetoxymethyl ester form for BAPTA (BAPTA-AM) is cell membrane permeable. Once inside cells, it is hydrolyzed by cell endogenous esterases into active form (BAPTA), which chelates intracellular Ca^{2+}.

3.3.4 INTRACELLULAR pH EXAMINATION WITH BCEF PROBE

FRTL-5 *wild type* were used to measure intracellular pH in functional *in vivo* experiments. Fluorescent BCECF (2,7,bis-carboxyethyl-5(6) carboxy-fluorescein) probe was employed. Also in this case the compound exists as membrane permeable acetoxymethyl ester (BCECF-AM), which enters whole cells and is converted into the acid form (BCECF) by cell esterases. This acid form is retained inside cells and shows a pH-dependent fluorescence response, because of its lateral chain bound to fluorescein, whose fluorescence intensity is progressively quenched by increasing acidity. Probe pKa is 6.98, suitable for cell analysis since their resting intracellular pH (pH_i) is close (7.4).

BCECF is characterized by these wavelengths (λ): pH-independent excitation 440 nm and pH-dependent 490 nm (fig. 3.15).
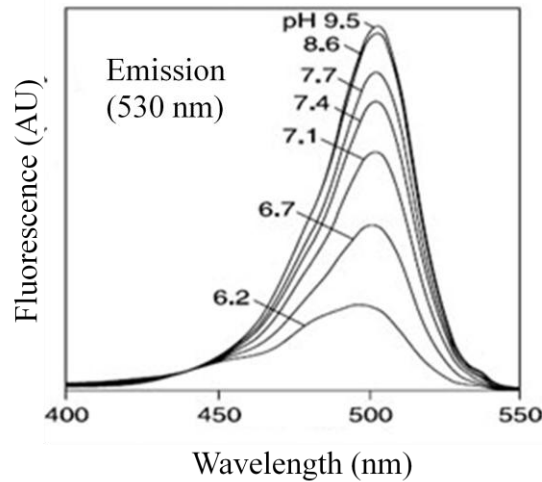
Fig. 3.15. BCECF excitation spectrum at different wavelengths (λ). λ= 490 nm pH-dependent, λ= 440 nm pH-independent.

Alterations in pH cause a shift in excitation wavelength, a fact that allows the use of the ratio between fluorescence signals (490/440) in order to normalize differences in probe loading among cells and *photobleaching* effects.

FRTL-5 were cultured on coverslips in 6well-plates as previously described. 5uM BCECF-AM, dissolved in 6H5 medium, was added to each coverslip fir 30'. Cells were washed with 6H5 medium twice and incubated in incubator 15' again, to allow BCECF-AM hydrolysis.

BCECF fluorescence was observed with specific filters at these wavelength (λ): pH-independent excitation 440 nm (XF1071) and pH-dependent 490 nm (XF1011) , emission 530 nm (XF3011).

Images were acquired every 5" with 10 ms exposition to avoid probe quick *photobleaching* effects.

For this kind of experiments, HBS (HEPES buffered saline) was used, which consists of:

❖ Hepes 10 mM

❖ NaCl 140mM

❖ KCl 5mM

❖ MgCl$_2$ 1,1mM

❖ CaCl$_2$ 0,7mM

Finally pH was adjusted to 7.4 with 1M NaOH.

Calibration curve for pH was performed with 4 solutions characterized by different pH (6.5, 7, 7.5 e 8) and high K$^+$ concentration (high K$^+$-HBS), with the following components:

❖ HEPES 10mM

❖ NaCl 5mM

❖ KCl 140mM

❖ MgCl$_2$ 1,1mM

❖ CaCl$_2$ 0,7mM

❖ nigericin 7µM

Nigericin is a ionophore which allows a rapid equilibration of intra- and extracellular H$^+$ and K$^+$ ions.

Protocol used for experiments with BCECF probe:

❖ cells were perfused with PBS (pH 7.4) for 2' (12-24 cycles);

❖ after, cells were perfused with HBS pH 7.4 for 2';

❖ cells were perfused with HBS pH 7.4+ 100 uM inhibitor for 2';

❖ cells were perfused with HBS pH 7.4 for 2'again;

❖ after, for creation of calibration curve, cells were perfused with:

    ❖ high K$^+$-HBS pH 8

    ❖ high K$^+$-HBS pH 7.5

    ❖ high K$^+$-HBS pH 7

    ❖ high K$^+$-HBS pH 6.5

Images were acquired every 5" with 10 ms exposition to avoid probe quick *photobleaching* effects.

3.3.5 INTRACELLULAR Ca $^{2+}$ MEASUREMENT WITH FURA-2

In vivo Ca^{2+}_i measurement was performed using Fura-2 probe, in *wild type* FRTL-5. Fura-2 undergoes an absorption spectrum shift depending on free Ca^{2+}_i concentration. Without Ca^{2+}_i , Fura-2 has a peak at 380 nm in excitation spectrum, with a wide range. In a solution with Ca^{2+}_i , Fura-2 binds to it and its excitation peak shifts to 340 nm. Bound to Ca^{2+}_i, Fura-2 emits an increased fluorescence (measured at 510 nm), without Ca^{2+}_i it is quenched (fig. 3.16).
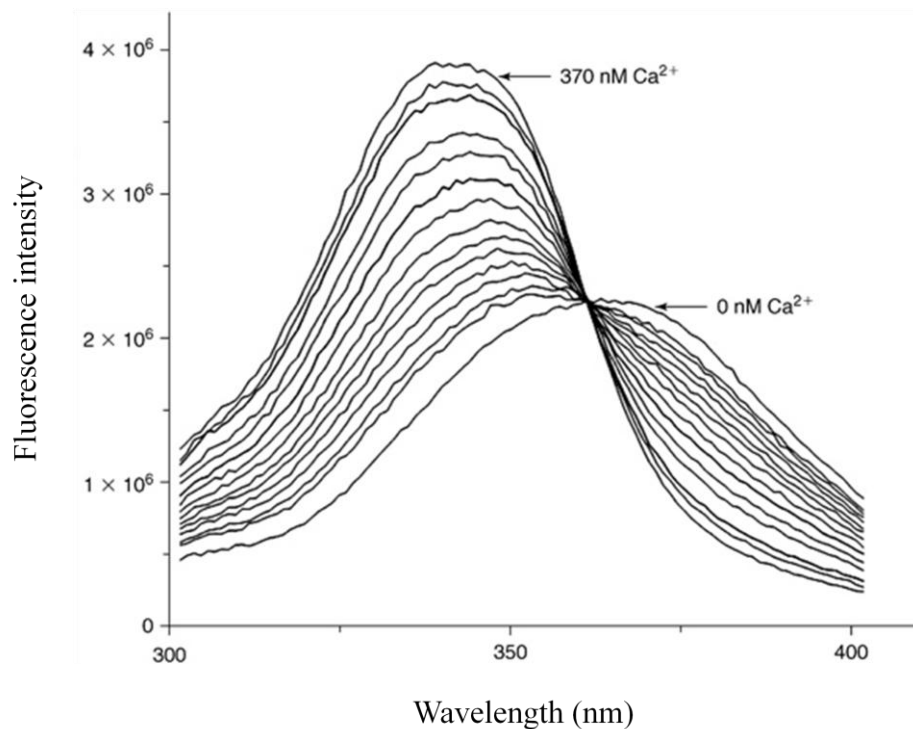

Fig. 3.16 Fura-2 absorbance spectrum at different wavelengths (λ) = 340, Ca $^{2+}$-dependent, λ= 380 Ca $^{2+}$-dependent.

The protocol used was the same as BCECF. Cell-permeable AM-variant Fura-2 (1 mM in DMSO), dissolved in 6H5, was added to each coverslip with cells (5 uM/ml

6H5) for 30', then washes of cells with PBS twice and 15' incubation again, to allow Fura-2 AM hydrolyzing by cell esterases.

Fura-2 wavelength are: excitation 340 nm (detection filter XF1093) and 380 nm (detection filter XF1094), emission λ at 510 nm (detection filter XF3043).

Images were acquired every 2'' with an exposure of 10 ms.

Solution used for this kind of experiment were PBS-based+ additives (compounds to test).

Protocol used for experiments with Fura-2 probe:

- ❖ cells were perfused with PBS (pH 7.4) for 2' (60 cycles);

- ❖ after, cells were perfused with PBS+ ATP 100uM+/-100 µM TA/FLUO/NFA or 25 uM BAPTA;

- ❖ cells were perfused with PBS again

Images were acquired every 5'' with exposition of 10 msec.

BCECF and Fura-2 are ratiometric probes: their shift based on pH/ Ca^{2+} fluctuations, allow correction of signal variations due to several parameters during experiments (i.e. probe accumulation, *photobleaching*, focalization plane shift, different optical pathway). Fluorescence signals were processed with excitation wavelength ratio (340/380 or 490/440) to evaluate the real intracellular $[Ca^2]$/ pH.

3.3.6 YFP-H148Q/I152L PROTEIN PRODUCTION

YFP-H148Q/I152L purified protein was used to detect direct interaction with screened compounds. To produce it, open reading frame (ORF) was cloned into a pGEX-4T-1 bacterial expression vector (GE Healthcare ©) (fig. 3.17), flanked by Glutathione S-transferase gene (GST). Fig. 3.18 shows YFP-H148Q/I152L sequence.
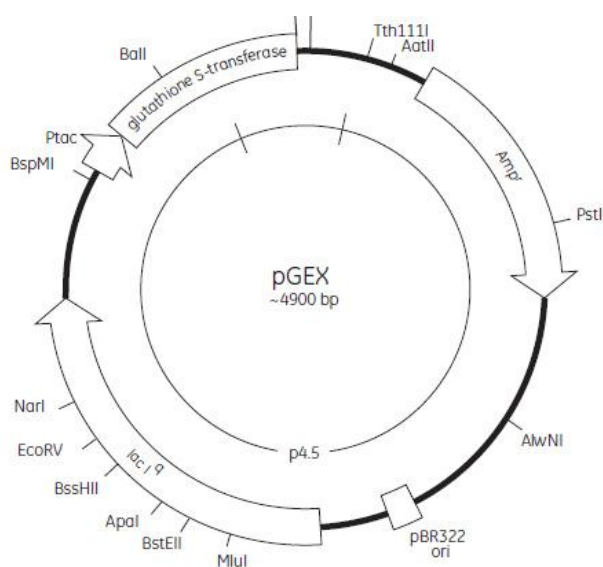
Fig. 3.17. pGEX-4T-1 bacterial expression empty vector (GE Healthcare ©).

YFP-H148Q/I152L

```
        10        20        30        40        50        60
         *                   *                   *                   *
ATGGTGAGCA AGGGCGAGGA GCTGTTCACC GGGGTGGTGC CCATCCTGGT CGAGCTGGAC
 M  V  S  K  G  E  E  L  F  T  G  V  V  P  I  L  V  E  L  D>

        70        80        90       100       110       120
         *                   *                   *                   *
GGCGACGTAA ACGGCCACAA GTTCAGCGTG TCCGGCGAGG GCGAGGGCGA TGCCACCTAC
 G  D  V  N  G  H  K  F  S  V  S  G  E  G  E  G  D  A  T  Y>

       130       140       150       160       170       180
         *                   *                   *                   *
GGCAAGCTGA CCCTGAAGTT CATCTGCACC ACCGGCAAGC TGCCCGTGCC CTGGCCCACC
 G  K  L  T  L  K  F  I  C  T  T  G  K  L  P  V  P  W  P  T>

       190       200       210       220       230       240
         *                   *                   *                   *
CTCGTGACCA CCTTCGGCTA CGGCCTGCAG TGCTTCGCCC GCTACCCCGA CCACATGAAG
 L  V  T  T  F  G  Y  G  L  Q  C  F  A  R  Y  P  D  H  M  K>

       250       260       270       280       290       300
         *                   *                   *                   *
CAGCACGACT TCTTCAAGTC CGCCATGCCC GAAGGCTACG TCCAGGAGCG CACCATCTTC
 Q  H  D  F  F  K  S  A  M  P  E  G  Y  V  Q  E  R  T  I  F>

       310       320       330       340       350       360
         *                   *                   *                   *
TTCAAGGACG ACGGCAACTA CAAGACCCGC GCCGAGGTGA AGTTCGAGGG CGACACCCTG
 F  K  D  D  G  N  Y  K  T  R  A  E  V  K  F  E  G  D  T  L>

       370       380       390       400       410       420
         *                   *                   *                   *
GTGAACCGCA TCGAGCTGAA GGGCATCGAC TTCAAGGAGG ACGGCAACAT CCTGGGGCAC
 V  N  R  I  E  L  K  G  I  D  F  K  E  D  G  N  I  L  G  H>

       430       440       450       460       470       480
         *                   *                   *                   *
AAGCTGGAGT ACAACTACAA CAGCCAGAAC GTCTATCTGA TGGCCGACAA GCAGAAGAAC
 K  L  E  Y  N  Y  N  S  Q  N  V  Y  L  M  A  D  K  Q  K  N>

       490       500       510       520       530       540
         *                   *                   *                   *
GGCATCAAGG TGAACTTCAA GATCCGCCAC AACATCGAGG ACGGCAGCGT GCAGCTCGCC
 G  I  K  V  N  F  K  I  R  H  N  I  E  D  G  S  V  Q  L  A>

       550       560       570       580       590       600
         *                   *                   *                   *
GACCACTACC AGCAGAACAC CCCCATCGGC GACGGCCCCG TGCTGCTGCC CGACAACCAC
 D  H  Y  Q  Q  N  T  P  I  G  D  G  P  V  L  L  P  D  N  H>

       610       620       630       640       650       660
         *                   *                   *                   *
TACCTGAGCT ACCAGTCCGC CCTGAGCAAA GACCCCAACG AGAAGCGCGA TCACATGGTC
 Y  L  S  Y  Q  S  A  L  S  K  D  P  N  E  K  R  D  H  M  V>

       670       680       690       700       710       720
         *                   *                   *                   *
CTGCTGGAGT TCGTGACCGC CGCCGGGATC ACTCTCGGCA TGGACGAGCT GTACAAGTAA
 L  L  E  F  V  T  A  A  G  I  T  L  G  M  D  E  L  Y  K  *>
```

Fig. 3.18 Coding sequence of YFP-H148Q/I152L (red: mutated aminoacids compared to original YFP protein)

Escherichia Coli (BL21 strain) bacteria were transformed with pGEX-4T-1-YFP-H148Q/I152L vector with heat-shock. Protein production was induced with isopropyl-β-D-tiogalatto-piranoside (IPTG, galattose-analogous inductor of genes under Lac operon control in *E. Coli*.). Bacterial lysis was performed with a lysis solution PBS 50mM (pH 7.4) containing:

- ❖ 1% NP-40, 5mM EDTA;

- ❖ 0.4 mg/ml lysozyme and protein inhinbitors cocktail (Roche®).

GST-YFP-H148Q/I152L fusion protein was purified with affinity chromatography using glutathione-agarose beads and eluted from column with a Cl⁻free buffer, which consisted of:

- ❖ sodium phosphate buffer 50 mM (pH 8.8);

- ❖ 25mM reduced glutathione

- ❖ 200mM sodium gluconate.

3.3.7 *YFP AND CACC INHIBITORS DIRECT INTERACTION*

YFP purified protein extracts were employed to determine direct interaction among YFP and CaCC screened inhibitors (tannic acid, niflumic acid, fluoxetin). Solutions:

- ❖ Sodium phosphate buffer pH 7.0 (SPB)

- ❖ NaI 2 mM in SPB

- ❖ NFA 300 μM in SPB

- ❖ NFA 100 μM in SPB

- ❖ NFA 300 μM + NaI 2mM in SPB

- ❖ NFA 100 μM + NaI 2mM in SPB

- ❖ TA 100 μM in SPB

- ❖ TA 100 μM + NaI 2mM in SPB

- ❖ FLUO 100 μM in SPB

- ❖ FLUO 100 μM + NaI 2mM in SPB

Solutions prepared were diluted with YFP in SPB (1:1), put on coverslip and observed with a 20X objective. Three images were acquired every 3" and exposition time was 500 msec.

CHAPTER 4

RESULTS

4.1 MOLECULAR CHARACTERIZATION OF TMEM16A IN THYROID GLAND

4.1.1 TMEM16A mRNA EXPRESSION IN HUMAN NORMAL THYROID GLAND

The molecular characterization of TMEM16A in human thyroid gland began with assessment its transcriptional expression by RT-PCR. TMEM16A mRNA was detected in normal human thyroid tissue together with NIS, a specific marker for this tissue. Fig. 4.1 illustrates the results of a representative RT-PCR experiment on three independent human normal thyroid samples from different patients, showing specific bands for TMEM16A with the expected amplicon size (110 bp).
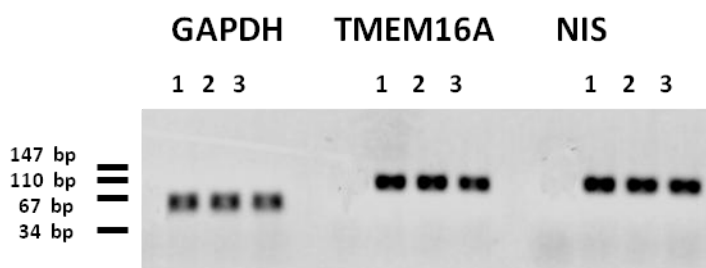
Fig 4.1 Transcript expression in human thyroid gland (n=3). Left: signal of hGAPDH *housekeeping* **gene mRNA (amplicon=69 bp), used as reaction positive control. Middle: hTMEM16A mRNA signal (amplicon=110 bp). Right: NIS mRNA gene signal used as thyroidal positive marker (amplicon=105 bp). RT- samples showed no signal (not shown).**

4.1.2 TMEM16A mRNA EXPRESSION IN HUMAN THYROID GLAND: COMPARISON BETWEEN NORMAL AND TUMOUR

Since TMEM16A transcript was detected in human normal thyroid gland, the next step was to control its expression in tumor thyroid tissue. Fig. 4.2 shows TMEM16A expression in 3 independent normal and tumor thyroid samples. Every normal/tumour couple was from the same patient carrying thyroid papillary tumour (biopsy from healthy or tumor portion of the same sample). These result demonstrate that TMEM16A expression is maintained also in thyroid tumor tissue. (in contrast to NIS, decreased 2/3 samples).
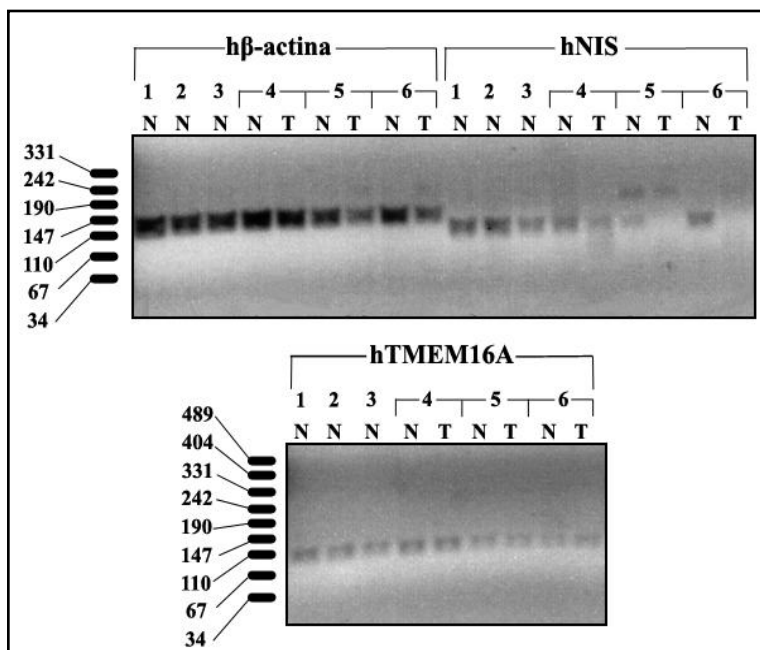
Fig. 4.2. Transcript expression in human thyroid gland (n=3 for coupled samples, + 3 normal samples). Upper image, left part: signal of hβ-actin *housekeeping* gene mRNA, used as technique positive control in 3 normal plus other 3 ,3 normal thyroid samples from different patients. Upper image, right part: NIS mRNA gene signal used as thyroid positive marker. Bottom image: hTMEM16A mRNA signal in the same samples. RT- samples showed no signal (not shown). N: normal tissue; T: tumour tissue.

4.1.3 TMEM16A mRNA EXPRESSION IN FRTL-5 CELLS

Since positive results were obtained in thyroid tissue, research continued to verify if TMEM16A transcript were also expressed in FRTL-5 cells (from rat normal thyroid gland), used as an experimental model. TMEM16A mRNA was detected by RT-PCR with specific primers for rTMEM16A (fig. 4.3), indicating that this cell line could be employed as a model to study the channel functionally.
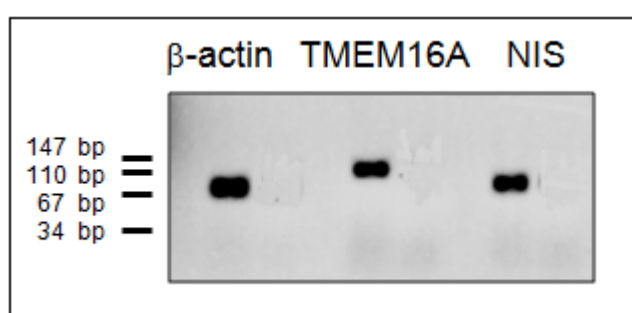

Fig. 4.3. Transcript expression in FRTL-5 cells (representative experiment). From left to right: signal of hβ-actin *housekeeping* **gene mRNA, used as reaction positive control, hTMEM16A mRNA signal, NIS mRNA gene signal used as thyroid positive marker. RT- samples showed no signal (not shown).**

4.1.4 EFFECT OF TSH HORMONE ON TMEM16A mRNA IN FRTL-5 CELLS

TSH is the main physiologic/endogenous regulator of thyroid gland, therefore effect of TSH on TMEM16A mRNA expression was examined in FRTL-5 cells. (TSH is a component of cell culture medium..for differentiation etc) . Cells were grown to 50% confluence, followed by TSH deprivation and readdition.
The effect of TSH on TMEM16A mRNA levels was compared with the effect on NIS mRNA, since NIS is known to be regulated by TSH. Results are shown in fig. 4.4. Real Time PCR (Quantitative PCR) technique was used to detect and quantify rTMEM16A transcript levels. A "time course" analysis was performed: FRTL-5 cells,

deprived of TSH for one week, on 7th day were treated differentially: some samples were maintained in TSH-free medium, other received TSH addition. Samples from both conditions (n=7) were collected after 6h, 12h, 24h to detect TSH-dependent changes in TMEM16A mRNA.

As expected, TSH deprivation led to a significant decrease of NIS transcript expression (100 fold less than control) and readdition of TSH partially restored NIS expression. In contrast, neither TSH deprivation nor readdition had any effect on TMEM16A mRNA expression levels (fig. 4.4). It remained high in both of conditions, suggesting that its expression is constitutive or at least TSH- independent.(**p<0.0001.**)
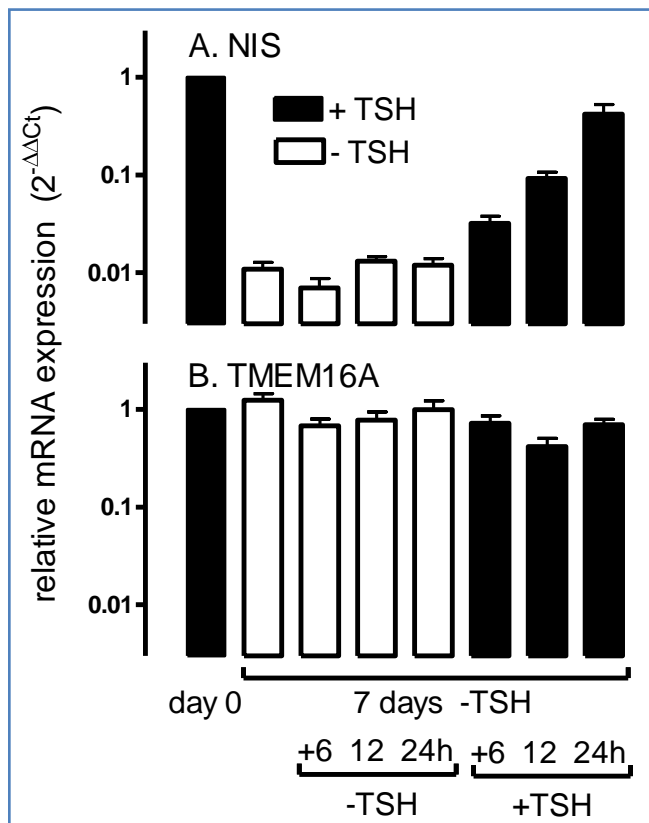
Fig. 4.4.   Real Time PCR experiments with FRTL-5 cells (n=7). From left to right: NIS/ hTMEM16A mRNA signal on day 0, after 7 days +/- TSH exposure : 0h, 6h,12h, 24h.

hβ-actin *housekeeping* gene used as reaction positive control. RT- samples showed no signal (not shown). NIS transcript decrease without TSH exposure in a statically significant manner p<0.0001.

4.1.5 EXPRESSION OF TMEM16A mRNA SPLICING ISOFORMS IN FRTL-5 CELLS

Having confirmed TMEM16A mRNA expression in human thyroid gland samples and in FRTL-5 cells, the expression of TMEM16A alternative isoforms in FRTL-5 cells was determined using primers specific for each isoform. Primers for segments *b*, *c* and *d* segments were designed for flanking regions, leading to two possible amplicon sizes representing the absence or presence or the corresponding segment: the lower band (175 bp for b, 118 for c, 230 for d) corresponds to the absence of segment in transcript, the upper to the presence of respective segment in transcript (amplicons: 241 for b, 130 for c, 305 for d). Primers for segment *a* were designed inside (amplicon: 267 bp). Fig. 4.6 shows results obtained. Amplicon specific for a segment was detected, thus it is contained in TMEM16 transcript expressed in 4 independent samples of FRTL-5 cells. Both of amplicons specific for b segment were detected, only the upper amplicon specific for c segment was detected, thus TMEM constitutively includes , only the lower amplicon specific for d segment was detected. Therefore, we concluded that TMEM16A/anoctamin-1alternative *splicing* isoforms expressed in FRTL-5 cells could include b segment, c segment was constitutively expressed but d segment was not included.

TMEM16A mRNA alternative maturation isoforms are suggested to be TMEM16A "abc" and "ac" in FRTL-5 cells.
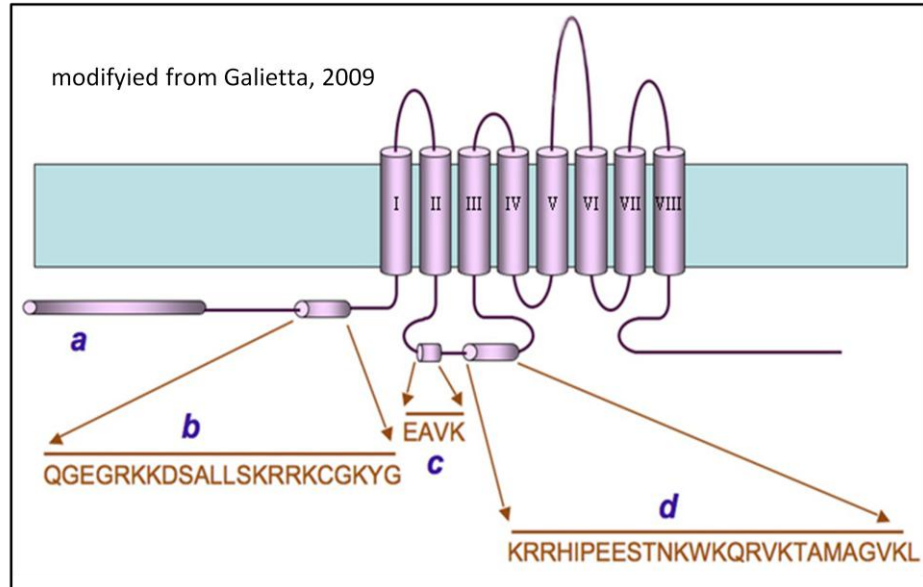
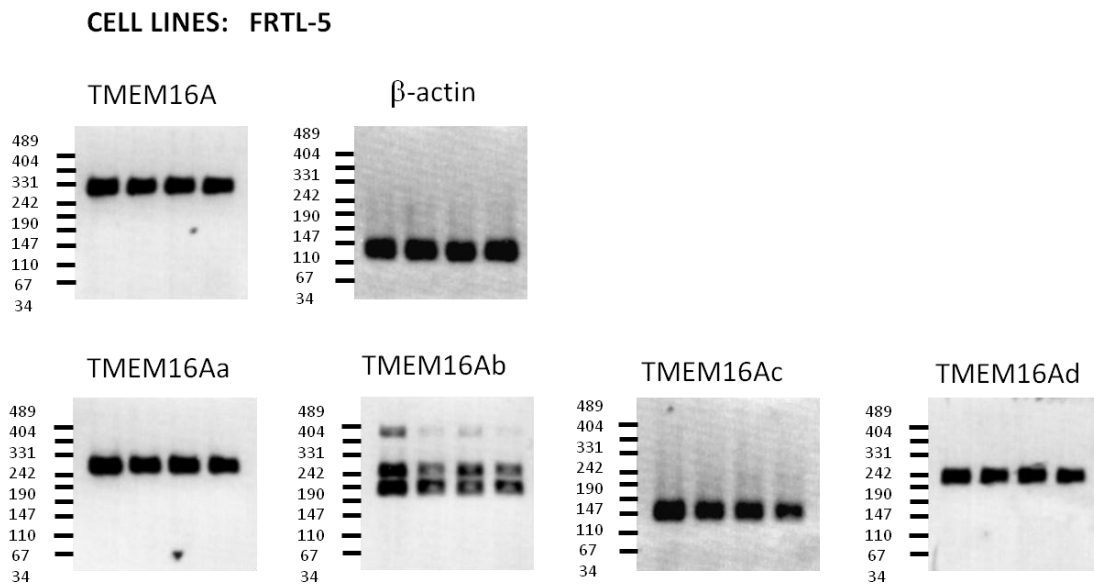**Fig. 4.5 Protein segments alternatively spliced in hTMEM16A.**

Fig.4.6. Upper line: TMEM16A transcript signal (305 bp) and b actin signal (hosekeeping gene). Lower line, from left to right: rTMEM16A mRNA signal related to a segment (amplicon 267 bp), b segment (amplicon 241/175 bp, b can be included or not in mature mRNA), c segment (amplicon 130/118 bp), d segment (amplicon 230 bp detected only, d segment not expressed), RT-samples showed no signal (not shown), (n=4 independent samples).

4.1.6 EXPRESSION OF ANOCTAMIN mRNA IN FRTL-5 CELLS.

In addition, (since TMEM16A belongs to family etc, containing conserved members,) the expression of these paralogs was also examined in FRTL-5 cells was checked with RT-PCR. Specific primers were used for every anoctamin to test 4 independent FRTL-5 samples.

Clear expression in FRTL-5 cells was observed for: TMEM16A, TMEM16F, TMEM16K, TMEM16H (respective amplicons: 305 bp, 304 bp, 280 bp, 324 bp). No signal was detected for either TMEM16B or TMEM16J (respective amplicons: 297 bp, 327 bp). Variable signals for TMEM16C, TMEM16D, TMEM16E, TMEM16G were detected: TMEM16C and TMEM16G signals (respective amplicons : 290 bp, 302 bp) were detected in ¾ samples, TMEM16D in ¼, TMEM16E (respective amplicons: 319 bp, 293 bp) in 2/4 samples faintly (fig. 4.7).

In conclusion, FRTL-5 showed a clear expression for TMEM16A, TMEM16F, TMEM16K, TMEM16H anoctamin transcripts.
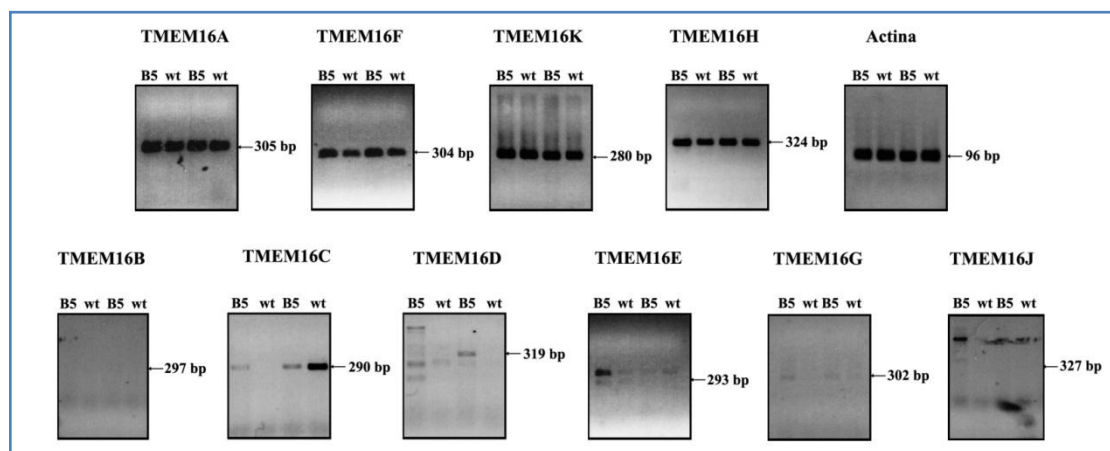

Fig. 4.7. Expression of anoctamins in FRTL-5 cells. Up, from left to right: TMEM16A, TMEM16F, TMEM16K, TMEM16H, β actin as *housekeeping* gene. Down, from left to right: TMEM16B, TMEM16C, TMEM16D, TMEM16E, TMEM16G, TMEM16J. RT- samples showed no signal (not shown), (n=4 independent samples).

4.2 FUNCTIONAL CHARACTERIZATION OF TMEM16A IN THYROID GLAND

Molecular characterization led to the conclusion that TMEM16A transcript is expressed in FRTL-5 cells. To determine whether TMEM16A is active in the thyroid gland as an anion channel, research continued by analyzing iodide transport in FRTL-5 cells. Specifically anion transport in FRTL-5 cells was characterized to determine whether it is compatible with the known characteristics of CaCC/TMEM16A described in literature.

4.2.1 IODIDE TRANSPORT IN THYROID CELLS: INFLUX ACTIVITY

Characterization experiments began with study of iodide influx in FRTL-5 cells, particularly selection clones that expressed YFP protein stably, as a halide biosensor (fig. 4.8, on the left). Galietta et al. (2001), measured I^- influx with YFP-H148Q/I152L-based assay, as a model of Cl^- transport, because YFP-H148Q/I152L has higher affinity for I^- than Cl^-. In this model, YFP-H148Q/I152L-expressing bronchial epithelium cells were perfused with solutions containing 100 mM, physiological concentration of Cl^-. Partial substitution of extracellular Cl^- with the same amount of I^- allowed indirect analysis of Cl^- flux. We used this model to characterize I^- flux due to other halide transporters less specific than NIS in FRTL-5.

4.2.1.1 Characterization of iodide flux in FRTL-5 cells

Continuous perfusion system exposed cells first to a physiological buffer (PBS) to form and stabilize the baseline during initial stages of the observation. Then FRTL-5 YFP-H148Q/I152L were exposed to PBS containing 100uM iodide, to study its influx specifically via NIS transporter, because NIS affinity constant is close to that value (Km ≈ 30uM). Cells showed a rapid decrease of fluorescence, indicator of iodide entry, of almost 50% compared to baseline. (after removal of extracellular iodide led to recovery fluorescencelevel etc) .

Depriving cells of TSH from the culture medium for at least one week, absence of fluorescence decrease was noticed when perfused with PBS+100uM iodide. This indicated absence of iodide transport via NIS due to inhibition of its expression without TSH. In the same conditions, instead, perfusing cells with PBS+100mM, a conspicuous fluorescence decrease was observed anyway, although less than the previous condition (fig. 4.8, on the right). Such a decrease of fluorescence signal is due to iodide entry through other transporters or channels.

Described observations are compatible with NIS sensitivity at iodide concentrations of uM order, instead sensitivity of chloride channels is of mM order.

In order to study TMEM16A function it is necessary to eliminate the contribution of NIS to iodide transport by maintaining FRTL-5 YFP-H148Q/I152L cells in a TSH-free medium (5H5) for at least 1 week. Under these conditions perfusion with a solution a 100mM external iodide concentration permitted the identification of iodide fluxes through pathways other than NIS.

FRTL-5 Fischer rat
thyroid cell line with
stable YFP expression
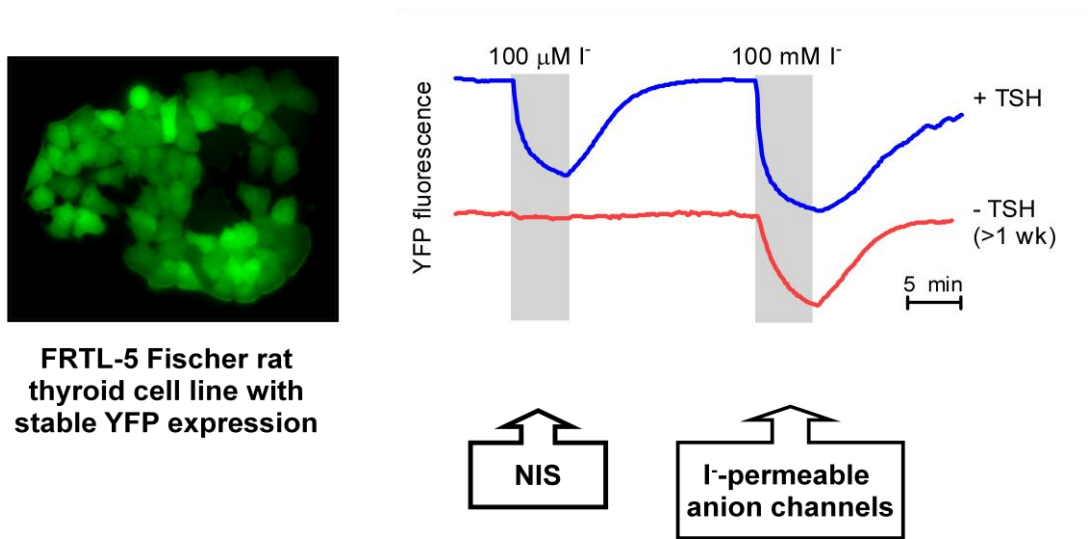
Rhoden et al Am J Physiol 2007

Fig.4.8 Left image: FRTL-5 Fischer rat thyroid cell line stably expressing YFP-H148Q/I152L, observed with inverted optical microscope at 40X objective (excitation 500 ± 12.5 nm and emission 545 ± 17.5 nm). Right image: iodide flow into FRTL-5 YFP-H148Q/I152L, absolute fluorescence is showed, exposed to 100uM/mM iodide, cultured with or without TSH for >1 wk).

4.2.1.2 Effect of nucleotides on iodide influx

 Since TMEM16A is known to be stimulated by purinergic agonists, their effect on NIS-independent iodide influx in TSH deprived FRTL-5-YFP cells was examined. Cells were exposed to ATP UDP ADP added to the perfusion solution containing 100mM K+I-. KI was used since TMEM16A is known to be activated by depolarization (Galietta et al., 2001). Particularly, exposure to nucleotides at different concentrations (0.1-100 uM) increasing the rate of decrease in fluorescence signal, All the three agonists let to a more rapid fluorescence decrease in response to iodide, suggesting that these agonists stimulated iodide influx. (fig.) This effect was concentration dependent for all three agonists, with the maximum effect occurring   at 100uM. The affinity of each nucleotide was obtained from the concentration response curve obtained by plotting the maximum rate of fluorescence change against concentration (Fig. 4.9, bottom on the left, n=3-6 for ATP, n=4-6 for UTP, n= 4-6 for UTP). Order of potency of agonists was ATP > UTP > ADP .

Since Depolarization activates (as previously mentioned) TMEM16A, stimulation of iodide influxes were examined in the presence of 100mM K (depolarization) or 100mM Na (control). The result indicate that the affinity of ATP was increased , compatinble with known properties of TMEM16A. (Fig. 4.9, bottom on the right).
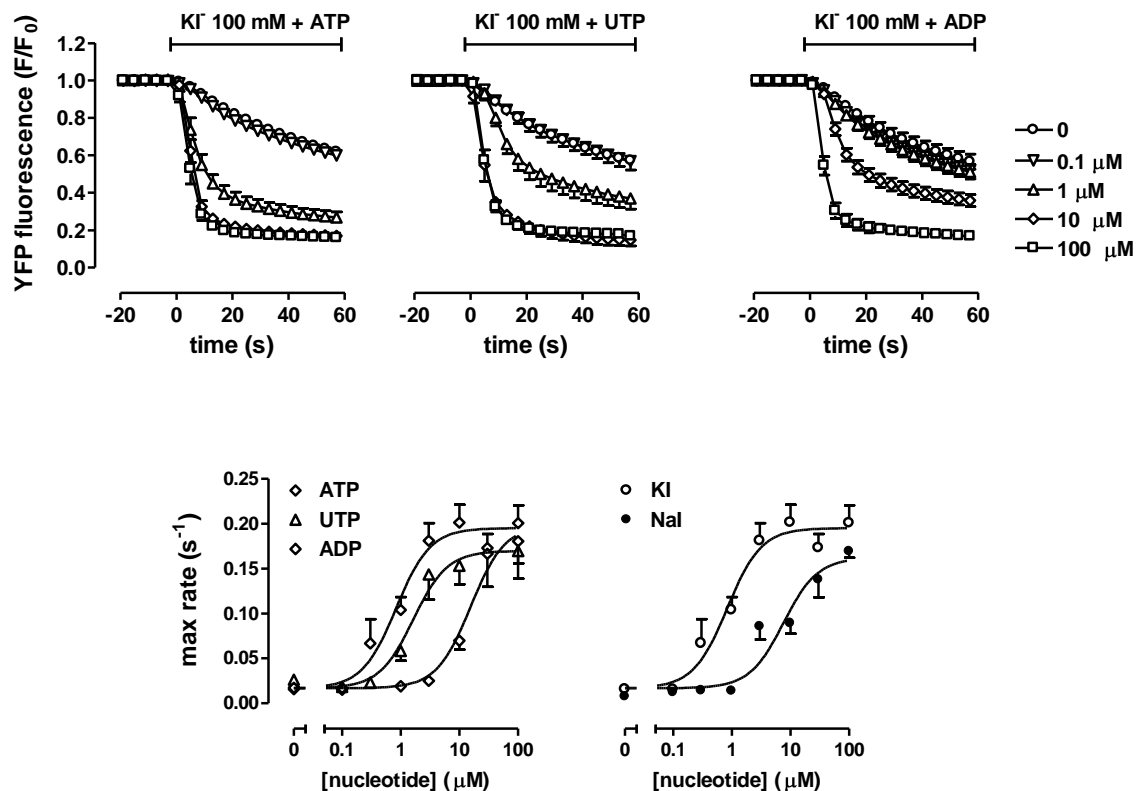
Fig. 4.9 Upper images: fluorescence signals are shown as F/F$_0$. FRTL-5 YFP-H148Q/I152L cells cultured in a TSH-free medium for at least 1 wk were exposed to 100mM K$^+$I$^-$ +/- ATP, UTP, ADP (0,1-100uM). Bottom images: fluorescence signals are showed as max rate (s-1) (influx), on the left nucleotide affinity curves are shown (fluorescence recovery rate versus time Δf /Δt for each nucleotide, compared to their concentration) on the right nucleotide affinity curves are shown in normal/depolarization conditions.(Logarithmic scale).

4.2.1.3 Effect of calcium on iodide influx stimulated by ATP and ionomycin

 Calcium effect on CaCC activity were characterized in FRTL-5 YFP-H148Q/I152L cells. Ionomycin was used as a ionophore, able to increase intracellular calcium concentration, rising permeability of cell and organelle membranes. Ionomycin is very powerful in stimulation of extracellular calcium entry and calcium release from intracellular stores through organelle membranes. It is active already at 1uM concentration.

Exposition to ATP produced the same effect at 100uM concentration, thus it is revealed less powerful than ionomycin, already active at 1uM.

In fig. 4. 10 it can be seen a marked decrease of fluorescence signal due to calcium-activated iodide entrance into FRTL-5 cells.

The next step was to establish if iodide influx were stimulated by calcium in PBS, so from extracellular compartment, or already present in cytoplasm, particularly from intracellular storage organelles. Therefore, FRTL-5 were exposed to PBS calcium-free. Besides, a chelating of intracellular calcium, BAPTA, was used to remove calcium effect and to observe, intracellular calcium contribution on iodide entry mediated by CaCC.

- ❖ In fig. 4.10 A control situation is shown. Perfusion solution (PBS) contains calcium (0,7 mM): expected iodide entry was observed into FRTL-5 in the presence of 1uM ionomycin and 100uM ATP compared to the baseline (n=6).

- ❖ In fig. 4.10 B situation Ca^{2+}-free is shown. With Ca^{2+}-free PBS, iodide entry into FRTL-5 could still be observed, stimulated by ionomycin and ATP (n=5).

- ❖ In fig. 4.10 C situation with BAPTA is shown. Cells were pre-incubated with 25 uM BAPTA and perfused with Ca^{2+}-free PBS. In this case a virtually complete inhibition of iodide influx could be observed. BAPTA, chelating intracellular calcium released from storage organelles, virtually removed every Ca^{2+} source from cells (n=3).
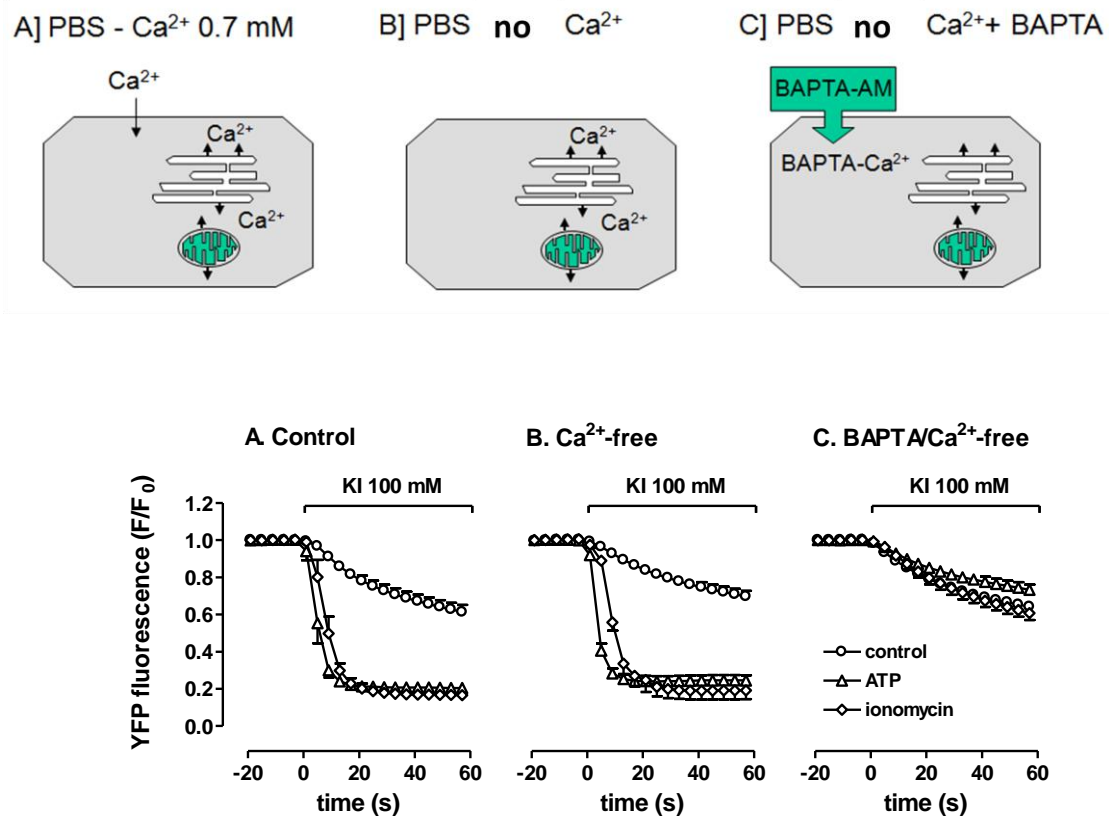
Fig. 4.10. Fluorescence signals are showed as F/F_0. **A**, control situation: FRTL-5 YFP-H148Q/I152L cells were perfused with KI PBS+calcium, then exposed to 1uM ionomycin and 100uM ATP (n=6). **B**, situation Ca^{2+}-free: Ca^{2+}-free PBS perfused FRTL-5 (n=5). **C**, situation with BAPTA: cells were pre-incubated with 25 uM BAPTA and perfused with Ca^{2+}-free PBS (n=3).

In conclusion, results showed in FRTL-5 cells that calcium-activated iodide influx depended on intracellular calcium only, released from stores of intracellular organelles (as the endoplasmic reticulum). Ca^{2+}-activated iodide flow properties, included activation by nucleotides and intracellular calcium, were coherent with known properties of TMEM16A calcium-activated channel.

4.2.2 IODIDE TRANSPORT IN THYROID CELLS: EFFLUX ACTIVITY

NIS-independent iodide influx into FRTL-5, was revealed to have properties coherent to CaCC. Attention was focused on activity of iodide efflux.

<u>4.2.2.1 Use of a experimental model for iodide efflux studies: CHOK-1 cells</u>

To begin characterization of iodide efflux, the same experimental conditions were reproduced as described before: presence or absence of extracellular calcium in PBS, presence or absence of intracellular calcium released by storage organelles, chelated by BAPTA. Before undertaking a depth study about FRTL-5 thyroid cells, iodide transport was characterized in a model cell system, CHOK-1 cell lines, to find and optimize the best experimental conditions, and to confirm functional properties of currents due to TMEM16A. CHO K1 cells were chosen because of their good adhesion to substrate, feature suitable for functional experiments, and lack of known endogenous CaCC expression.

<u>4.2.2.2 Expression of TMEM16A mRNA in CHOK-1 *wild type* / NIS/ YFP-hTMEM16A cells</u>

 First of all, the chosen experimental model CHOK-1 cells were considered about the endogenous TMEM16A expression. This study was carried out by RT-PCR, on *wild type* cells previously. Neither TMEM16A transcript expression was observed, nor evidence was found in literature so far, thus CHOK-1 cell lines were chosen as a model definitively.
 Stable clones of CHOK-1, selected and established previously in our lab, expressing hNIS and YFP-H148Q/I152L were employed. Absence of endogenous TMEM16A mRNA expression was confirmed. Besides, maintenance of hNIS and YFP-H148Q/I152L expression, after long culture and cryopreservation periods, was verified before employing them in the next characterization functional studies.

 Fig. 4.11 shows that CHOK-1- hNIS/YFP-H148Q/I152L stable clones do not express TMEM16A endogenously, thus they can be used as a cell model for negative control in functional experiments. Besides, cells preserve intact exogenous hNIS and YFP-H148Q/I152L expression, and are adequate for functional characterization of iodide transport. Transfection with hTMEM16A cDNA led to transient exogenous expression of hTMEM16A by CHOK-1- hNIS/YFP-H148Q/I152L, detectable by RT-PCR (fig. 4.11): amplicon specific for hTMEM16A (305 bp) was detected.
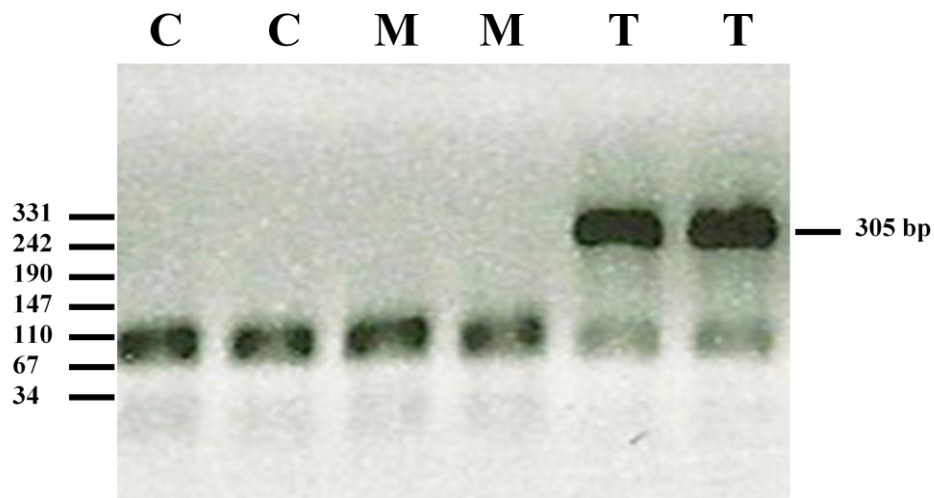
Fig. 4.11. From left to right, in duplicate samples of CHOK-1 YFP-H148Q/I152L/hNIS cells (control, C), transfected with pcDNA3.1 (mock, M), transfected (T) with pcDNA3.1hTMEM16A (expressing hTMEM16A transiently). Amplicon specific for hTMEM16A is detected (305 bp).

Since mRNA signal were detected in CHOK-1 expressing hTMEM16A transiently, this model cell was tested to know effects of exogenous hTMEM16 expression on iodide efflux, to be compared with putative endogenous CaCC/rTMEM16A functional activity expressed in FRTL-5 cell lines.

4.2.2.3 Effect of ionomycin on iodide efflux in CHOK-1 *wild type* / NIS-YFP-hTMEM16A cells

Calcium-activated iodide conductance in efflux, due to hTMEM16A transporter, expressed in stable clones CHOK-1-hNIS/YFP-H148Q/I152L transiently was evaluated. Aim was observation of efflux properties, to have a model of functional response and, going on with studies on FRTL-5, making a comparison between expected and obtained results observed in this model system.

Analogous experiments were performed, similar to experiments made to study iodide influx, adapting protocol to efflux situation. Perfusion solution (PBS as usual) contained 1uM ionomycin, to stimulate intracellular calcium concentration. First of all, clones without TMEM16A exogenous expression were used to detect any iodide

transport due to other endogenous transporters or to other isoforms belonging to anoctamin family.

- ❖ Fig. 4.14 A shows CHOK-1-hNIS/YFP-H148Q/I152L cells perfused with PBS (control).

- ❖ Fig. 4.14 E shows cells, pre-loaded with iodide, exposed to 1uM ionomycin for 2'. A small fluorescence decrease can be observed, likely due to pH variation provoked by ionomycin.

- ❖ Fig. 4.14 B shows CHOK-1-hNIS/YFP-H148Q/I152L-pcDNA3.1 cells (mock), perfused with PBS in efflux stage (control) (n = 210 cells).

- ❖ Fig. 4.14 F shows absence of iodide efflux in mock cells exposed to 1uM ionomycin, compared to control conditions. Cell clones are adequate negative controls, without detectable functional expression of transporters involved in calcium-activated iodide efflux (n =234 cells).

- ❖ Finally, fig. 4.14 C shows CHOK-hNIS/YFP-H148Q/I152L stable clones with transient hTMEM16A expression perfused with PBS in efflux stage (control)(n =214 cells).

- ❖ Fig. 4.14 G shows actual fluorescence increase in efflux stage with 1uM ionomycin in CHOK-hNIS/YFP-H148Q/I152L stable clones with transient hTMEM16A expression. After initial fluorescence decrease, due to extracellular iodide entry (10' exposition to iodide 100uM as usual), exposition to PBS only let the "wash-out" of intracellular iodide slowly (20' for a basal levels complete recovery), not detectable during the short time interval considered. Instead, addition of ionomycin to cells provoked a rapid fluorescence decrease, due to iodide efflux out of cells. Particularly, 79/488

cells responded to ionomycin, depending on tranfection efficiency (qualitative and quantitative) (n=488 cells).

Observed properties of calcium-activated iodide efflux are compatible with known properties of TMEM16A calcium-activated channel.
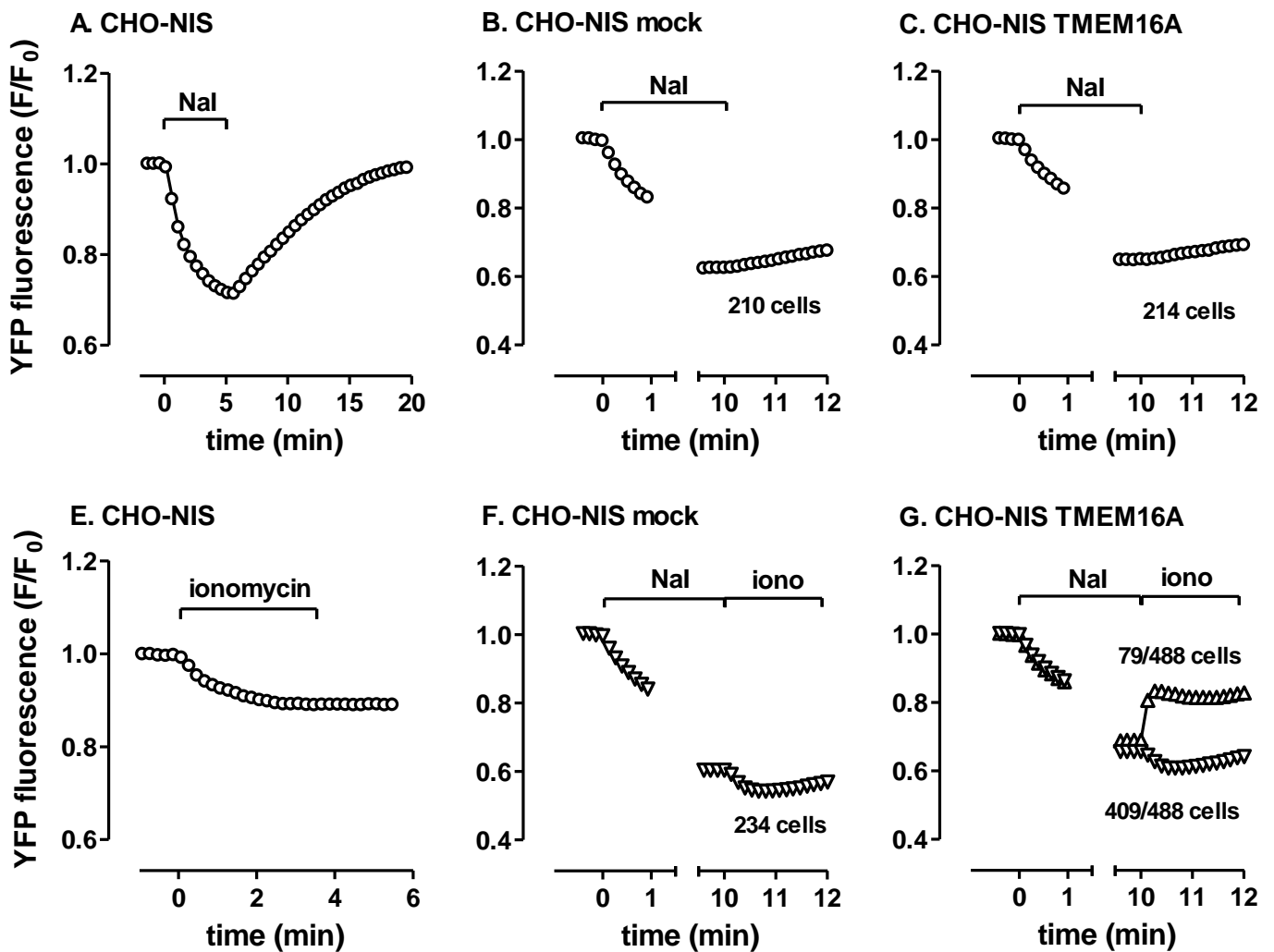

Fig. 4.14. Fluorescence signals are showed as F/F_0 . A: CHOK-1-hNIS/YFP-H148Q/I152L cells perfused with PBS (control). E: cells exposed to 1uM ionomycin. B: CHOK-1-hNIS/YFP-H148Q/I152L-pcDNA3.1 cells (mock)(PBS in efflux stage, control). F: mock cells exposed to 1uM ionomycin, compared to control conditions. C: CHOK-hNIS/YFP-H148Q/I152L stable clones with transient hTMEM16A expression (control), exposed to PBS in efflux stage. G: CHOK-hNIS/YFP-H148Q/I152L-hTMEM16A cells exposed to 1uM ionomycin.

In conclusion, it can be asserted that transient exogenous hTMEM16A expression, in CHOK-1-hNIS/YFP-H148Q/I152L stable cell clones, led to functional expression of a Ca^{2+}-activated iodide transport in efflux, whose properties are coherent with characteristics of TMEM16A endogenously expressed, described in literature.

Then, characterization of Ca^{2+}-activated iodide transport in efflux in FRTL-5 cell lines was started, to understand if it could take place via CaCC/TMEM16A endogenously expressed in FRTL-5 cells. The same experimental model was used, as previously: exposition of cells to PBS with 1uM ionomycin after verifying iodide influx into the cells.

4.2.2.4 Effect of ionomycin and ATP on iodide efflux in FRTL-5 cells: calcium-dependence

Analysis continued testing effect of calcium on iodide efflux in FRTL-5 cells. The same system was employed as described for iodide influx experiments: ionomycin or ATP to stimulate CaCC activity and intracellular calcium chelation with BAPTA.
Fig. 4.16 shows all performed conditions. Fig. 4.16 A, B, C show relative fluorescence due to iodide flow; fig. 4.16 D shows maximum rate of iodide flow (n=4).

  ❖ A, control condition: FRTL-5 cells perfused with PBS+100uM iodide (10'as usual). Cells uptook iodide; during pause of image acquisition, iodide uptake reached the steady state. Following perfusion with PBS+100uM ATP or PBS+1uM ionomycin (2' as usual) stimulated iodide efflux, with a maximum peak reached instantaneously. Cells perfused only with PBS showed a slow iodide efflux.

  ❖ B, calcium-free condition: when iodide uptake reached the steady state, FRTL-5 cells were perfused with calcium-free PBS+100uM iodide. Calcium-

free PBS+100uM ATP or calcium-free PBS+1uM ionomycin stimulated instantaneous iodide efflux, also in absence of extracellular calcium.

- ❖ C, calcium-free condition+ BAPTA: FRTL-5 cells pre-incubated with BAPTA (45' as usual) and perfused with calcium-free PBS+100uM iodide, when iodide uptake reached the steady state. PBS+100uM ATP or PBS+1uM ionomycin did not stimulate instantaneous iodide efflux in absence of intracellular calcium.

- ❖ D, graph shows comparison among maximum rate of iodide efflux. Particularly, as it can be seen on the right, deprivation of intracellular calcium did not allow iodide efflux activation.

Also in iodide efflux stage, results suggested a fundamental role of intracellular calcium in activation of iodide efflux, which is extracellular calcium-independent.
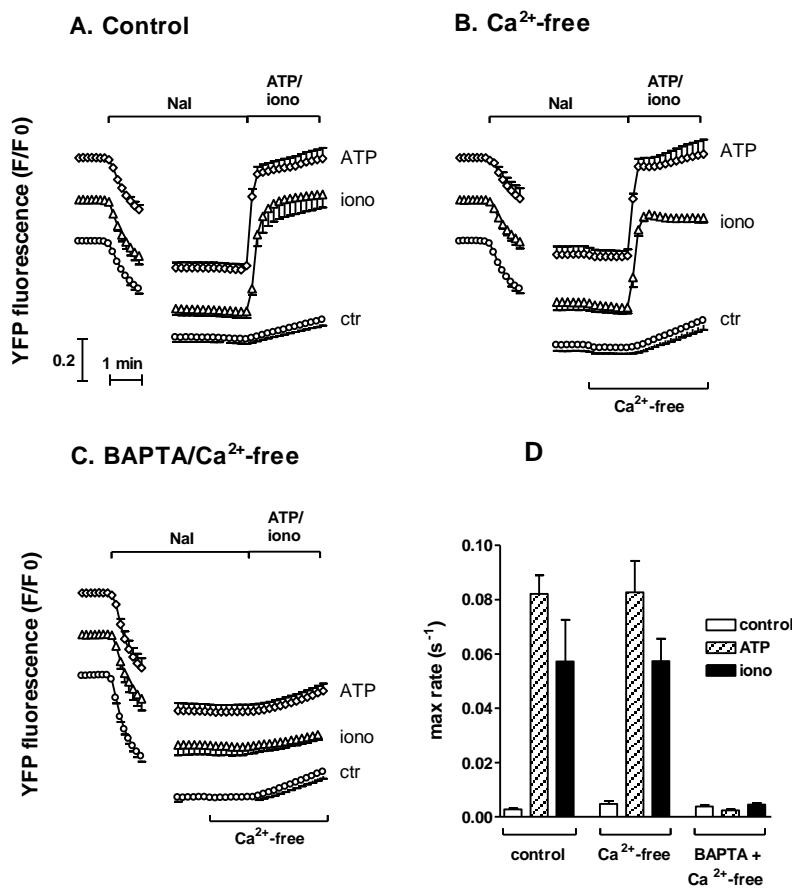
Fig. 4.16. fluorescence signals are showed as F/F_0. A, control condition: FRTL-5 cells perfused with PBS+100uM iodide, +/- 100uM ATP or 1uM ionomycin. B, calcium-free condition: FRTL-5 cells were perfused with calcium-free PBS+100uM iodide +/- 100uM ATP or 1uM ionomycin. C, calcium-free condition+ BAPTA: FRTL-5 cells pre-incubated with BAPTA and perfused with calcium-free PBS+100uM iodide (n=4). D, comparison among maximum rate of iodide efflux. Data points or bars represent means ± standard errors of 4 measurements.

4.2.2.5 Effect of receptor agonists on iodide efflux in FRTL-5 cells

Receptor agonists effect on iodide transport in efflux in FRTL-5 cells was characterized. Cells were exposed to increasing extracellular agonist concentration, to verify which agonists were the most effective. In general potency was revealed bigger at 100uM concentration. Agonists screened were ATP, epinephrine, dopamine, acetylcholine, histamine, serotonin (5HT), TSH.

❖ Fig. 4.17 A: among tested agonists, only two produced iodide efflux responses, ATP and epinephrine (100uM)(2' as usual). ATP-dependence and response entity were coherent with calcium-activated iodide current provoked by TMEM16A in CHOK-1-hNIS/YFP-H148Q/I152L-hTMEM16A, observed during previous experiments. With the other agonists fluorescence recovery was similar to control. Dopamine and acetylcholine produced not reproducible responses.(n=6-11 for ATP and epinephrine, n=5-7 for dopamine, and acetylcholine, n=4-8 for histamine, TSH, 5-HT).

❖ Fig. 4.17 B, only epinephrine and ATP produce a statistically significant response compared to control situation (p<0,01).
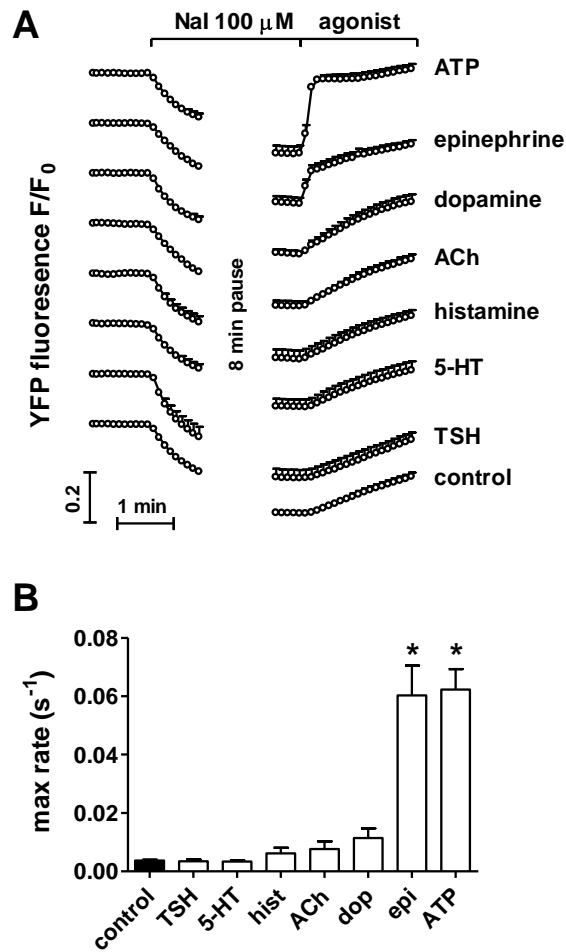
Fig. 4.17. Fluorescence signals are showed as F/F_0. A: Tested agonists, ATP, epinephrine, dopamine, acetylcholine, histamine, serotonin, TSH. B, maximum rate in iodide efflux stimulated by screened agonists. Statistical analysis performed with ANOVA one way method ($p < 0.0001$), and Dunnett's multiple comparison post test to compare every treatment with control. (* : $p < 0,01$).

4.2.2.6 Effect of ATP/UTP/ADP nucleotides on iodide efflux in FRTL-5

Sensitivity of iodide transporters, involved in observed efflux response, to nucleotides was analyzed.

- ❖ Fig. 4.18 A: FRTL-5 cells exposed to different ATP nucleotide concentration (2' as usual). Response of efflux caused by ATP was dose-dependent. Tested concentration in PBS were 1, 10, 100 uM: at increasing used concentration, response of efflux was more intense and showed the highest slope for every effective concentration, virtually instantly (n=6-11).

- ❖ Fig. 4.18 B: same experiment was performed, using UTP nucleotide. Observed efflux responses had the same properties of those detected exposing FRTL-5 cells to ATP. Responses were concentration-dependent and maximum at 100uM concentration. However, entity of induced response was less than the entity due to exposition to ATP, for every employed concentration (n=5-7).

- ❖ Fig. 4.18 C: exposition of FRTL-5 to increasing nucleotide concentrations, ADP in this case. Effect on efflux response was active but in a more modest manner compared to that detected with previous nucleotides, at 100uM ADP only (n=4-8).

- ❖ Fig. 4.18 D: exposition to nucleotides let iodide efflux increase in a concentration-dependent manner with a potency order ATP > UTP > ADP (maximum rate graph that represents affinity curve for each agonist) (ATP Ec_{50}=4,9 uM , UTP Ec_{50} =>10 uM, ADP Ec_{50}=>100uM).

- ❖ Fig. 4.18 E: depolarization conditions (100mM K+PBS) did not alter ATP affinity on its own receptors in FRTL-5 cells (curve slope not modified).

- ❖ Fig. 4.18 F: chloride-free PBS conditions (100mM K+PBS) did not alter iodide efflux response in FRTL-5 cells. This activity was chloride-independent.

Hence, it can be asserted that response of iodide efflux is evoked in FRTL-5 in a concentration-dependent manner, with a maximum peak at 100uM, characterized by potency order of nucleotides on involved receptors below: ATP >UTP> ADP, compatible with P2Y receptor properties. Neither cell membrane depolarization nor chloride provoked effect on iodide efflux response in FRTL-5 cells.
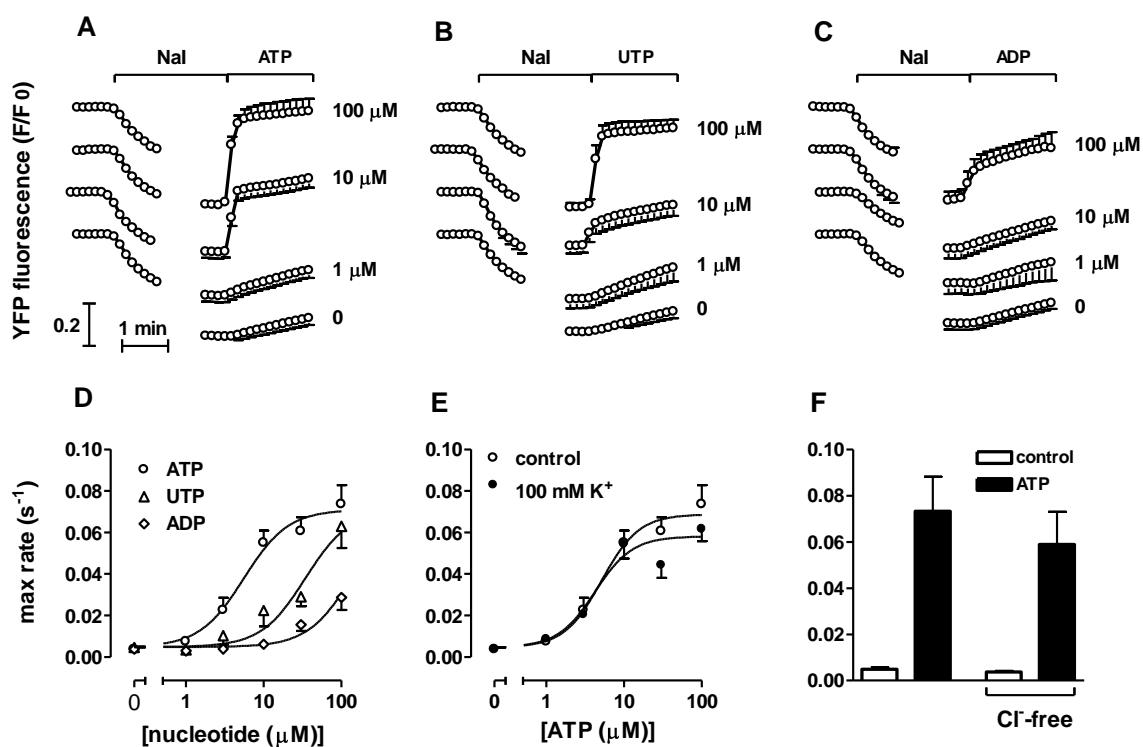

Fig. 4.18. Fluorescence signals are showed as F/F$_0$. A: FRTL-5 cells exposed to different ATP concentration (1, 10, 100 uM) (n=6-11). B: same experiment was performed, using UTP nucleotide (n=5-7). C: exposition of FRTL-5 to increasing ADP nucleotide concentrations (n=4-8). D: fluorescence signals are showed as max rate (s-1) (influx), nucleotide affinity curves are shown for nucleotides ATP, UTP, ADP (fluorescence recovery rate versus time Δf /Δt for each nucleotide, compared to their concentration) (logarithmic scale)) (ATP Ec$_{50}$=4,9 uM , UTP Ec$_{50}$ =>10 uM, ADP Ec$_{50}$=>100uM) . E: ATP affinity curves are shown in normal/depolarization conditions (100mM K+PBS). F: comparison between control and chloride-free PBS conditions under ATP exposure. Data points or bars represent means ± standard errors.

4.2.2.7 Properties of ATP and calcium-mediated iodide efflux response in FRTL-5: duration

Iodide efflux stimulated by nucleotides, ATP particularly, and by cytoplasmic ATP increase, was characterized further to analyze its duration as well as its intensity. FRTL-5 cells were exposed to PBS containing 100uM iodide, 100uM ATP or 1uM ionomycin, as previously.

❖ Fig. 4.19 A, exposition to PBS with 100uM iodide (10') caused high iodide influx into cells, also up to 50% compared to baseline, as expected in FRTL-5 cells cultured at usual conditions, with TSH. Afterwards cells were perfused with PBS, conditions which provoked iodide efflux as expected, through non-specific transporters (n=1).

❖ Fig. 4.19 B shows situation of perfusion with PBS, without 100uM iodide, with 100 uM ATP (20'), to check nucleotide effects in control conditions. No ATP-dependent effect was detected on baseline, except to a small fluorescence increase, likely caused by pH increase after exposition of the cells to ATP.

❖ Fig. 4.19 C shows situation of perfusion with PBS, without 100uM iodide, with 1uM ionomycin (10'), to check effects of cytoplasmic calcium increase in control conditions. In this case, baseline was slightly increased, likely caused by pH increase after exposition of cells to ionomycin.

❖ Fig. 4.19 D shows situation of perfusion with PBS+100uM iodide (10'), then with PBS containing 100uM ATP (20'). A rapid response of efflux, developed virtually instantaneously, could be seen.

❖ Fig. 4.19 E, shows a different situation: in the efflux stage, FRTL-5 cells kept on being perfused with PBS+100uM iodide. Iodide efflux evoked by exposition with PBS+iodide+ATP100uM (20') took place, response was rapid, instantaneous and intense but temporary: in few less than 10', baseline was increased with a peak, as seen in control conditions + ATP100uM but without iodide. However, the interesting result is that, immediately after, iodide began to enter the cells again, as it could be detected by fluorescence signal decrease. Thus, response of efflux is transient, with iodide perfused continuously, involved transporters and channels did not keep on responding to ATP.

❖ Fig. 4.19 F: FRTL-5 cells were perfused before with PBS + 100uM iodide (10'), then with PBS + ionomycin 1uM (10'). A rapid response of efflux could be detected, developed virtually instantly. Contemporary presence of ionomycin allowed iodide efflux out of FRTL-5 cells anyway.

❖ Fig. 4.19 G: during the efflux stage, FRTL-5 cells kept on perfusing with PBS containing 100uM iodide. Iodide efflux evoked by exposition with PBS and iodide+ionomycin (10') took place, but contemporary presence of ionomycin and iodide did not allow complete iodide flow out of cells. A rapid and intense response of efflux was observed but, in 10', baseline was increased with a well pronounced peak, as seen in control conditions with ionomycin but without iodide. However also in this case, immediately after, iodide began to enter the cells with bigger quickness compared to condition with ATP, as it could be detected by fluorescence signal decrease. Also in this case efflux response was transient, with iodide continuously, involved transporters and channels did not keep on responding to ionomycin.

In conclusion, in the light of the obtained results, transporters and channels responsible of calcium-activated iodide efflux showed a rapid activation, virtually immediate but transient. This suggested that CaCC began insensitive with iodide perfused continuously after the first activation.
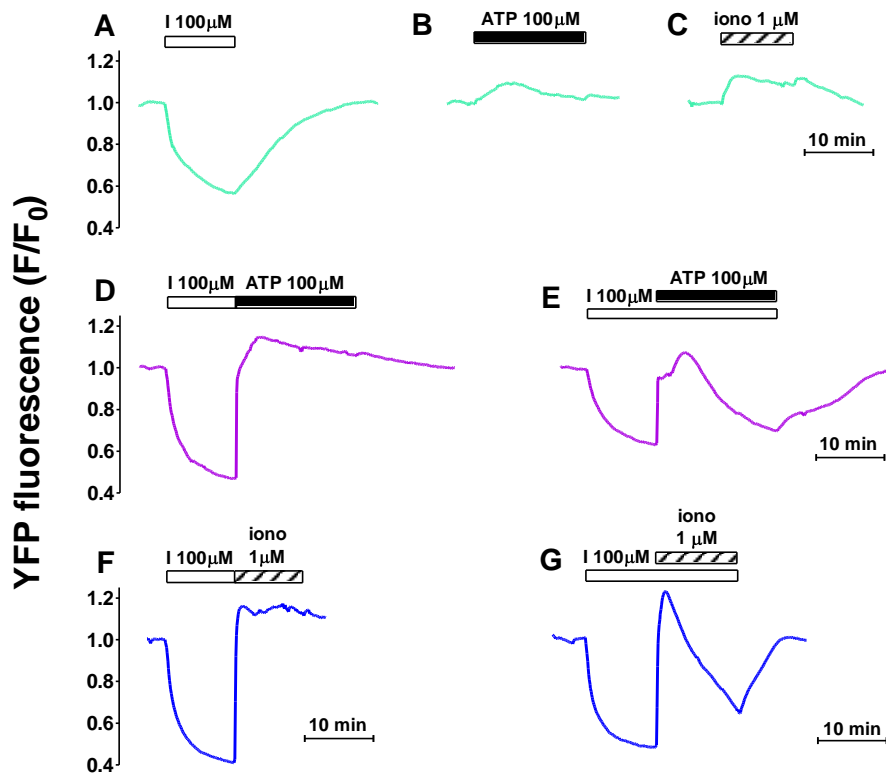
Fig. 4.19. Fluorescence signals are showed as F/F_0. A: exposition of FRTL-5 to PBS with 100uM iodide (10') and PBS on efflux stage. B: perfusion with PBS, without 100uM iodide, + 100 uM ATP (20'). C: perfusion with PBS, without 100uM iodide, + 1uM ionomycin (10'). D: perfusion with PBS+100uM iodide (10'), then with PBS + 100uM ATP (20'). E:during efflux stage, FRTL-5 cells continuously perfused with PBS+100uM iodide. F: FRTL-5 cells were perfused before with PBS + 100uM iodide (10'), then with PBS + ionomycin 1uM (10'). G: during the efflux stage, FRTL-5 cells continuously perfused with PBS+100uM iodide , then with PBS and iodide+ionomycin (10') (n=1).

4.2.2.8 Effect of catecholamines on iodide efflux

Calcium-activated iodide efflux was characterized further, also considering receptor agonists of catecholaminergic system. FRTL-5 cells were perfused with PBS at increasing concentrations of epinephrine or norepinephrine to examine their effects and compare them with those detected during iodide influx studies in FRTL-5. Finally were compared effects of adrenergic antagonists to noepinephrine-induced iodide efflux.

Effect of endogenous receptor agonists

- ❖ Fig. 4.20 (upper, on the left): fluorescence signals are related to iodide efflux experiments, carried out exposing iodide-preloaded FRTL-5 cells to PBS+ epinephrine (epi) at concentration range of 0,01-10uM (2'). Response of calcium-activated iodide efflux was detected and resulted characterized by concentration-dependent intensity, with a maximum at 10uM. It showed a virtually immediate activation (a few seconds) (n=7-8)

- ❖ Fig. 4.20 (bottom, on the right): the same kind of experiment can be seen, but exposing FRTL-5 cells to PBS+ norepinephrine (NE) at concentration range of 0,01-10uM (2'). Response signals produced are similar for entity and properties, also in this case maximum at 10uM (n=5-6).

Effect of endogenous and exogenous receptor agonists: comparison among affinities

- ❖ Fig. 4.20 (bottom, on the left): comparison among affinities of different receptor agonists of catecholaminergic system, maximum rate affinity curve. Iodide-preloaded FRTL-5 were exposed to PBS+/- thyroid endogen/synthetic agonists (0.01-100uM, 2'). Epinephrine and norepinephrine (selective α receptors more than β) were shown the most active on receptors involved in response, compared to other screened agonists, phenylephrine (PE) (selective for α1 receptors) and isoproterenol (iso) (selective for β receptors), at the same concentration range (synthetic agonists) (epinephrine Ec_{50}=4.1uM,

norepinephrine $Ec_{50}= 5.1uM$, phenylnephrine $Ec_{50}=3.7$ uM). Isoproterenol did not induce any response.

❖ Fig. 4.20 (bottom, on the right) shows comparison among effects of norepinephrine (NE, agonist) and prazosin (PRAZ), phentolamine (PHE), propranolol (PROP) (antagonists of catecholaminergic system, respectively selective for α1 receptors, α1/ α2, β) on norepinephrine-induced iodide efflux response. Graph shows maximum rate levels (affinity curves). Iodide-preloaded FRTL-5 were exposed to PBS+/- thyroid antagonists (100uM, 2'). Prazosin and phentolamine showed to inhibit norepinephrine-activated iodide efflux response, propranolol showed to be inactive.
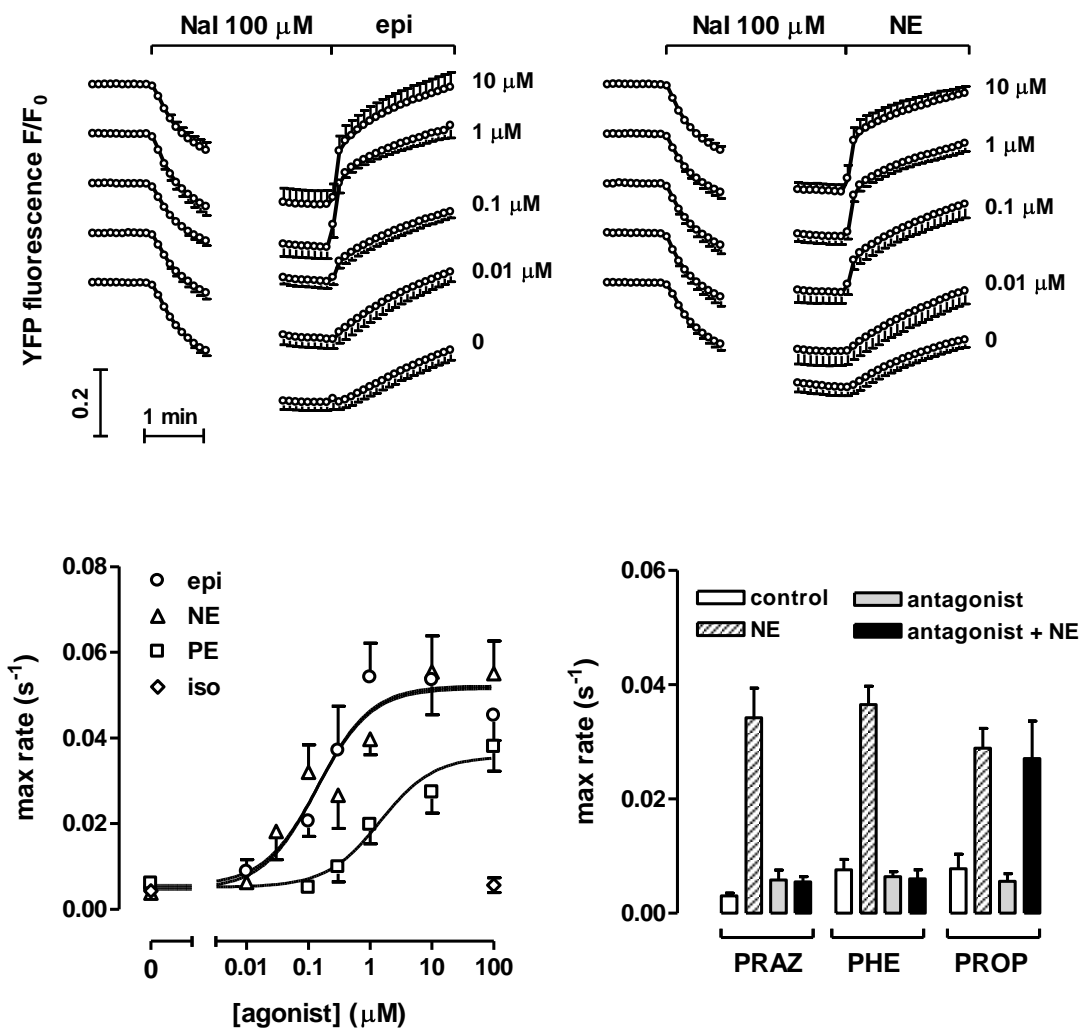
Fig. 4.20. Fluorescence signals are showed as F/F$_0$. Upper images: FRTL-5 cells perfused with PBS+/- epinephrine (epi) (left,n=7-8) or PBS+/-norepinephrine (NE) (right, n=5-6) (0,01-10uM). Bottom images: fluorescence signals are showed as max rate (s-1) (influx), nucleotide affinity curves are shown for epinephrine, norepinephrine, phenylephrine (PE), isoproterenol (iso) (fluorescence recovery rate versus time $\Delta f / \Delta t$ for each agonist, compared to their concentration) (logarithmic scale)) (epinephrine Ec$_{50}$=4.1 uM , norepinephrine Ec$_{50}$ =5.1 uM, phenylephrine Ec$_{50}$=3.7 uM) at increasing concentrations (left); comparison among affinities at 100 uM for antagonists (prazosin PRAZ, phentolamine PHE, propranolol PROP) +/- NE induced-iodide efflux response (right). Data points or bars represent means ± standard errors.

4.2.2.9 Catecholaminergic receptorial agonists: effect of isoproterenol/isoprenaline on intracellular calcium.

 As a cell model FRTL-5 cells not expressing YFP were employed. To measure intracellular calcium levels FURA-2 probe was used.

 Cells were incubated 30' membrane permeable FURA-2-AM form, hydrolysed by cell esterases to obtain FURA-2 active form.

 Exposure of cells to various agonists tested (ATP, epinephrine or adrenaline, norepinephrine, or noradrenaline, isoprenaline and dopamine) increased intracellular levels of calcium.

 In particular, ATP caused the highest increase in intracellular calcium levels among all the agonists screened (fig. 4.21), consistent with the most active stimulation of CaCC produced by ATP, as seen in fig. 4.18.

 Interestingly, isoprenaline induces increase in intracellular calcium levels, although lower than the other agonists (fig. 4.21). Previously, it was seen that this agonist was not able to stimulate iodide efflux. These data suggested the existence of a threshold level of intracellular calcium, above which activates the channel.
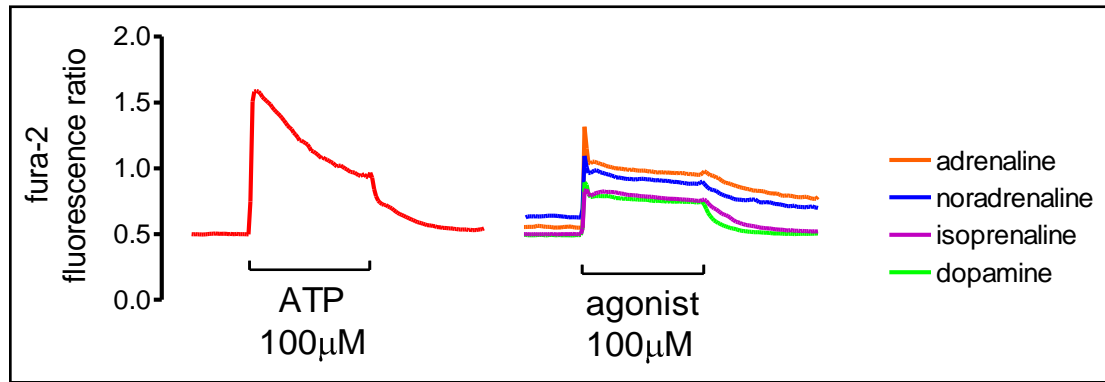
Fig. 4.21. Fluorescence signals are showed as F_{340}/F_{380} of fura-2 probe. Adrenaline/epinephrine, noradrealine/norepinephrine, isoprenaline/isoproterenol, dopamine agonists tested on FRTL-5 cells. Single representative experiment.

4.2.2.10 Effect of Ca^{2+} on iodide efflux stimulated by epinephrine

Similarly, effect of epinephrine was tested, to confirm if it could stimulate CaCC activity also in efflux stage, checking also its dependence on calcium.

Fig. 4.22 shows all performed conditions. Fig. 4.22 A, B, C show relative fluorescence due to iodide flow; fig. 4.22 D shows maximum rate of iodide flow (n=3-5).

- ❖ A: control condition. FRTL-5 cells perfused with PBS+100uM iodide (10'). Cells uptook iodide; during pause of image acquisition, iodide uptake reached the steady state. Following perfusion with PBS+100uM epinephrine (1') stimulated iodide efflux, with a maximum peak reached instantaneously. Cells perfused only with PBS show a slow iodide efflux (recovery in almost 20').

- ❖ B: calcium-free condition. When iodide uptake reached the steady state, FRTL-5 cells were perfused with calcium-free PBS+100uM iodide (2'). Calcium-free PBS+100uM epinephrine (1') stimulated instantaneous iodide efflux, also in absence of extracellular calcium, but less than control condition (PBS).

- ❖ Calcium-free condition+ BAPTA: FRTL-5 cells pre-incubated with BAPTA (45'), preloaded with PBS+100uM iodide (10') and perfused with calcium-free PBS+100uM iodide (1'). Calcium-free PBS+100uM epinephrine (1') did not stimulate iodide efflux.

❖ Graph shows comparison among maximum rate of iodide efflux in all the conditions. In the middle condition B is showed: absence of extracellular calcium activated iodide efflux but with a rate smaller than control situation. On the right condition C is showed: deprivation of intracellular calcium did not allow iodide efflux activation.

Effect of extracellular calcium on epinephrine-activated iodide efflux appears more marked than ATP or ionomycin. Lack of extracellular calcium did not allow the same instantaneous iodide efflux as seen in control condition. Lack of extracellular calcium and total depletion of intracellular calcium with BAPTA blocked every iodide efflux response.
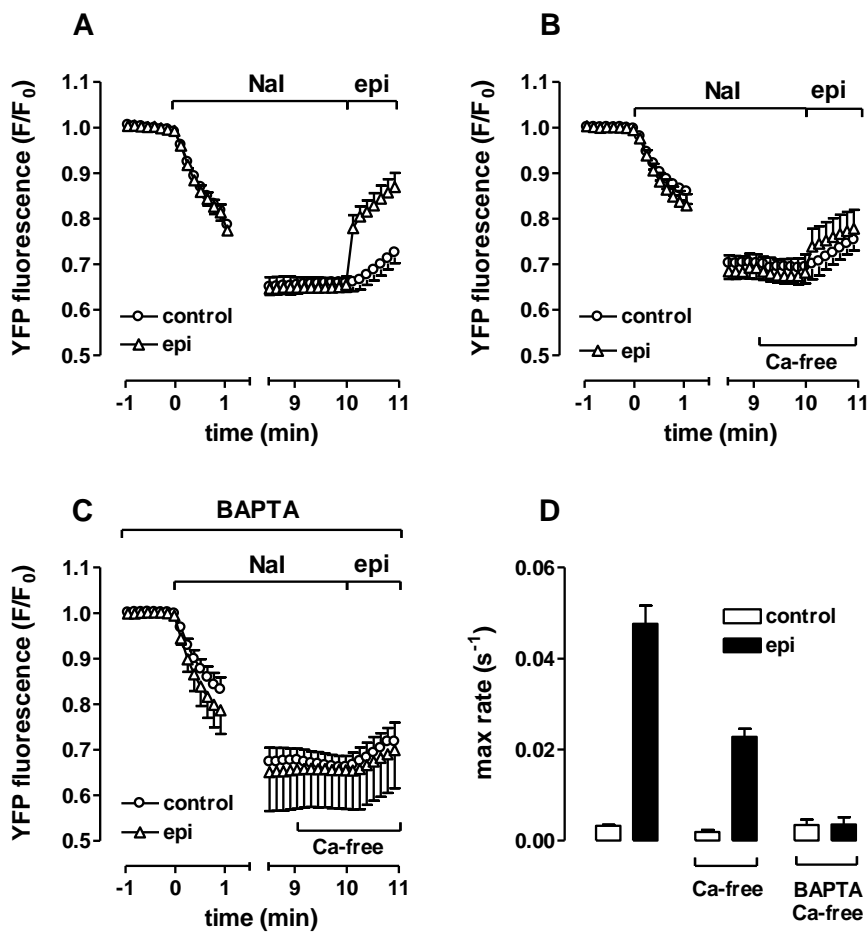
Fig. 4.22. Fluorescence signals are showed as F/F_0. A: FRTL-5 cells perfused with PBS+/- epinephrine (100uM) (control). B: FRTL-5 cells perfused with PBS+/- epinephrine (100uM) (in Ca^{2+} free PBS). C: FRTL-5 cells, pre-incubated with BAPTA, perfused with PBS+/- epinephrine (100uM) (in Ca^{2+} free PBS) (n=3-5). D: maximum rate graph of the three conditions described: effects of perfusion with PBS, Ca^{2+} free PBS, Ca^{2+} free PBS + BAPTA on epi stimulated iodide efflux. Data points or bars represent means ± standard errors of 3-5 measurements.

4.2.2.11 Effect of CaCC/TMEM16A inhibitors on iodide efflux stimulated by ATP

 Specific CaCC inhibitors described in literature: niflumic acid (NFA), tannic acid (TA), were screened to detect any effect on iodide efflux stimulated by ATP (n=6-7).

❖ Fig. 4.23 A (left): control condition: FRTL-5 cells pre-loaded with PBS+100uM iodide (10'). Perfusion with NFA/TA 100uM showed no effect on iodide basal efflux. Interestingly, TA produced a increased basal iodide level, as shown with fluorescence baseline lowering after acquisition pause, compared to control.

❖ Fig. 4.23 A (right): ATP effect (100uM). FRTL-5 cells pre-loaded with PBS+100uM iodide (10'). Perfusion with NFA/TA 100uM inhibited rapid ATP-stimulated iodide efflux: NFA partly, TA completely, producing, also in this case, a increased basal iodide level, as shown with fluorescence baseline lowering after acquisition pause, compared to control.

❖ Fig. 4.23 B (left): maximum rate graph for conditions described below with comparison between influx and efflux stages. TA inhibited iodide efflux and increased basal iodide level in a statistically significant manner.

❖ Fig. 4.23 B (right): steady state graph for conditions described below. TA and NFA inhibited iodide efflux a statistically significant manner (p< 0,01).

Fig. 4.23. Fluorescence signals are showed as F/F_0. A (left): FRTL-5 cells perfused with PBS+/-NFA/TA (100uM) (control). A (right): FRTL-5 cells perfused with PBS+/- NFA/TA (100uM) (+ATP 100uM) (n=6-7). B (left): maximum rate graph for conditions described below. B (right): steady state graph for conditions described below. Statistical analysis performed with ANOVA one way method (p< 0.0001), and Dunnett's multiple comparison post test to compare every treatment with control. (* : p< 0,01).

4.2.2.12 Effect of CaCC/TMEM16A inhibitors on iodide efflux stimulated by epinephrine and comparison with iodide efflux stimulated by ATP

Specific CaCC inhibitors described in literature: niflumic acid (NFA), tannic acid (TA), were screened to detect any effect on iodide efflux stimulated by epinephrine.

- ❖ Fig. 4.24 A: control condition: FRTL-5 cells pre-loaded with PBS+100uM iodide (10'). Perfusion with NFA/TA 100uM (100uM) showed no effect on iodide basal efflux. Also in this condition, TA produced a increased basal iodide level, as shown with fluorescence baseline lowering after acquisition pause, compared to control.

- ❖ Fig. 4.24 B: epinephrine effect (100uM). FRTL-5 cells pre-loaded with PBS+100uM iodide (10'). Perfusion with NFA/TA 100uM inhibited rapid epinephrine-stimulated iodide efflux: NFA partly, TA completely, producing, also in this case, a increased basal iodide level, as shown with fluorescence baseline lowering after acquisition pause, compared to control.

- ❖ Fig. 4.24 C: maximum rate graph for conditions described below with comparison between influx and efflux stages. TA inhibited iodide efflux and increased basal iodide level in a statistically significant manner, presumilbly for increased iodide retention inside cells (p< 0.01).

- ❖ Fig 4.24 (bottom): comparison between maximum rate graphs of ATP and epinephrine-stimulated iodide efflux response. TA and NFA blocked iodide efflux response in both cases (ATP and epinephrine).
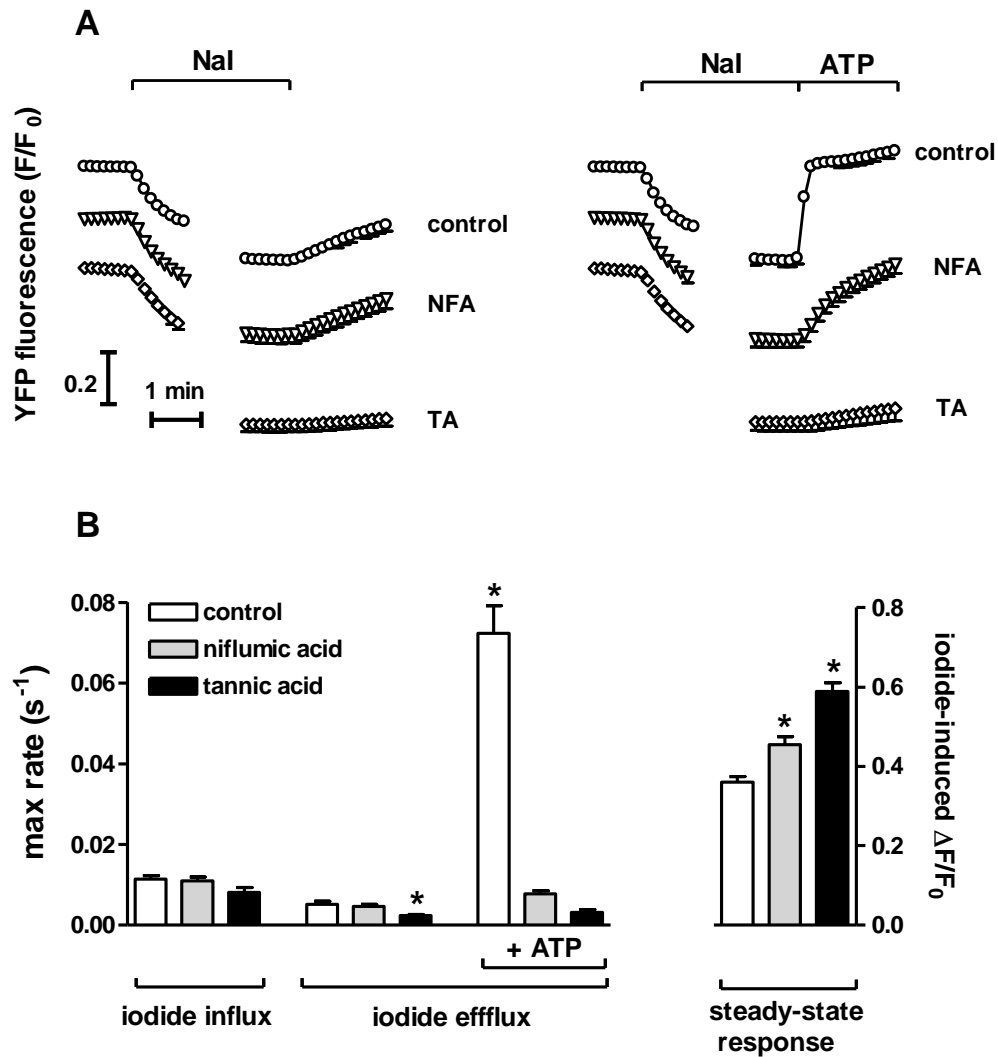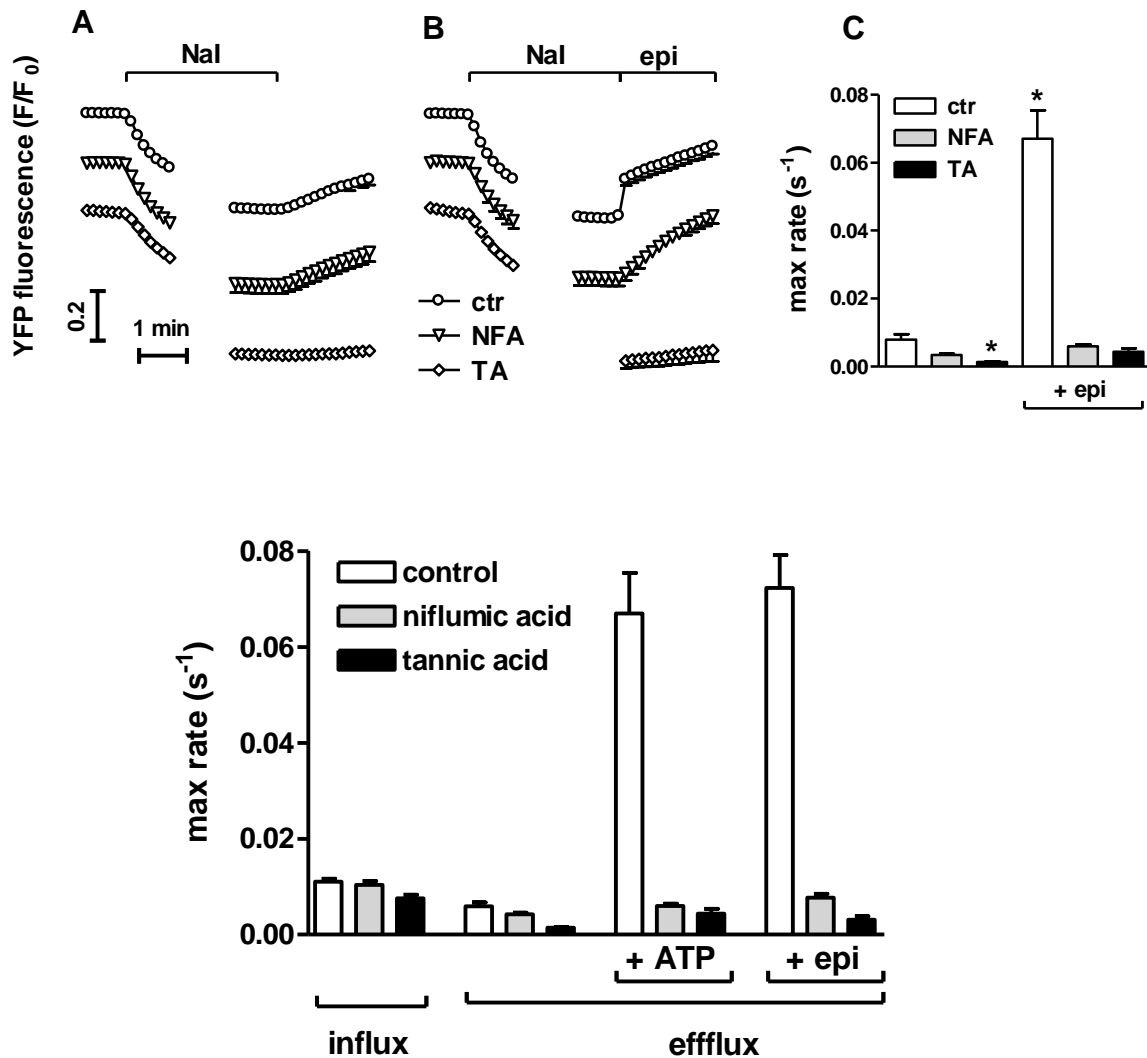
Fig. 4.24. Fluorescence signals are showed as F/F_0. A: FRTL-5 cells perfused with PBS+/- NFA/TA (100uM) (control). B: FRTL-5 cells perfused with PBS+/- NFA/TA (100uM) (+epinephrine 100uM). C: maximum rate graph for conditions described below. Statistical analysis performed with ANOVA one way method (p< 0.0001), and Dunnett's multiple comparison post test to compare every treatment with control. (* : p< 0,01). Bottom: comparison between maximum rate graphs of ATP and epinephrine-stimulated iodide efflux response. Data points or bars represent means ± standard errors of measurements.

<u>4.2.2.13 YFP protein binding assay with iodide efflux inhibitors</u>

Detected effect of iodide efflux inhibition was tested, to understand possible non specific effects of inhibitors rather than an actual effect on CaCC in FRTL-5 cells during iodide efflux stage. Niflumic acid (NFA) and tannic acid (TA) were tested.

❖ Fig. 4.25 A: Fluorescence signals are showed as F/F_0; FRTL-5 cells were perfused with PBS+/- NFA/TA (100uM) (5') (control). TA produced quenching of YFP resting fluorescence (10%) , while NFA quenched resting YFP fluorescence more (25%), plateaux reached after 5' and complete fluorescence recovery after other 5'.

To detect mechanism which altered YFP fluorescence by inhibitors, possible intracellular pH variations and binding with YFP were considered in different buffers (SPB and HEPES).

❖ Fig. 4.25 B: detection of inhibitors-dependent intracellular pH variations. FRTL-5 cells were perfused with PBS+/- NFA/TA (100uM) (5'). pH signal was detected with BCECF probe and resulted decreased (>10%) during exposition with NFA. TA showed no effect on intracellular pH.

❖ Fig. 4.25 C: YFP protein-binding assays with TA/NFA (0-100uM) (relative fluorescence, control fluorescence: 100%). NFA showed no effect on YFP purified protein fluorescence, while TA produced more quenching of YFP fluorescence at increasing TA concentrations employed (10-30-100 uM), up to 80% with 100uM TA..

❖ Fig. 4.25 D: affinity curve for iodide of TA(10uM) and NFA. Both of inhibitors produced no effect on YFP affinity for iodide.

Taken together, these results suggested that NFA effect on iodide efflux was due partially to its acidification effect inside cells but not to direct binding to YFP protein expressed exogenously by FRTL-5 cells. Different buffers used (SPB and HEPES) did not alter fluorescence YFP, which is only dose-dependent.

TA showed to have a effect on intracellular acidification and, interestingly, seemed to have a direct binding with YFP protein, since interaction between TA and YFP purified protein led to fluorescence quenching.
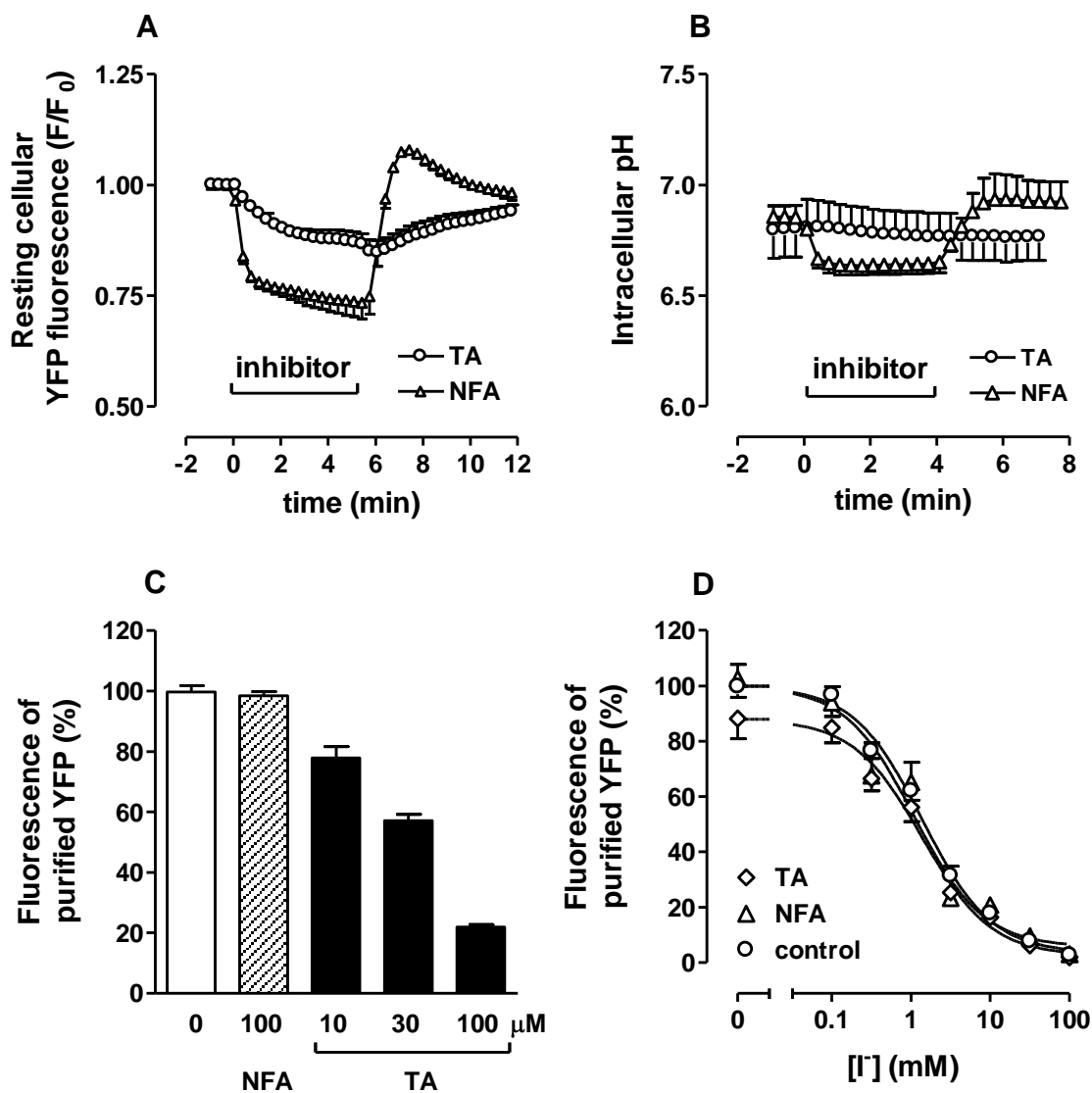
Fig. 4.25. A: Fluorescence signals are showed as F/F_0; FRTL-5 cells perfused with PBS+/-NFA/TA (100uM) (control). B: detection of inhibitors-dependent intracellular pH variations. C: YFP protein-binding assays with TA/NFA (relative fluorescence, control fluorescence: 100%). Data points or bars represent means ± standard errors of 3 measurements. D: affinity curve for iodide of TA and NFA. TA IC_{50} 1.4 mM (TA 10uM), Control IC_{50} 0.98 mM. (IC: intracellular concentration).

4.2.2.14 Effect of RNA interference on rTMEM16A transcript in FRTL-5

 Endogenous rTMEM16A transcriptional expression knock-down was performed with three different siRNAs specifically designed against TMEM16A (#75, #76, #77, Sigma) and three different constructs for delivery into cells.
FRTL-5 YFP-H148Q/I152L cells were treated to siRNA constructs for 2 or 5 days with three delivery systems:

❖ Fig. 4.26 A: FRTL-5 were exposed to N-TER nanoparticles™ and 100nM siRNAs against TMEM16A (#75, #76, #77, Sigma) for 2 days. The first experiment seemed to show a knock-down of rTMEM16A transcript, whose levels were almost 2 fold less than control samples, while the other experiments showed decreased rTMEM16A transcript also without specific siRNA (with buffer blank, universal negative control siRNA, no treatment). Low knock-down signals probably resulted by low transfection efficiency in FRTL-5 cells. This evidence suggested that system could be used but with optimized experimental conditions (n=3-4).
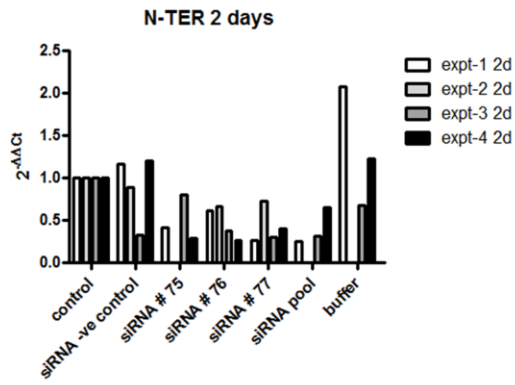
❖ Fig. 4.26 B: FRTL-5 were exposed to N-TER nanoparticles™ and 100nM siRNAs against TMEM16A (#75, #76, #77, Sigma) for 5 days. Not marked knock-down effect, observed after 2 days, was lost after 5 days of treatment, suggesting a short-term effect of mRNA silencing.

❖ Fig. 4.26 C: FRTL-5 were exposed to Lipofectamine 2000® (lipo) and to Superfect® (SF) and 50/100nM siRNAs against TMEM16A (#75, #76, #77, Sigma) for 2 days. No evidence of knock-down could be detected with this construct.

❖ Fig. 4.26 D: Mean + SEM graph for 2 days N-TER reagent treatment, for n=3 independent experiments. Exposure to specific siRNA against rTMEM16A produce a two-fold decrease in rTMEM16A expression compared to control.

Results appeared difficult to interpret so far, acid nucleic delivery conditions have to be improved to obtain reproducible and significant effects.

A

N-TER 2 days

Legend: expt-1 2d, expt-2 2d, expt-3 2d, expt-4 2d

X-axis: control, siRNA -ve control, siRNA # 75, siRNA # 76, siRNA # 77, siRNA pool, buffer

Y-axis: $2^{-\Delta\Delta Ct}$

B

N-TER 5 days

Legend: expt-2 5d, expt-3 5d, expt-4 5d

X-axis: control, siRNA -ve control, siRNA # 75, siRNA # 76, siRNA # 77, siRNA pool, buffer

Y-axis: $2^{-\Delta\Delta Ct}$

C

Superfect/lipofectamine 2 days

Legend: expt 1 SF 2d 50nM, expt 1 SF 2d 100 nM, expt 1lipo 2d 50nM, expt 1 lipo 2d 100nM

X-axis: control, siRNA -ve control, siRNA # 75, siRNA # 76, siRNA # 77, siRNA pool

Y-axis: $2^{-\Delta\Delta Ct}$

Fig. 4.26. RNA interference of rTMEM16A in FRTL-5 cells with different techniques. A: 2 days-treatment with N-TER™ nanoparticle and three different siRNA (100 nM) again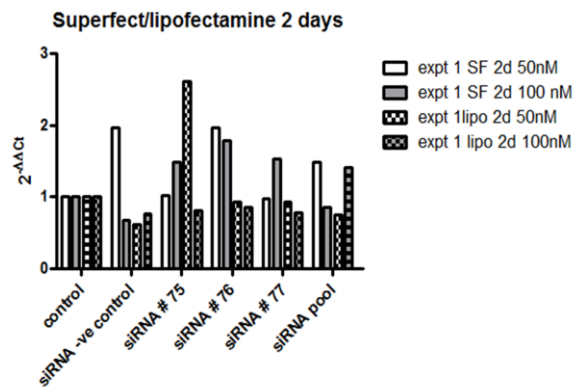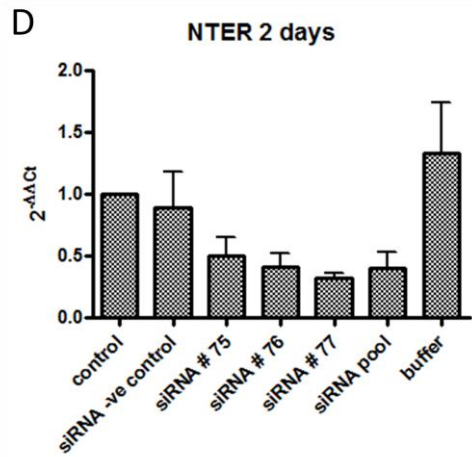st TMEM16A (*n*=3-4). B: 5 days-treatment with N-TER reagent.. C: 2 days-treatment with Superfect®, Lipofectamine 2000® and three different siRNA (50/100 nM) against rTMEM16A (*n*=1). D: Mean+SEM for siRNA treatment against rTMEM16A with N-TER reagent (2 days, n=3).

Effect of RNA interference of TMEM16A transcript on ATP-induced iodide efflux response in FRTL-5

After TMEM16A transcriptional expression knock-down and functional characterization of calcium-activated iodide efflux in FRTL-5, effects of TMEM16A mRNA interference was checked also at functional level, to detect any consequent variations in iodide efflux response .

FRTL-5 cells were treated to siRNA constructs for 2 days with three different siRNAs specifically designed against TMEM16A (100nM) SASI_Rn02_00230075, SASI_Rn02_00230076, SASI_Rn02_00230077 (Sigma), using N-TER nanoparticles™ (Sigma). (Single representative experiments, n=19-24 cells).
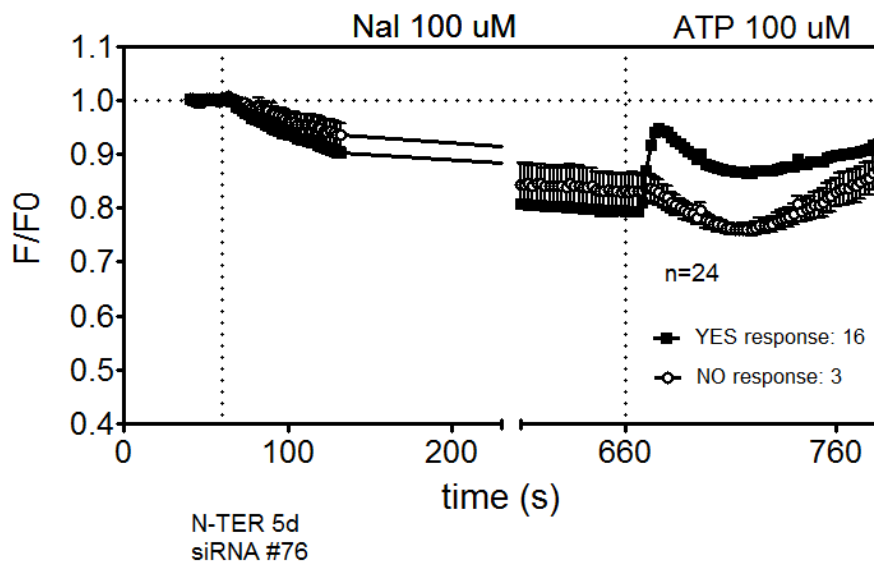
❖ Fig. 4.27 up: FRTL-5 cells, treated with specific siRNA#76 (100uM) against TMEM16A mRNA for 2 days, perfused with PBS+ATP 100uM in efflux stage, responding/not responding to ATP.

❖ Fig. 4.27 bottom: FRTL-5 cells, treated with universal negative control (100uM) for siRNA for 2 days, perfused with PBS+ATP 100uM in efflux stage, responding/ not responding to ATP.

Among the tested cells were excluded those that were unable to load iodide, probably because of toxicity effect of buffer or silencing-induced cellular stress, with resulting depriovation of a a gene product necessary for normal function, as putatively TMEM16A is for thyroid cells.

An effective suppression of the activation of efflux of iodide induced by ATP following treatment with the siRNA 76 (4.27). Considering, however, the toxic effects of treatment and the low transfection efficiency data are difficult to interpret.

Several cells treated with siRNA against TMEM16A showed blockade in ATP-induced iodide efflux. Response induced in the other cells probably was due to little efficacy of treatment, since FRTL-5 cells are characterized by low transfection efficiency. This evidence suggested that system could be used but with optimized experimental conditions.
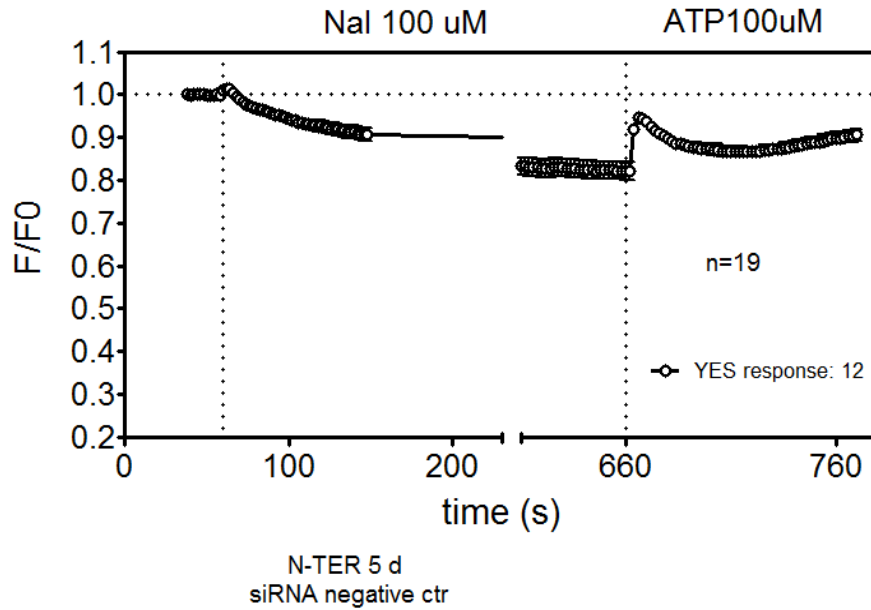
Fig. 4.27. Fluorescence signals are showed as F/F_0 . FRTL-5 cells preloaded with PBS+I- 100uM and perfused with PBS+/- ATP 100uM. Up: FRTL-5 cells, treated with specific siRNA#76 against TMEM16A mRNA, perfused with PBS+ATP 100uM in efflux stage, responding (16) or not responding (3) to ATP. Bottom: FRTL-5 cells, treated with universal negative control for siRNA, perfused with PBS+ATP 100uM in efflux stage, responding (12) to ATP. Single representative experiment for each figure. Black lines: mean signal from single cell in one experiment.

4.3 ONGOING EXPERIMENTS

 Recently, molecular analysis of TMEM16A was enriched with study of protein expression. This aspect was developed at Dr. Diego Alvarez De La Rosa Rodríguez's laboratory, Pharmacology Unit, Canary University Hospital, La Laguna University, Tenerife.

4.3.1 DETECTION OF hTMEM16A-EYFP PROTEIN IN CHO K1 hTMEM16A CELLS

 First of all, hTMEM16A was expressed in CHO K1 cells transiently. Membrane proteins were obtained from CHO K1-hTMEM16A cell samples and tested with 2-D electrophoresis. Before performing proteomic experimental set, prediction of

hTMEM16A isoelectric point and molecular weight was calculated with specific software found on http://scansite.mit.edu/. Check of human TMEM16A protein NCBI Reference Sequence, NP_060513.5, and EYFP sequence showed predicted molecular weight of 114,1 kDa and 11,3 kDa respectively, and an isoelectric point of 8,76 and 5,90 respectively, in absence of phosphates groups. Addiction of more phosphate groups should make proteins more acid, as showed in section 3.2.11. According to these predictions, first dimension was tested with a 3-10 pH range, second dimension with 8,5% acrylamide concentration in electrophoresis gel. More than 100ug membrane proteins were loaded for each sample. Gel stained was made with Sypro Ruby® (Sigma), a fluorescent probe, and detected under UV light.

Fig. 4.28 shows two gels. The initial approach to detect the right spot pattern, coherent with hTMEM16A predicted parameters, was comparison between *wild type* CHO K1 and CHO K1 expressing hTMEM16A transiently.

- ❖ Left fig.: membrane fractions from *wild type* CHOK-1 (negative control) do showed no spot in 8-10 pH range. A group of spots could be detected, as expected, at 6-7 pH range.

- ❖ Right fig.: membrane fractions from CHOK-1-hTMEM16A showed a group of close spots: interestingly, after electrophoretic migration, this spot group, not detected in control samples, was localized in a region coherent with hTMEM16A predicted molecular weight and isoelectric point (114,1 kDa and 8,76 pH). Also here, as found in control samples, a group of spots could be detected at 6-7 pH range, with a shift on the right compared to control, maybe due to a sample artefact.

- ❖ Comparing the two gels (control/exogenous hTMEM16A) some protein spots detected in recombinant system were absent in negative control. Their location was actually compatible with predicted isoelectric point and molecular weight.

This preliminary result (*n*=1) suggested that proteomic approach could be used to detect proteins with migration pattern compatible with hTMEM16A. One or more spots could be hTMEM16A protein signals, suitable for next sequencing with MALDI-TOF technique.

Fig. 4.28. Sypro Ruby® staining of 2-D electrophoresis gel. First dimension: 3-10 pH range; second dimension: gel with 8,5% acrylamide. Left image: >100 ug membrane protein loaded (*n*=1) from *wild type* CHO K1. Right image: >100 ug membrane protein loaded (*n*=1) from CHO K1 expressing hTMEM16A transiently.

4.3.2 DETECTION OF hTMEM16A-EYFP PROTEIN IN CHO K1 hTMEM16A-EYFP CELLS

After the first preliminary result, detection system was performed: membrane protein samples from CHO K1 expressing hTMEM16A-EYFP fusion protein transiently were tested with Western Blot technique, detecting protein signal with monoclonal antibody against pan-FP, to have a specific spot to compare with the previous approach.

Fig. 4.29 shows two different acrylamide gels, to compare protein signal obtained with staining and antibody recognition and to identify putative hTMEM16A protein signal more precisely.

❖ Left: the same gel showed in lower fig. 4.29, membrane fractions from CHOK-1-hTMEM16A showed a group of close protein spots in 8-10 pH range.

❖ Right: 2-D electrophoresis of membrane fractions from CHOK-1-hTMEM16A-EYFP revealed two spots in 100-150 kDa range. Predicted

molecular weight of fusion protein was 125,4 kDa, coherent with detected signals, and isoelectric point 8,6 pH or less depending on phosphate groups added to TMEM16A during post-translational modification processes. Probably the lowest signal detected post-translational modification-free hTMEM16A-EYFP form, the highest detected a protein form with two putative post-translational modifications: one phosphorylation, which decreases pI, and one glycosylation, which increases molecular weight.

Taken together, these preliminary results suggested that proteomic approach could be employed to characterize hTMEM16A protein in several aspects, such as post-translational modifications, and represent another useful protein detection system to be compared with specific antibodies recognition, once available.

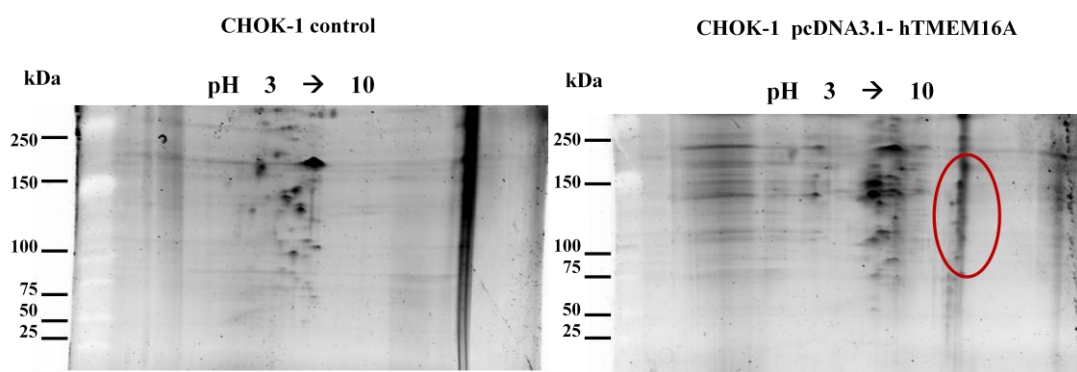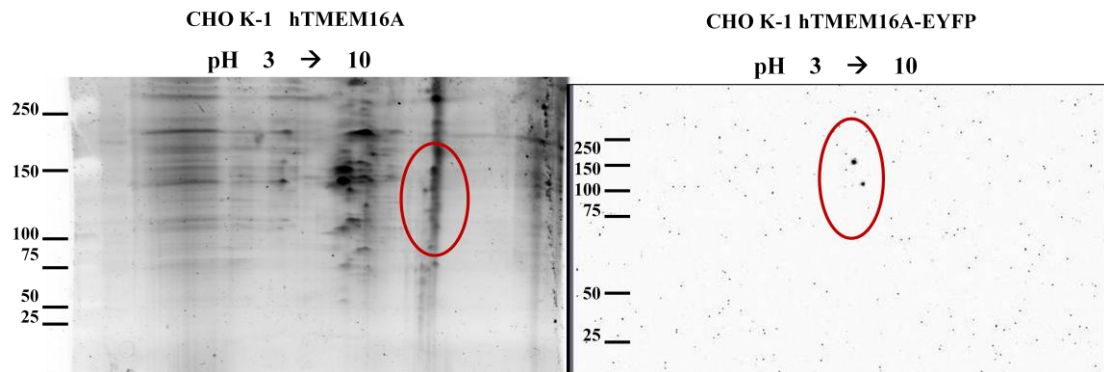**Fig. 4.29. Left image: Sypro Ruby® staining of a 2-D electrophoresis gel. First dimension: 3-10 pH range; second dimension: gel with 8,5% acrylamide. >100 ug membrane protein loaded (*n*=1) from CHO K1 expressing hTMEM16A transiently. Right image: Western Blot of a 2-D electrophoresis gel. >100 ug membrane protein loaded (*n*=1) from CHO K1 expressing hTMEM16A-EYFP transiently.**

CHAPTER 5

DISCUSSION

Topic of our research is iodide transport in thyroid follicular cells. Iodide influx into thyrocytes through their basolateral membrane is well known, but less is known about iodide efflux through apical membrane, towards the follicular lumen. Among the feasible involved proteins, a novel calcium-activated chloride channel, TMEM16A/ANO1 (Galietta et al., 2008, Yang et al., 2008, Schroeder et al, 2008), seems to have adequate properties to exert a role in this activity. This channel belongs to a family of protein, "anoctamins", with specific structural and functional features: eight transmembrane domains and involvement in anion transport. So far, known members of this family are ten in humans, called TMEM16A/ANO1, TMEM16B/ANO2 up to TMEM16K/ANO10) (Schreiber et al., 2010).

Published results on mouse tissues (Schreiber et al., 2010) showed that ANO1, 6, 7, 8, 9, 10 were mostly expressed in epithelial tissues, while ANO2, 3, 4, 5 were common in neuronal and muscle tissues. When expressed in Fisher Rat Thyroid (FTR) cells (polarized but not differentiated cell line), all anoctamins localized to plasma membrane but only ANO1, 2, 6, and 7 produced CaCC. ANO1, ANO6 and 10 produced chloride currents, very different on to each other. It seemed that each tissue was characterized by its own anoctamin expression pattern, a tissue-specific set, to produce tissue specific CaCC (Ca^{2+} activated chloride conductance) (Schreiber et al., 2010).

Gene expression profiles, available on BioGPS portal (http://biogps. gnf.org), suggested that TMEM16A was expressed in tissues (human, mouse, rat) with different levels and, particularly, up-regulated in some tumours (i.e. human colon carcinoma). In human thyroid gland TMEM16A seemed to be expressed more than background expression levels.

According to this, TMEM16A was chosen as a object of study, putative responsible of CaCC in thyroid gland, among other anoctamins with a known CaCC function: TMEM16A/ANO1, TMEM16B/ANO2, TMEM16B/ANO2, TMEM16F/ANO6, TMEM16H/ANO8, TMEM16K/ANO10 (Schreiber,2010, Suzuki, 2004). Activity of TMEM16A and TMEM16B was more marked than the other, but TMEM16B seemed to be not expressed in thyroid gland (Schreiber, 2010). Finally, research focused on TMEM16A. Besides, cells expressing TMEM16A show channels with the following permeability sequence to anions: $NO_3^- > I^- > Br^- > Cl^- > F^-$ (Yang, 2008): evidence of permeability to iodide higher than chloride, supported our hypothesis about involvement of TMEM16A in iodide flow in thyroid follicular cells.

The first important result was TMEM16A mRNA expression in human normal thyroid gland.

Then, also its expression in human tumour thyroid gland was considered. Screening was performed on coupled samples (normal and tumour portion from the same patient with thyroid papillary tumour). It revealed that TMEM16A mRNA was maintained in thyroid cancer.

Besides, it was investigated if TMEM16A transcript expression could undergo regulation by TSH. TSH is the main regulator hormone of thyroid gland. To study TSH effect on TMEM16A transcript in thyroid gland, FRTL-5 cell lines (Fisher rat normal thyroid gland follicular cells) were used as a model, suitable for functional experiments and established for a long time and employed in many studies on thyroid.

We found that FRTL-5 expressed TMEM16A transcript with RT-PCR experiments, so resulted to be suitable as a model also for next studies. Moreover, QRT-PCR experiments showed that TSH did not regulate TMEM16A in FRTL-5, suggesting that apical iodide efflux was constitutive. FRTL-5 not exposed to TSH did not express NIS mRNA, confirming actual TSH effect.

Characterization of TMEM16A continued with detection of its alternative *splicing* isoforms mRNA in FRTL-5 cells. TMEM16A protein has got four segments subject to alternative *splicing* of their codified mRNA, each isoform contains or not a specific segment ("a", "b", "c", "d"). Particularly some works (Ferrera et al., 2011), showed correlation between *splicing* isoforms and functional properties. Every transcript, in

fact, produces a protein isoform containing or not codified peptide segments. Alternative *splicing* of TMEM16A transcript could be a system for channel tissue-specificity, based on functional properties as voltage-dependence as calcium sensitivity (Ferrera et al., 2011). "B" and "c" segments seemed to be inside a region important for calcium sensitivity and membrane potential dependence. Primers for b, c and d segments were designed outside of each segment to distinguish segments expressed in TMEM16A mRNA (Manoury, 2010). Therefore, we observed that TMEM16A/anoctamin-1 alternative *splicing* mRNA isoforms expressed in FRTL-5 cells did not contain d segment, instead c segment was constitutively expressed.

Next step was investigation of expression profile of other members belonging to anoctamin family as well as TMEM16A/ANO1 in FRTL-5 cells, to discover if some members could be suitable targets of further functional studies on iodide transport in thyroid gland. All anoctamin expression was detected with RT-PCR experiments. Results showed that TMEM16A/ANO1, TMEM16F/ANO6, TMEM16H/ANO8, TMEM16K/ANO10 mRNA were expressed in FRTL-5 cells. The other members, TMEM16C/ANO3, TMEM16D/ANO4, TMEM16E/ANO5, TMEM16G/ANO7, resulted to be expressed weakly and in a variable manner. Instead, TMEM16B/ANO2 and TMEM16J/ANO9, showed no signal but their specific primers were designed on mouse sequences instead of rat, because rat TMEM16A coding sequences were still not registered.

To confirm TMEM16A mRNA expression with an alternative approach, transcriptional expression knock-down was performed with three different siRNAs (100nM) specifically designed against TMEM16A. Best results were obtained with a peptide-based transfecting agent, N-TER nanoparticles™, after 2 days treatment. Experiments showed knock-down of rTMEM16A transcript. Low knock-down signals probably resulted by low transfection efficiency in FRTL-5 cells. The same approach was performed in FRTL-5 cells tested with functional assay. Several cells treated with siRNA against TMEM16A showed blockade in ATP-induced iodide efflux.

This evidence suggested that system could be used, optimizing experimental conditions, and in previous studies it revealed successful (i.e. on bronchial epithelium cell lines, Galietta, 2008).

FRTL-5 cells are from Fisher rat normal thyroid gland and express all thyroid markers. After previous selection of stable clones in our laboratory (Rhoden et al., 2007) FRTL-5 cells expressed stably an exogenous protein, YFP-H148Q/I152L. YFP-H148Q/I152L is a fluorescent protein that results very useful as a halide biosensor, particularly it has got high affinity for iodide. Its fluorescence signal is quenched when iodide enters the cells, compared to baseline, but recovers when iodide flows out of the cells.

To begin the characterization of calcium-activated iodide conductance in FRTL-5, putatively mediated by TMEM16A in our hypothesis, experiments were performed to study iodide influx as a model of chloride, with a partial substitution of chloride with iodide. Iodide flows into thyrocytes through NIS, so it was necessary deletion of its contribute to iodide transport to analyze only iodide flow via other channels, such as putative TMEM16A. Therefore, FRTL-5 cells were cultured for at least one week without TSH hormone, to inhibit NIS expression. TSH is the most relevant regulator of growth and differentiation of thyroid gland. Among TSH fundamental functions there are induction of NIS transcriptional and protein expression, NIS transport to cell membrane (Carrasco et al, 2003).

Iodide influx, in FRTL-5 not exposed to TSH, took place only at high iodide concentrations (mM), via channels (i.e. chloride channels) less specific for iodide than NIS, not expressed in this condition. Response of iodide influx, by cells cultured with TSH, was evoked by both chloride channels and NIS, if exposed to 100mM iodide.
Calcium-activated chloride conductance was stimulated by purine nucleotides, such as UTP (Galietta et al., 2008). Then, nucleotides were tested to characterize it, particularly in FRTL-5 cell lines model, to verify if they stimulated chloride influx via TMEM16A CaCC channel. CaCC are activated by intracellular calcium concentration increase, event provoked also by nucleotides.

Two mechanisms for intracellular calcium increase can be theorized: (i) nucleotides bind to P2X purinergic receptors, which stimulate sodium influx and, accordingly,

membrane action potential variation that provokes voltage-dependent calcium channels opening; (ii) nucleotides bind to P2Y purinergic receptors, G_q-coupled, with consequent activation of PLC, which causes IP_3 increase and, accordingly, calcium release from intracellular stores.

At the end, result is intracellular calcium-activated influx of calcium again, via store-operated channels (SOC). Our experiments confirm this mechanism and indicate that P2Y purinergic receptors could be involved, because observed order of nucleotide potency on receptors was ATP > UTP > ADP in FRTL-5, as it happens on P2Y receptors. Differences on fluorescence reflected differences on iodide entry into FRTL-5, due to different potency of nucleotides on their own receptors. Indirectly such a difference suggested a different affinity of nucleotides on studied channels activity. Order of nucleotide potency is compatible with P2Y purinergic receptors.

Another aspect analyzed was behaviour of CaCC when cell membrane was depolarized in FRTL-5 cells. Perfusion with K-PBS provoked depolarization in cell membrane of FRTL-5. Also with less than 1uM ATP, iodide influx was higher, confirming a property of TMEM16A already described: increased activation in depolarization conditions. Since CaCC are active with membrane potential depolarization condition (Galietta et al., 2001), used PBS contained 100mM K^+Cl^- instead of 100mM Na^+Cl^-.

Taken together, these evidences suggested presence of a thyroid CaCC, TMEM16A, as a putative molecular target.

Calcium can active and open channels directly or through calcium-calmodulin complex, with activation of calmodulin-dependent kinase II, that phosphorylates channels. Intracellular calcium increase, stimulated by ionomycin, a ionophore selective for calcium, was actually responsible for iodide influx in our cell model. Lack of extracellular calcium in perfusion solution (PBS) allowed iodide influx. Next step was to establish origin of calcium capable to activate channels. Perfusing cells with Ca^{2+} free PBS, but chelating also intracellular calcium with BAPTA compound,

iodide influx could not take place into FRTL-5 cells. This evidence suggested activation of channels by calcium released from intracellular store organelles only.

Our results were compatible with the expression of a CaCC (Ca $^{2+}$ activated chloride conductance/ channel) such as TMEM16A in FRTL-5.

After, since channels responsible of iodide apical efflux are not all known, our work focused on a potential role of TMEM16A in iodide transport, as well as chloride, in thyroid, for iodide accumulation in the follicular lumen.

To begin characterization of iodide efflux, the same previous experimental conditions were reproduced, such as presence of absence of extracellular calcium in PBS, presence of absence of intracellular calcium released by storage organelles, chelated by BAPTA compound. Before undertaking a depth study about FRTL-5 thyroid cells, iodide transport was characterized in a model cell system, CHOK-1 cell lines, to find and optimize the best experimental conditions and to confirm functional properties of currents due to TMEM16A.

First of all, the chosen experimental model CHOK-1 cells, were considered about the endogenous TMEM16A mRNA expression. No TMEM16A transcript expression was observed, thus CHOK-1 cell lines were chosen as a model definitively, since *wild type* cells were a good negative control. Clones of CHOK-1 stably expressing hNIS and YFP-H148Q/I152L were selected and established previously in our laboratory. Absence of endogenous TMEM16A mRNA expression was confirmed. Besides, maintenance of hNIS and YFP-H148Q/I152L expression after long culture and cryopreservation periods, was verified.

Characterization continued on calcium-activated iodide conductance in efflux, due to hTMEM16A transporter, expressed in stable clones CHOK-1-hNIS/YFP-H148Q/I152L transiently. Aim was observation efflux properties, to have a model of functional response and, going on with studies on FRTL-5, making a comparison between obtained results and expected observed in the model system.

Thus, analogous experiments were performed, similar to experiments made to study iodide influx. PBS contained ionomycin, to stimulate intracellular calcium concentration increase, at 1uM concentration. First of all, clones without TMEM16A exogenous expression showed no iodide transport due to other endogenous transporters such as members of anoctamin family. Then, CHOK-hNIS/YFP-H148Q/I152L stable clones, with transient hTMEM16A expression, were checked. After initial fluorescence decrease, due to extracellular iodide entry, exposition to PBS only let the "wash-out" of intracellular iodide but slowly (20'), not detectable during the short time interval considered (usually 5'). Instead, exposure of cells to PBS+1uM ionomycin provoked a rapid fluorescence decrease, due to iodide efflux out of cells.

Observed properties of calcium-activated iodide efflux were compatible with known properties of TMEM16A calcium-activated channel.

Thus, FRTL-5 expressing NIS were employed. They were subjected to iodide pre-loading, mediated by NIS, responsible only for iodide influx. Experiments similar to influx were performed, but on the iodide efflux stage, testing nucleotides (ATP, UTP, ADP 100uM) and ionomycin-activated intracellular calcium increase.
Our results showed actual iodide efflux increase due to ionomycin exposition, as detected by starting fluorescence recovery, in a few seconds, instead of 20 minutes requested usually.

Screening with receptor agonists was performed to detect their effect on iodide efflux.
First of all TSH, histamine, acetilcholin, serotonin, dopamin were tested. TSH was found to generate a I-/Cl- current in FRTL-5 cells (electrophysiological studies , Yoshida et al. of 1999) but in our system produced no effect, likely because of different sensitivity of technique.
Histamine is present in mast cells residing in thyroid gland (Melander et al., 1973), seretonin is able to activate intracellular pathways that culminate in increased cytoplasmic calcium in cells FRTL-5 (Tamir et al., 1992), and stimulates iodide organification and thyroid hormones synthesis (Melander, 1970), but no effect was detected our experiments.

Thyroid gland is innervated by cholinergic nerves (Van Sande et al., 1980) and acetylcholine is able to stimulate the efflux of radioiodide in FRTL-5, interacting with muscarinic receptor (Di Girolamo et al. 1991), but in our system produced no effect.

Dopamine was found to induce organification of iodide and is present in mast cells residing in thyroid gland and in parafollicular cells (Melander et al., 1973). No effect on iodide efflux was detected in our experimental system.

Since thyroid gland is innervated by sympathetic nervous system (Tice and Creveling, 1975) and catecholamines (including epinephrine and norepinephrine) stimulate the synthesis of thyroid hormones (Melander, 1970), we wanted to test some endogenous catecholaminergic receptor agonists epinephrine and norepinephrine.
Epinephrine and norepinephrine, can interact with all the adrenergic receptors ($\alpha 1$, $\alpha 2$, $\beta 1$, $\beta 2$, $\beta 3$), thus, to identify receptor that mediates effect of these agonists on iodide efflux in FRTL-5 B5 cells, were tested two more selective exogenous adrenergic agonists: phenylephrine, which binds $\alpha 1$ receptors, and isoprenaline, which interacts with β receptors.
Epinephrine and norepinephrine were able to stimulate iodide efflux strongly, also at 1uM. It was demonstrated that phenylephrine, unlike isoprenaline, was able to stimulate iodide efflux, even though it is much less potent endogenous agonists. From this result, it can be concluded that adrenergic agonists act in FRTL-5 cells through $\alpha 1$ receptor.

Since ATP is able to stimulate calcium-activated channels interacting with purinergic receptors (Verkman and Galietta, 2009), was evaluated its effect on iodide efflux in FRTL-5 cells.
ATP, epinephrine and norepinephrine were found to stimulate iodide efflux more than other tested previously. ATP was more effective than epinephrine and norepinephrine in channel activation, because fluorescence recovers more rapidly (1'-2'), anyway epinephrine and norepinephrine very potent in iodide efflux stimulation also at low concentrations (uM). Channel activity is dose-dependent.
Iodide efflux increased stimulated also with exposition to purine nucleotides, as detected by starting fluorescence recovery, virtually instantly, instead of 20 minutes

requested usually. Also in efflux we found the same nucleotide potency order ATP > UTP > ADP on involved receptors.

Another property compatible with TMEM16A is its transient activation, characteristic we found in iodide efflux activity in FRTL-5 cells. Iodide efflux was stimulated by ATP and ionomycin in FRTL-5; afterwards (in 10') with contemporary presence of iodide and ATP/ionomycin, they accumulated iodide again. Hence, activation of channels involved in iodide efflux seems to be transient, fact that suggested CaCC are characterized by a refractory period, in which their status is inactive.

To distinguish the precise class of adrenergic receptors involved in iodide efflux, we needed more selective exogenous agonists, because epinephrine and norepinephrine are not so specific (they can bind to all of kinds, α_1, α_2, β_1, β_2, β_3). Phenylephrine, which binds α_1 receptors, and isoproterenol, which binds all β receptors, were used for this aim. Only phenylephrine could stimulate iodide efflux in FRTL-5 cells. Isoproterenol could not stimulate iodide efflux, but it was observed also that intracellular calcium increase was lower than phenylephrine-induced. This is coherent with existence of a threshold level of calcium for activation of channel involved in iodide efflux.

Also in experiments on iodide efflux, origin of calcium capable to activate channels was established. Chelation of intracellular calcium with BAPTA compound, in FRTL-5 cells perfused with Ca^{2+} free PBS, did not allow iodide efflux in FRTL-5 cells. This evidence suggested activation of channels by calcium released from intracellular store organelles only. Not only calcium-dependent iodide efflux response, but also ATP and epinephrine –dependent response were tested to know source of calcium responsible for iodide efflux. BAPTA pre-incubation /calcium-free perfusion solution revealed also in this case that, in FRTL-5 cells, response depended on increase of calcium from intracellular store organelles only.

According to recent studies (Caputo et al., 2008; Hartzell et al., 2009), niflumic acid (NFA) is a CaCC inhibitor. Use of NFA could identify mediator of iodide efflux.

NFA was used to check if it could inhibit stimulation of iodide efflux due to ATP. Tannic acid is a compound present in several natural products, i.e. green tea and red wine. TA seems to be a highly selective TMEM16A inhibitor (Namkung et al., 2010), putative responsible of iodide efflux in thyrocytes according to working hypothesis. Experiments on I⁻ efflux demonstrated their effectiveness in inhibiting effect of ATP stimulation, but, these compounds have been shown to be highly specific for TMEM16A channel and being characterized by certain properties that can influence the evaluation of data obtained. Niflumic acid and tannic acid inhibitors were showed to change basal fluorescence in FRTL-5 YFP used in our experiments. To detect any non specific effect, pH changes (with BCECF probe-based functional assay) and direct interaction with YFP protein was checked.

Niflumic acid led to intracellular pH decrease, tannic acid was shown to have a direct binding of YFP purified protein without changing in iodide affinity. Interestingly, tannic acid increased basal iodide levels.

Finally, through cloning expression, a fusion protein between hTMEM16A and EYFP (Enhanced YFP) (C-term *tag*), was expressed transiently in a exogenous system, CHOK-1 cells. CHOK-1-hTMEM16A-EYFP cell samples (membrane fractions), were tested with 2-dimensional (2-D) electrophoresis gel. Detection was performed with Western Blot, using a specific antibody against GFP and all its variant. Isoelectric point and molecular weight of recombinant protein were predicted with software found on http://scansite.mit.edu/ webpage (respectively, 8.6 and 125,43 kDa). 2-D gel electrophoresis pointed out two protein signals compatible with theoretical values of hTMEM16A-EYFP fusion protein, located beyond pH 7 and between 100 and 150 kDa (preliminary result). Moreover, presence of two signals is compatible with some post-translational modifications undergone by proteins, such as glycosylations (higher molecular weight), phosphorylations (isoelectric point lower), acetylations (isoelectric point lower). Actually TMEM16A has a conserved N-linked glycosylation site between seventh and eighth transmembrane domain (Hartzell, 2009).

Our working hypothesis is based on a putative role of TMEM16A channel in iodide efflux in thyroid. Iodide flows into thyrocyte through basal membrane via NIS, that lets its intracellular accumulation and concentration up to 100 times more, compared to cytoplasm. Then, iodide diffuses into follicular lumen through apical membrane via other channels, such as pendrin. ATP and other less specific nucleotides active TMEM16A (or other CaCC), iodide flows out of thyrocyte into follicular lumen in a rapid and transient manner. Inactivated channel cannot transport iodide out, so high intracellular iodide concentration can be recovered via NIS.

Thyroid shows expression of purinergic receptors and is innerved by ANS nervous fibers. Nucleotides as ATP may be involved as cotransmitters. Their functional role could be thyroid hormone synthesis increase, and our experiments confirm this putative function, since iodide can be more available (more influx and efflux).

ATP is necessary for homeostasis and energy production for body metabolism and is produced ubiquitously. In nervous system districts and inflammatory tissues higher ATP levels were found, also released by inflammatory cells (Pellegatti et al., 2008). Inflammatory responses and high metabolic activities take place around and inside tumour cells, events which would explain high extracellular ATP levels around tumour cells.

Activation of calcium-activated iodide conductance in efflux, mediated by TMEM16A, could be one reason of poor results of radioiodide-therapy applied to some patients. Some classes of thyroid cancer with poor prognosis, as metastatic and anaplastic, do not response to therapy because not able to load radioiodide anymore. NIS transporter is little or not expressed, with consequent less iodide influx, factor that makes more difficult their treatment. Besides, efficacy of radioiodide-therapy depends upon not only iodide influx via NIS, but also iodide retention inside thyroid tumour cells and iodide lost, caused by its efflux. Tumour cells are little or not polarized, so they lack normal follicular architecture that allows iodide accumulation. The more extracellular ATP is produced there, the more would be iodide efflux and lost from tumour cells. Pharmacological characterization of inhibitors of channel involved in this activity, such as TMEM16A, could lead to improve the current therapy.

CHAPTER 6

CONCLUSIONS

Our working hypothesis asserted that molecular responsible of iodide efflux in FRTL-5 cells was TMEM16A protein. This channel transports Cl^-/I^- in a $Ca2^+$ - dependent manner, properties of CaCC activity. Research was performed to characterize iodide efflux activity and discover if could have properties coherent with TMEM16A.

Molecular evidences:

❖ TMEM16A mRNA wss expressed in human normal and tumour thyroid gland and in FRTL-5 cell lines;

❖ TMEM16A mRNA was not dependent on TSH hormone in FRTL-5 cells;

❖ TMEM16A mRNA alternative *splicing* isoforms expressed in FRTL-5 cells were "abc" and "ac";

❖ anoctamins expressed in FRTL-5 cells were: TMEM16A, F, K, H;

Functional evidences (iodide influx):

❖ iodide transport is coherent with TMEM16A functional properties:

❖ activation due to ATP, UTP, ADP had potency order ATP> UTP> ADP, typical of P2Y purinergic receptors, probably involved in this transduction pathway in FRTL-5 cells;

❖ affinity of nucleotides on their own receptors increased in depolarization conditions in FRTL-5 cells;

❖ activation of iodide influx was due to calcium released from intracellular stores in FRTL-5 cells, and is extracellular calcium-independent

Molecular evidences:

❖ CHO K1-NIS/ YFP- expressing cells showed no endogenous mRNA expression of hTMEM16A;

Functional evidences (iodide efflux):

❖ CHO K1-NIS/ YFP- hTMEM16A expressing cells showed calcium-activated iodide efflux;

❖ activation of calcium-induced iodide efflux was due to calcium released from intracellular stores in FRTL-5 cells, and is extracellular calcium-independent;

❖ ATP and epinephrine stimulated iodide efflux in FRTL-5 cells;

❖ activation due to ATP, UTP, ADP had potency order ATP> UTP> ADP, typical of P2Y purinergic receptors, probably involved in this transduction pathway in FRTL-5 cells;

❖ iodide efflux calcium-dependent activation was transient in FRTL-5 cells;

❖ epinephrine and norepinephrine agonists activated iodide efflux at uM concentrations in FRTL-5 cells;

❖ prazosin and phentolamine antagonists blocked epinephrine-activated iodide efflux in FRTL-5 cells;

- ❖ epinephrine, norepinephrine and isoproterenol increased intracellular calcium levels in FRTL-5, but isoproterenol with not marked entity, not enough to elicit a calcium-activated iodide efflux response;

- ❖ activation of epinephrine-induced iodide efflux was due to calcium released from intracellular stores in FRTL-5 cells, and is extracellular calcium-independent;

- ❖ ATP/epinephrine-dependent Ca2+-activated iodide efflux was inhibited by specific inhibitors such as niflumic acid and tannic acid in FRTL-5 cells;

- ❖ tannic acid blocked iodide efflux but also increased basal intracellular iodide levels in FRTL-5 cells;

- ❖ niflumic acid led to decrease in intracellular pH in FRTL-5 cells;

- ❖ tannic acid seemed to have a direct binding with YFP protein in FRTL-5 cells;

- ❖ specific siRNA against TMEM16A knocked-down its transcriptional expression in FRTL-5 cells but result has to be confirmed;

- ❖ RNA interference treatment against TMEM16A provoked inhibition of ATP-dependent iodide efflux response in FRTL-5 cells which sufficiently received interfering construct.

Novel approaches for characterization of anoctamins:

- ❖ 2-D electrophoresis on CHO K1 expressing hTMEM16A-YFP fusion protein revealed two spots, recognized by specific antibodies against YFP, with isoelectric point and molecular weight compatible with hTMEM16A protein, suggesting its post-translational modifications such as glycosylation and phosphorylation.

In conclusion, we demonstrated a calcium-activated iodide conductance in efflux, with properties compatible with CaCC/TMEM16A activity. These results suggest that TMEM16A does play a role in mediation of iodide efflux in thyroid gland.

CHAPTER 7

PERSPECTIVES

❖ Sequencing of anoctamins transcripts expressed in FRTL-5 cells

❖ Western Blot and immunocytochemistry to detect TMEM16A protein in FRTL-5 cells with specific antibodies

❖ Optimization of RNA interference assay on TMEM16A transcript in FRTL-5 cells

❖ Complete functional characterization of iodide efflux in FRTL-5 cells with CaCC inhibitors, receptor agonists/antagonists

❖ New experiments with 2-D SDS-PAGE and sequencing of TMEM16A protein with gas-mass spectrometry (MALDI-TOF, time-of-flight mass spectrometer) to detect *splicing* isoforms expressed in FRTL-5 cells

❖ Detection of post-translational modification of TMEM16A protein in FRTL-5 cells with proper enzymatic treatments

❖ Application of these technique to rat and human thyroid tissues to investigate TMEM16A and the other anoctamins expression

❖ Study of interaction between TMEM16A splicing isoforms one to each other and with other anoctamins, to detect involvement in CaCC activity in thyroid, specifically of iodide efflux.

BIBLIOGRAPHY

Akinc A., Thomas M., Klibanov AM., Langer R. (2004). Exploring polyethylenimine-mediated DNA transfection and the proton sponge hypothesis". Journal of Gene Medicine **7** (5): 657–663.

Ambesi-Impiombato F. S. et al., "Colture of hormone-dependent functional epithelial cells from rat thyroids" Proc Natl Acad Sci 77, 6 3455-3459 , 1980

Armstrong, J. W., Cragoe, E. J., Jr., Bourke, J. R., Huxham, G. J., and Manley, S. W. (1992). Chloride conductance of apical membrane in cultured porcine thyroid cells activated by cyclic AMP. Mol Cell Endocrinol 88, 105-110.

ATCC ,The Global Bioresource Center "www.atcc.org"

Baschieri, L., Benedetti, G., Deluca, F., And Negri, M. (1963). Evaluation And Limitations Of The Perchlorate Test In The Study Of Thyroid Function. J Clin Endocrinol Metab 23, 786-791.

Bera, T. K., Das, S., Maeda, H., Beers, R., Wolfgang, C. D., Kumar, V., Hahn, Y., Lee, B., and Pastan, I. (2004). NGEP, a gene encoding a membrane protein detected only in prostate cancer and normal prostate. Proc Natl Acad Sci U S A 101, 3059-3064.

Bidart JM., Mian C., Lazar V., Russo D., Filetti S., Caillou B., Schlumberger M., 2000, Epression of pendrin and the Pendred syndrome (PDS) gene in human thyroid tissues. J Clin Endocrinol Metab 85, 2028-2033

Bizhanova, A., and Kopp, P. (2009). Minireview: The sodium-iodide symporter NIS and pendrin in iodide homeostasis of the thyroid. Endocrinology 150, 1084-1090.

Boland, A., Ricard, M., Opolon, P., Bidart, J. M., Yeh, P., Filetti, S., Schlumberger, M., and Perricaudet, M. (2000). Adenovirus-mediated transfer of the thyroid sodium/iodide symporter gene into tumors for a targeted radiotherapy. Cancer Res 60, 3484-3492.

Bonora, E., Porcelli, A. M., Gasparre, G., Biondi, A., Ghelli, A., Carelli, V., Baracca, A., Tallini, G., Martinuzzi, A., Lenaz, G., et al. (2006). Defective oxidative phosphorylation in thyroid oncocytic carcinoma is associated with pathogenic mitochondrial DNA mutations affecting complexes I and III. Cancer Res 66, 6087-6096.

Cahmann HJ., Pommier J., Nunez J., 1977, Spatial requirement for coupling of iodotyrosine residues to form thyroid hormone. Proc Natl Acad Sci 74, 5333-5335.

Caillou, B., Troalen, F., Baudin, E., Talbot, M., Filetti, S., Schlumberger, M., and Bidart, J. M. (1998). Na$^+$/I$^-$ symporter distribution in human thyroid tissues: an immunohistochemical study. J Clin Endocrinol Metab 83, 4102-4106.

Caputo, A., Caci, E., Ferrera, L., Pedemonte, N., Barsanti, C., Sondo, E., Pfeffer, U., Ravazzolo, R., Zegarra-Moran, O., and Galietta, L. J. (2008). TMEM16A, a membrane protein associated with calcium-dependent chloride channel activity. Science 322, 590-594.

Carrasco N., 1993, Iodide transport in the thyroid gland. Biochim Biophys Acta 1154, 65-82.

Castro M. R. et al. "Monoclonal antibodies against the human sodium iodide symporter: utility for immunocytochemistry of thyroid cancer" J Endocrin 163, 495-504, 1999)

Chalfie M., Tu Y., Euskirchen G., Ward W. W., Prasher D. C., 1994, Green fluorescent protein as a marker for gene expression. Science 263, 802-805.

Cho J. Y. et al. "Hormonal regulation of radioiodide uptake activity and Na^+/I^- symporter expression in mammary glands" J Clin Endocrinol Metab 85,2936-2943 (2000)

Chomczynski P. and Sacchi N., (1987) Single-step method of RNA isolation by acid guanidinium thiocyanate-phenol-chloroform Anal Biochem. 1987 Apr;162(1):156-9.

Cianchetta, S., di Bernardo, J., Romeo, G., and Rhoden, K. J. (2010). Perchlorate transport and inhibition of the sodium iodide symporter measured with the yellow fluorescent protein variant YFP-H148Q/I152L. Toxicol Appl Pharmacol 243, 372-380.

Clementi F., Fumagalli G. (1999) Farmacologia generale e molecolare, UTET.

Cone, R. D., Platzer, M., Piccinini, L. A., Jaramillo, M., and Davies, T. F. (1988). HLA-DR gene expression in a proliferating human thyroid cell clone (12S). Endocrinology 123, 2067-2074.

Corda D., Kohn L. D. (1985) Thyrotropin upregulates alpha 1-adrenergic receptors in rat FRTL-5 thyroid cells. Proc Natl Acad Sci U S A. Dec;82(24):8677-80.

Corda, D., Marcocci, C., Kohn, L. D., Axelrod, J., and Luini, A. (1985). Association of the changes in cytosolic Ca2+ and iodide efflux induced by thyrotropin and by the stimulation of alpha 1-adrenergic receptors in cultured rat thyroid cells. J Biol Chem 260, 9230-9236.

Cubitt A. B., Heim R., Adams SR., Boyd AE., Gross LA., Tsien RY.,1995, Understanding, using and improving green fluorescent protein. Trends Biochem Sci 20, 448-455.

Day G., Levi O., Carrasco N. "Cloning and characterization of the thyroid iodide transporter" Nature 379,458-460 (1996)

De la Vieja A., Ginter C.S., Carrasco N. "Topology of the sodium/iodide symporter. Program of the 12th International Thyroid Congress, Kyoto, Japan, p 162,abstract P-225 (2000)

De Luca, F., Trimarchi, F., Sferlazzas, C., Benvenga, S., Costante, G., Mami, C., Di Pasquale, G., and Magazzu, G. (1982). Thyroid function in children with cystic fibrosis. Eur J Pediatr 138, 327-330.

Devuyst, O., Golstein, P. E., Sanches, M. V., Piontek, K., Wilson, P. D., Guggino, W. B., Dumont, J. E., and Beauwens, R. (1997). Expression of CFTR in human and bovine thyroid epithelium. Am J Physiol 272, C1299-308.

Di Girolamo, M., D'Arcangelo, D., Bizzarri, C., and Corda, D. (1991). Muscarinic regulation of phospholipase A2 and iodide fluxes in FRTL-5 thyroid cells. Acta Endocrinol (Copenh) 125, 192-200.

Dohán O. et al. "Na^+/I^- symporter activity requires a small and uncharged amino acid residue at position 395" Mol Endocrinol 16,1893-1902 (2002)

Dohan, O., Baloch, Z., Banrevi, Z., Livolsi, V., and Carrasco, N. (2001). Rapid communication: predominant intracellular overexpression of the Na(+)/I(-) symporter (NIS) in a large sampling of thyroid cancer cases. J Clin Endocrinol Metab 86, 2697-2700.

Dohan, O., De la, V. i. A., Paroder, V., Riedel, C., Artani, M., Reed, M., Ginter, C. S., and Carrasco, N. (2003). The sodium/iodide Symporter (NIS): characterization, regulation, and medical significance. Endocr Rev 24, 48-77.

Dohan, O., Portulano, C., Basquin, C., Reyna-Neyra, A., Amzel, L. M., and Carrasco, N. (2007). The Na+/I symporter (NIS) mediates electroneutral active transport of the environmental pollutant perchlorate. Proc Natl Acad Sci U S A 104, 20250-20255.

Elsliger, M. A., Wachter, R. M., Hanson, G. T., Kallio, K., and Remington, S. J. (1999). Structural and spectral response of green fluorescent protein variants to changes in pH. Biochemistry 38, 5296-5301.

Eng P. H. K. "Regulation of the sodium iodide symporter by iodide in FRTL-5 cells" Eur J Endocrinol 144,139-144 (2001)

Eng, P. H., Cardona, G. R., Fang, S. L., Previti, M., Alex, S., Carrasco, N., Chin, W. W., and Braverman, L. E. (1999). Escape from the acute Wolff-Chaikoff effect is associated with a decrease in thyroid sodium/iodide symporter messenger ribonucleic acid and protein. Endocrinology 140, 3404-3410.

Eskandari S. et al. "Thyroid Na$^+$/I$^-$ symporter. Mechanism, stoichiometry and specificity" J Biol Chem 272,27230-27238 (1997)

Espinosa, I., Lee, C. H., Kim, M. K., Rouse, B. T., Subramanian, S., Montgomery, K., Varma, S., Corless, C. L., Heinrich, M. C., Smith, K. S., et al. (2008). A novel monoclonal antibody against DOG1 is a sensitive and specific marker for gastrointestinal stromal tumors. Am J Surg Pathol 32, 210-218.

Estour, B., Van Herle, A. J., Juillard, G. J., Totanes, T. L., Sparkes, R. S., Giuliano, A. E., and Klandorf, H. (1989). Characterization of a human follicular thyroid carcinoma cell line (UCLA RO 82 W-1). Virchows Arch B Cell Pathol Incl Mol Pathol 57, 167-174.

Everett LA., Glaser B., Beck JC., Idol JR., Buchs A., Heyman M., Adawi F., Hazani E., Nassir E., Baxevanis AD., Sheffield VC., Green ED. 1997, Pendred syndrome is caused by mutations in a putative sulphate transporter gene (PDS). Nat Genet 17, 411-422.

Everett, L. A., Belyantseva, I. A., Noben-Trauth, K., Cantos, R., Chen, A., Thakkar, S. I., Hoogstraten-Miller, S. L., Kachar, B., Wu, D. K., and Green, E. D. (2001). Targeted disruption of mouse Pds provides insight about the inner-ear defects encountered in Pendred syndrome. Hum Mol Genet 10, 153-161.

Fabien, N., Fusco, A., Santoro, M., Barbier, Y., Dubois, P. M., and Paulin, C. (1994). Description of a human papillary thyroid carcinoma cell line. Morphologic study and expression of tumoral markers. Cancer 73, 2206-2212.

Ferrera, L., Caputo, A., Ubby, I., Bussani, E., Zegarra-Moran, O., Ravazzolo, R., Pagani, F., and Galietta, L. J. (2009). Regulation of TMEM16A chloride channel properties by alternative splicing. J Biol Chem 284, 33360-33368.

Fraser GR., 1965, Association of congenital deafness with goitre (Pendred's syndrome) a study of 207 families. Ann Hum Genet 28, 201-249.

Friedrich, T., Breiderhoff, T., and Jentsch, T. J. (1999). Mutational analysis demonstrates that ClC-4 and ClC-5 directly mediate plasma membrane currents. J Biol Chem 274, 896-902.

Furlanetto T. W. et al. "Estradiol increases proliferation and down-regulates the sodium/iodide symporter gene in FRTL-5 cells" Endocrinology 140,5705-5711 (1999)

Galietta L. J. V. et al. "An electrogenic amino acid transporter in the apical membrane of coltured human bronchial epithelial cells" Am Physiol Soc L,917-923 (1998)

Galietta, L. J. (2009). The TMEM16 protein family: a new class of chloride channels?. Biophys J 97, 3047-3053.

Galietta, L. J., Haggie, P. M., and Verkman, A. S. (2001a). Green fluorescent protein-based halide indicators with improved chloride and iodide affinities. FEBS Lett 499, 220-224.

Galietta, L. V., Jayaraman, S., and Verkman, A. S. (2001b). Cell-based assay for high-throughput quantitative screening of CFTR chloride transport agonists. Am J Physiol Cell Physiol 281, C1734-42.

Gasparre, G., Bonora, E., Tallini, G., and Romeo, G. (2010). Molecular features of thyroid oncocytic tumors. Mol Cell Endocrinol 321, 67-76.

Gerdes H.H., Kaether C., 1996, Green fluorescent protein: applications in cell biology. FEBS Lett 389, 44–47.

Ghada Fallah, Thomas Romer, Silvia Detro-Dassen, Ursula Braam, Fritz Markwardt, and Gunther Schmalzing (2011) TMEM16A(a)/anoctamin-1 Shares a homodimeric Architecture with CLC Chloride Channels, Molecular & Cellular Proteomics 10: 10.1074/mcp.M110.004697, 1–10.

Gillam, M. P., Sidhaye, A. R., Lee, E. J., Rutishauser, J., Stephan, C. W., and Kopp, P. (2004). Functional characterization of pendrin in a polarized cell system. Evidence for pendrin-mediated apical iodide efflux. J Biol Chem 279, 13004-13010.

Graham FL, van der Eb AJ (1973). A new technique for the assay of infectivity of human adenovirus 5 DNA. *Virology* 52 (2): 456–67.

Grynkiewicz, G., Poenie, M., and Tsien, R. Y. (1985). A new generation of Ca2+ indicators with greatly improved fluorescence properties. J Biol Chem 260, 3440-3450.

Gunther, W., Luchow, A., Cluzeaud, F., Vandewalle, A., and Jentsch, T. J. (1998). ClC-5, the chloride channel mutated in Dent's disease, colocalizes with the proton pump in endocytotically active kidney cells. Proc Natl Acad Sci U S A 95, 8075-8080.

Hannon, G. J., and Rossi, J. J. (2004). Unlocking the potential of the human genome with RNA interference. Nature 431, 371-378.

Hartzell, C., Putzier, I., and Arreola, J. (2005). Calcium-activated chloride channels. Annu Rev Physiol 67, 719-758.

Hartzell, C., Qu, Z., Putzier, I., Artinian, L., Chien, L. T., and Cui, Y. (2005). Looking chloride channels straight in the eye: bestrophins, lipofuscinosis, and retinal degeneration. Physiology (Bethesda) 20, 292-302.

Hartzell, H. C., Yu, K., Xiao, Q., Chien, L. T., and Qu, Z. (2009). Anoctamin/TMEM16 family members are Ca^{2+}-activated Cl^- channels. J Physiol 587, 2127-2139.

Heim, R., Prasher, D. C., and Tsien, R. Y. (1994). Wavelength mutations and posttranslational autoxidation of green fluorescent protein. Proc Natl Acad Sci U S A 91, 12501-12504.

Hilditch T. E. et al. "Defects in intrathyroid binding of iodine and the perchlorate discharge test" Acta Endocrinol (Copenh) 100,237-244 (1982)

Ishizaka, Y., Ushijima, T., Sugimura, T., and Nagao, M. (1990). cDNA cloning and characterization of ret activated in a human papillary thyroid carcinoma cell line. Biochem Biophys Res Commun 168, 402-408.

Jayaraman, S., Haggie, P., Wachter, R. M., Remington, S. J., and Verkman, A. S. (2000). Mechanism and cellular applications of a green fluorescent protein-based halide sensor. J Biol Chem 275, 6047-6050.

Jentsch, T. J., Stein, V., Weinreich, F., and Zdebik, A. A. (2002). Molecular structure and physiological function of chloride channels. Physiol Rev 82, 503-568.

John T. Sheridan, Erin N. Worthington, Kuai Yu, Sherif E. Gabriel, H. Criss Hartzell, and Robert Tarran (2010). Characterization of the Oligomeric Structure of the Ca^{2+}-activated Cl^- Channel Ano1/TMEM16A JBC Papers in Press, November 5 2010 Published, DOI 10.1074/jbc.M110.174847

Katoh, M., and Katoh, M. (2004a). Identification and characterization of TMEM16E and TMEM16F genes in silico. Int J Oncol 24, 1345-1349.

Katoh, M., and Katoh, M. (2004b). Characterization of human TMEM16G gene in silico. Int J Mol Med 14, 759-764.

Katoh, M., and Katoh, M. (2005). Identification and characterization of TMEM16H gene in silico. Int J Mol Med 15, 353-358.

Klopfleisch R., Klose P., Weise C., Bondzio A., Multhaup G., Einspanier R., Gruber AD. (2010). Proteome of metastatic canine mammary carcinomas: similarities to and differences from human breast cancer. J Proteome Res 9 (12): 6380–91.

Kogai T. et al. "Enhancement of sodium/iodide symporter expression in thyroid and breast cancer" Rev. Endocrine-Related Cancer (2006)

Kogai T. et al. "Induction of follicle formation in long-term cultured normal human thyroid cells treated with thyrotropin stimulates iodide uptake but not sodium/iodide symporter messenger RNA and protein expression" J Endocrinol 167,125-135 (2000)

Kohn LD., Suzuki K., Nakazato M., Royaux I., Green ED., 2001, Effects of thyroglobulin and pendrin on iodide flux through the thyrocyte. Trends Endocrinol Metab 12, 10-16.

Koong, S. S., Reynolds, J. C., Movius, E. G., Keenan, A. M., Ain, K. B., Lakshmanan, M. C., and Robbins, J. (1999). Lithium as a potential adjuvant to 131I therapy of metastatic, well differentiated thyroid carcinoma. J Clin Endocrinol Metab 84, 912-916.

Kopp, P. (1999). Pendred's syndrome: identification of the genetic defect a century after its recognition. Thyroid 9, 65-69.

Kopp, P., Pesce, L., and Solis-S, J. C. (2008). Pendred syndrome and iodide transport in the thyroid. Trends Endocrinol Metab 19, 260-268.

Kraiem Z., Heinrich R., Sadeh O., Shiloni E., Nassir E., Hazani E., Glaser B., 1999, Sulfate transport is not impaired in pendred syndrome thyrocytes. J Clin Endocrinol Metab 84, 2574-2576.

Kunzelmann, K., Kongsuphol, P., Aldehni, F., Tian, Y., Ousingsawat, J., Warth, R., and Schreiber, R. (2009). Bestrophin and TMEM16-Ca(2+) activated Cl(-) channels with different functions. Cell Calcium 46, 233-241.

Kunzelmann, K., Milenkovic, V. M., Spitzner, M., Soria, R. B., and Schreiber, R. (2007). Calcium-dependent chloride conductance in epithelia: is there a contribution by Bestrophin?. Pflugers Arch 454, 879-889.

Lacroix L., Mian C., Caillou B., Talbot M., Filetti S., Schlumberger M., Bidart JM., 2001, Na^+/I^- symporter and Pendred syndrome gene and protein expressions in human extra-thyroidal tissues. Eur J Endocrinol 144, 297-302.

Levi O. et al. "Identification of a structural requirement for thyroid Na^+/I^- symporter (NIS) function for analysis of a mutation that causes human congenital hypothyroidism" FEBS Lett 429,36-40 (1998)

Levy O. et al. "Characterization of the thyroid Na^+/I^- symporter with an anti-COOH terminus antibody" Proc Natl Acad Sci USA 94,5568-5573 (1997)

Levy, O., De la, V. i. A., Ginter, C. S., Riedel, C., Dai, G., and Carrasco, N. (1998). N-linked glycosylation of the thyroid Na+/I- symporter (NIS). Implications for its secondary structure model. J Biol Chem 273, 22657-22663.

Lewin. Gene (2004)

Livak, K. J., and Schmittgen, T. D. (2001). Analysis of relative gene expression data using real-time quantitative PCR and the 2(-Delta Delta C(T)) Method. Methods 25, 402-408.

Mandell, R. B., Mandell, L. Z., and Link, C. J., Jr. (1999). Radioisotope concentrator gene therapy using the sodium/iodide symporter gene. Cancer Res 59, 661-668.

Manoury, B., Tamuleviciute, A., and Tammaro, P. (2010). TMEM16A/anoctamin 1 protein mediates calcium-activated chloride currents in pulmonary arterial smooth muscle cells. J Physiol 588, 2305-2314.

Mansoura, M. K., Biwersi, J., Ashlock, M. A., and Verkman, A. S. (1999). Fluorescent chloride indicators to assess the efficacy of CFTR cDNA delivery. Hum Gene Ther 10, 861-875.

Mc Cruden D. C. Et al. "Duration of antithyroid action of methimazole estimated with an intravenous perchlorate discharge test" Clin Endocrinol (Oxf) 26,33-39 (1987)

Melander A., Ljunggren J. G., Norberg K. A., Persson B., Rosengren E., Sundler F., Tibblin S., Westgren U (1978) Sympathetic innervation and noradrenaline content of normal human thyroid tissue from fetal, young, and elderly subjects. J Endocrinol Invest. Apr;1(2):175-7.

Melander, A. (1970). Amines and mouse thyroid activity: release of thyroid hormone by catecholamines and indoleamines and its inhibition by adrenergic blocking drugs. Acta Endocrinol (Copenh) 65, 371-384.

Melander, A., Sundler, F., and Westgren, U. (1973). Intrathyroidal amines and the synthesis of thyroid hormone. Endocrinology 93, 193-200.

Milenkovic, V. M., Brockmann, M., Stohr, H., Weber, B. H., and Strauss, O. (2010). Evolution and functional divergence of the anoctamin family of membrane proteins. BMC Evol Biol 10, 319.

Mizukami Y. et al. "Changes in localization of ouabain-sensitive, potassium-dependent p-nitrophenylphosphatase activity in human thyroid carcinoma cells" Lab Invest 48,411-418 (1983)

Mizuta, K., Tsutsumi, S., Inoue, H., Sakamoto, Y., Miyatake, K., Miyawaki, K., Noji, S., Kamata, N., and Itakura, M. (2007). Molecular characterization of GDD1/TMEM16E, the gene product responsible for autosomal dominant gnathodiaphyseal dysplasia. Biochem Biophys Res Commun 357, 126-132.

Mount, D. B., and Romero, M. F. (2004). The SLC26 gene family of multifunctional anion exchangers. Pflugers Arch 447, 710-721.

Namkung, W., Phuan, P. W., and Verkman, A. S. (2010a). TMEM16A inhibitors reveal TMEM16A as a minor component of calcium-activated chloride channel conductance in airway and intestinal epithelial cells. J Biol Chem 286, 2365-2374.

Namkung, W., Thiagarajah, J. R., Phuan, P. W., and Verkman, A. S. (2010b). Inhibition of Ca^{2+}-activated Cl^- channels by gallotannins as a possible molecular basis for health benefits of red wine and green tea. FASEB J 24, 4178-4186.

NCBI "http://www.ncbi.nlm.nih.gov"

Nilsson, M., Bjorkman, U., Ekholm, R., and Ericson, L. E. (1990). Iodide transport in primary cultured thyroid follicle cells: evidence of a TSH-regulated channel mediating iodide efflux selectively across the apical domain of the plasma membrane. Eur J Cell Biol 52, 270-281.

Ormo M., Cubitt A. B., Kallio K., Gross L. A., Tsien R. Y., Remington S. J., 1996, Crystal structure of the Aequorea victoria green fluorescent protein. Science 273, 1392-5.

Otowa, T., Yoshida, E., Sugaya, N., Yasuda, S., Nishimura, Y., Inoue, K., Tochigi, M., Umekage, T., Miyagawa, T., Nishida, N., et al. (2009). Genome-wide association study of panic disorder in the Japanese population. J Hum Genet 54, 122-126.

Ousingsawat, J., Martins, J. R., Schreiber, R., Rock, J. R., Harfe, B. D., and Kunzelmann, K. (2009). Loss of TMEM16A causes a defect in epithelial Ca^{2+}-dependent chloride transport. J Biol Chem 284, 28698-28703.

Pellegatti, P. et al. (2008). Increased level of extracellular ATP at tumor sites: in vivo imaging with plasma membrane luciferase. PLoS One 3.

Pfaffl, M. W. (2001). A new mathematical model for relative quantification in real-time RT-PCR. Nucleic Acids Res. 2001 May 1;29(9):e45.

Pifferi, S., Dibattista, M., and Menini, A. (2009). TMEM16B induces chloride currents activated by calcium in mammalian cells. Pflugers Arch 458, 1023-1038.

Piwon, N., Gunther, W., Schwake, M., Bosl, M. R., and Jentsch, T. J. (2000). ClC-5 Cl- -channel disruption impairs endocytosis in a mouse model for Dent's disease. Nature 408, 369-373.

Prasher D. C., Eckenrode V. K., Ward W. W., Prendergast F. G., Cormier M. J., 1992, Primary structure of the Aequorea victoria green-fluorescent protein. Gene 111, 229-33.

Pryor, S. P. et al. (2005). SLC26A4/PDS genotype-phenotype correlation in hearing loss with enlargement of the vestibular aqueduct (EVA): evidence that Pendred syndrome and non-syndromic EVA are distinct clinical and genetic entities. J Med Genet 42, 159-165.

Raben, M. S. (1949). The paradoxical effects of thiocyanate and of thyrotropin on the organic binding of iodine by the thyroid in the presence of large amounts of iodide. Endocrinology 45, 296-304.

Reid B. G., Flynn G. C., 1997, Chromophore formation in green fluorescent protein. Biochemistry 36, 6786-6791.

Reizer, J., Reizer, A., and Saier, M. H., Jr. (1994). A functional superfamily of sodium/solute symporters. Biochim Biophys Acta 1197, 133-166.

Rhoden K. J. "Cell-based imaging of sodium iodide symporter activity with the yellow fluorescent protein variant YFP-H148Q/I152L" Am J Physiol Cell Physiol 292,814-823 (2007)

Rhoden, K. J., et al. (2008). Fluorescence quantitation of thyrocyte iodide accumulation with the yellow fluorescent protein variant YFP-H148Q/I152L. Anal Biochem 373, 239-246.

Riedel C. et al. "Post-transcriptional regulation of the sodium/iodide symporter by thyrotropin" J Biol Chem 276,21458-21463 (2001)

Riedel, C., Levy, O., and Carrasco, N. (2001). Post-transcriptional regulation of the sodium/iodide symporter by thyrotropin. J Biol Chem 276, 21458-21463.

Rillema J., Melissa AH., 2003, Pendrin transporter carries out iodide uptale into MCF-7 human mammary cancer cells. Exp Biol Med 288, 1078-1082.

Rock, J. R., and Harfe, B. D. (2008). Expression of TMEM16 paralogs during murine embryogenesis. Dev Dyn 237, 2566-2574.

Rock, J. R., Futtner, C. R., and Harfe, B. D. (2008). The transmembrane protein TMEM16A is required for normal development of the murine trachea. Dev Biol 321, 141-149.

Rock, J. R., O'Neal, W. K., Gabriel, S. E., Randell, S. H., Harfe, B. D., Boucher, R. C., and Grubb, B. R. (2009). Transmembrane protein 16A (TMEM16A) is a Ca2+-regulated Cl- secretory channel in mouse airways. J Biol Chem 284, 14875-14880.

Rodriguez A.M. et al. "Identification and characterization of putative human iodide transporter located at the apical membrane of thyrocytes" J Clin Endocrinol Metab 87,3500-3503 (2202)

Rodriguez AM., Perron B., Lacroix L., Caillou B., Leblanc G., Schlumberger M., Bidart JM., Pourcher T., 2002, Identification and characterization of a putative human iodide transporter located at the apical membrane of thyrocytes. J Clin Endocrinol Metab. 87, 3500-3503.

Rotman-Pikielny P., Hirschberg K., Maruvada P., Suzuki K., Royaux IE., Green ED., Kohn LD., Lippincott-Schwartz J., Yen PM., 2002, Retention of pendrin in the endoplasmic reticulum is a major mechanism for Pendred syndrome. Hum Mol Genet 11**,** 2625–2633.

Royaux IE., Suzuki K., Mori A., Katoh R., Everett LA., Kohn LD., Green ED., 2000, Pendrin, the protein encoded by the Pendred syndrome gene (PDS), is an apical porter of iodide in the thyroid and is regulated by thyroglobulin in FRTL-5 cells. Endocrinology 141**,** 839–845.

Royaux IE., Wall SM., Karniski LP., Everett LA., Suzuki K., Knepper MA., Green ED., 2001, Pendrin, encoded by the Pendred syndrome gene, resides in the apical region of renal intercalated cells and mediates bicarbonate secretion. Proc Natl Acad Sci 98, 4221–4226.

Rudolph C., Lausier J., Naundorf S., Müller RH., Rosenecker J. (2000). In vivo gene delivery to the lung using polyethylenimine and fractured polyamidoamine dendrimers. Journal of Gene Medicine 2 (4): 269–78.

Ryu, K. Y. et al. "Promoter characterization of the human Na$^+$/I$^-$ symporter" Journal of Clinical Endocrinology and Metabolism 83,3247-3251 (1998)

Saito, T., Endo, T., Kawaguchi, A., Ikeda, M., Katoh, R., Kawaoi, A., Muramatsu, A., and Onaya, T. (1998). Increased expression of the sodium/iodide symporter in papillary thyroid carcinomas. J Clin Invest 101, 1296-1300.

Saito, T., Endo, T., Kawaguchi, A., Ikeda, M., Nakazato, M., Kogai, T., and Onaya, T. (1997). Increased expression of the Na$^+$/I$^-$ symporter in cultured human thyroid cells exposed to thyrotropin and in Graves' thyroid tissue. J Clin Endocrinol Metab 82, 3331-3336.

Scheel, O., Zdebik, A. A., Lourdel, S., and Jentsch, T. J. (2005). Voltage-dependent electrogenic chloride/proton exchange by endosomal CLC proteins. Nature 436, 424-427.

Schlumberger M. J. "Papillary and follicular thyroid carcinoma" N Engl J Med 338,297-306 (1998)

Schneppenheim, R., Castaman, G., Federici, A. B., Kreuz, W., Marschalek, R., Oldenburg, J., Oyen, F., and Budde, U. (2007). A common 253-kb deletion involving VWF and TMEM16B in German and Italian patients with severe von Willebrand disease type 3. J Thromb Haemost 5, 722-728.

Schreiber, R., Uliyakina, I., Kongsuphol, P., Warth, R., Mirza, M., Martins, J. R., and Kunzelmann, K. (2010). Expression and function of epithelial anoctamins. J Biol Chem 285, 7838-7845.

Schroeder, B. C., Cheng, T., Jan, Y. N., and Jan, L. Y. (2008). Expression cloning of TMEM16A as a calcium-activated chloride channel subunit. Cell 134, 1019-1029.

Schweppe, R. E., Klopper, J. P., Korch, C., Pugazhenthi, U., Benezra, M., Knauf, J. A., Fagin, J. A., Marlow, L. A., Copland, J. A., Smallridge, R. C., and Haugen, B. R. (2008). Deoxyribonucleic acid profiling analysis of 40 human thyroid cancer cell lines reveals cross-contamination resulting in cell line redundancy and misidentification. J Clin Endocrinol Metab 93, 4331-4341.

Scott D.A. et al. "The Pendred syndrome gene encodes a chloride-iodide transport protein" Nat Gen 21,40-443 (1999)

Scott DA., Karniski LP., 2000, Human pendrin expressed in Xenopus laevis oocytes mediates chloride/formate exchange. Am J Physiol Cell Physiol. 278, C207-211.

Scott DA., Wang R., Kreman TM., Sheffield VC., Karniski LP., 1999, The Pendred syndrome gene encodes a chloride-iodide transport protein. Nat Genet 21, 440-443.

Shimomura O., Johnson F. H., Saiga Y., 1962, Extraction, purification and properties of aequorin, a bioluminescent protein from the luminous hydromedusan, Aequorea. J Cell Comp Physiol 59, 223-39.

Simpson, J. E., et al. (2005). Chloride conductance of CFTR facilitates basal Cl-/HCO3- exchange in the villous epithelium of intact murine duodenum. Am J Physiol Gastrointest Liver Physiol 288, G1241-51.

Smallridge, R. C., and Gist, I. D. (1994). P2-purinergic stimulation of iodide efflux in FRTL-5 rat thyroid cells involves parallel activation of PLC and PLA2. Am J Physiol 267, E323-30.

Smanik P. A. et al. "Cloning of the human sodium iodide symporter. Biochem Biophys Res Commun 226,339-345 (1996)

Smanik P. A. et al. "Expression, exon-intron organization, and chromosome mapping of the human sodium iodide symporter" Endocrinology 138, 3555-3558 (1997)

Soleimani M., Greeley T., Petrovic S., Wang Z., Amlal H., Kopp P., Burnham CE., 2001, Pendrin: an apical $Cl^-/OH^-/HCO_3^-$ exchanger in the kidney cortex. Am J Physiol Renal Physiol 280, F356-364.

Spitzweg C., Morris J.C. "The sodium iodide symporter: its pathophysiological and therapeutic implications"(Rev.) Clinical Endocrinology 57,559-574 (2002)

Spitzweg, C., O'Connor, M. K., Bergert, E. R., Tindall, D. J., Young, C. Y., and Morris, J. C. (2000). Treatment of prostate cancer by radioiodine therapy after tissue-specific expression of the sodium iodide symporter. Cancer Res 60, 6526-6530.

Stephan, A. B., Shum, E. Y., Hirsh, S., Cygnar, K. D., Reisert, J., and Zhao, H. (2009). ANO2 is the cilial calcium-activated chloride channel that may mediate olfactory amplification. Proc Natl Acad Sci U S A 106, 11776-11781.

Stohr, H., Heisig, J. B., Benz, P. M., Schoberl, S., Milenkovic, V. M., Strauss, O., Aartsen, W. M., Wijnholds, J., Weber, B. H., and Schulz, H. L. (2009). TMEM16B, a novel protein with calcium-dependent chloride channel activity, associates with a presynaptic protein complex in photoreceptor terminals. J Neurosci 29, 6809-6818.

Suzuki, J., Umeda, M., Sims, P. J., and Nagata, S. (2010). Calcium-dependent phospholipid scrambling by TMEM16F. Nature 468, 834-838.

Suzuki, K., and Kohn, L. D. (2006). Differential regulation of apical and basal iodide transporters in the thyroid by thyroglobulin. J Endocrinol 189, 247-255.

Suzuki, K., Mori, A., Saito, J., Moriyama, E., Ullianich, L., and Kohn, L. D. (1999). Follicular thyroglobulin suppresses iodide uptake by suppressing expression of the sodium/iodide symporter gene. Endocrinology 140, 5422-5430.

Tamir, H., Hsiung, S. C., Yu, P. Y., Liu, K. P., Adlersberg, M., Nunez, E. A., and Gershon, M. D. (1992). Serotonergic signalling between thyroid cells: protein kinase C and 5-HT2 receptors in the secretion and action of serotonin. Synapse 12, 155-168.

Taylor JP., Metcalfe RA., Watson PF., Weetman AP., Trembath RC., 2002, Mutations of the PDS gene, encoding pendrin, are associated with protein mislocalization and loss of iodide efflux: implications for thyroid dysfunction in Pendred syndrome. J Clin Endocrinol Metabol 87**,** 1778–1784.

Tazebay U. H. et al. "The mammary gland iodide transporter is expressed during lactation and in breast cancer" Nat Med 6,871-878 (2000)

Thomas, J. A., Buchsbaum, R. N., Zimniak, A., and Racker, E. (1979). Intracellular pH measurements in Ehrlich ascites tumor cells utilizing spectroscopic probes generated in situ. Biochemistry 18, 2210-2218.

Tice LW., Creveling CR. (1975) Electron microscopic identification of adrenergic nerve endings on thyroid epithelial cells. Endocrinology. Nov;97(5):1123-9.

Tsutsumi, S., Kamata, N., Vokes, T. J., Maruoka, Y., Nakakuki, K., Enomoto, S., Omura, K., Amagasa, T., Nagayama, M., Saito-Ohara, F., et al. (2004). The novel gene encoding a putative transmembrane protein is mutated in gnathodiaphyseal dysplasia (GDD). Am J Hum Genet 74, 1255-1261.

V**an den, H. o. M., Croizet-Berger, K., Jouret, F., Guggino, S. E., Guggino, W. B., Devuyst, O., and Courtoy, P. J.** (2006). The loss of the chloride channel, ClC-5, delays apical iodide efflux and induces a euthyroid goiter in the mouse thyroid gland. Endocrinology 147, 1287-1296.

Van Sande, J., Dumont, J. E., Melander, A., and Sundler, F. (1980). Presence and influence of cholinergic nerves in the human thyroid. J Clin Endocrinol Metab 51, 500-502.

Vancha AR., et al. (2004). Use of polyethyleneimine polymer in cell culture as attachment factor and lipofection enhancer. BMC Biotechnology 4: 23.

Vassart G., Dumont J. E. "The thyrotropin receptor and the regulation of thyrocyte function and growth" Endocr Rev 13,596-611 (1992)

Verkman, A. S., and Galietta, L. J. (2009). Chloride channels as drug targets. Nat Rev Drug Discov 8, 153-171.

Vermeer, S., Hoischen, A., Meijer, R. P., Gilissen, C., Neveling, K., Wieskamp, N., de Brouwer, A., Koenig, M., Anheim, M., Assoum, M., et al. (2010). Targeted next-generation sequencing of a 12.5 Mb homozygous region reveals ANO10 mutations in patients with autosomal-recessive cerebellar ataxia. Am J Hum Genet 87, 813-819.

Virion A., Pommier J., Deme D., Nunez J., 1981, Kinetics of thyroglobulin iodination and thyroid hormone synthesis catalyzed by peroxidase: the role of H_2O_2. Eur J Biochem 117, 103-109.

Wachter, R. M., and Remington, S. J. (1999). Sensitivity of the yellow variant of green fluorescent protein to halides and nitrate. Curr Biol 9, R628-9.

Wachter, R. M., Yarbrough, D., Kallio, K., and Remington, S. J. (2000). Crystallographic and energetic analysis of binding of selected anions to the yellow variants of green fluorescent protein. J Mol Biol 301, 157-171.

Waltz et al. (2010). A nonradioactive iodide uptake assay for sodium iodide symporter function. Anal Biochem 396, 91-95.

Weiss, S. J., Philp, N. J., Ambesi-Impiombato, F. S., and Grollman, E. F. (1984a). Thyrotropin-stimulated iodide transport mediated by adenosine 3',5'-monophosphate and dependent on protein synthesis. Endocrinology 114, 1099-1107.

Weiss, S. J., Philp, N. J., and Grollman, E. F. (1984b). Effect of thyrotropin on iodide efflux in FRTL-5 cells mediated by Ca2+. Endocrinology 114, 1108-1113.

Wilkins M.R., Pasquali C., Appel R. D., Ou K., Golaz O., Sanchez J. C., Yan J. X., Gooley A. A., Hughes G., Humphery-Smith I., Williams K. L. & Hochstrasser D. F. (1996). From Proteins to Proteomes: Large Scale Protein Identification by Two-Dimensional Electrophoresis and Arnino Acid Analysis. Nature Biotechnology 14 (1): 61–65.

Wolff et al. (1949) The temporary nature of the inhibitory action of excess iodide on organic iodide synthesis in the normal thyroid Endocrinology 45,504

Wolff J. (1964) Transport of iodide and other anions in the thyroid gland Physiol Rev 44,45-90

Wolff, J. (1983). Congenital goiter with defective iodide transport. Endocr Rev 4, 240-254.

Wolff, J. (2005). What is the role of pendrin?. Thyroid 15, 346-348.

Wolff, J., and Chaikoff, I. L. (1948). Plasma inorganic iodide as a homeostatic regulator of thyroid function. J Biol Chem 174, 555-564.

Xu J. et al. "A GC box in the human sodium iodide symporter gene promoter is essential for full activity" Thyroid 12,107-114 (2002)

Yang F., Moss L. G., Phillips G. N Jr., 1996, The molecular structure of green fluorescent protein. Nat Biotechnol 14, 1246-1251.

Yang, Y. D., Cho, H., Koo, J. Y., Tak, M. H., Cho, Y., Shim, W. S., Park, S. P., Lee, J., Lee, B., Kim, B. M., et al. (2008). TMEM16A confers receptor-activated calcium-dependent chloride conductance. Nature 455, 1210-1215.

Yoshida A. et al. (1998) Differences in the electrophysiological response to I- and the inhibitory anions SCN⁻ and ClO₄⁻ , studied in FRTL-5 cells Biochim Biophys Acta 1414,231-237

Yoshida A., Hisatome I., Taniguchi S., Sasaki N., Yamamoto Y., Miake J., Fukui H., Shimizu H., Okamura T., Okura T., Igawa O., Shigemasa C., Green ED., Kohn LD., Suzuki K., (2004) Mechanism of iodide/chloride exchange by pendrin. Endocrinology 145, 4301-4308.

Yoshida A., Taniguchi S., Hisatome I., Royaux I. E., Green E. D., Kohn L. D., Suzuki K., (2002) Pendrin is an iodide-specific apical porter responsible for iodide efflux from thyroid cells. J Clin Endocrinol Metab 87, 3356–3361.

Yoshida, A., Hattori, K., Hisatome, I., Taniguchi, S., Ueta, Y., Hukui, H., Santo, Y., Igawa, O., Shigemasa, C., Kosugi, S., and Grollman, E. F. (1999). A TSH/dibutyryl cAMP activated Cl-/I-channel in FRTL-5 cells. Biochem Biophys Res Commun 259, 631-635.

DOTTORATO DI RICERCA IN BIOCHIMICA
Estratto del verbale della seduta del 9 febbraio 2012

L'anno 2012, addì 9 del mese di febbraio in Bologna, nell'aula del Dipartimento di Biochimica "G.Moruzzi" alle ore 15.00 si è riunito il Collegio dei Docenti del Corso di Dottorato di ricerca in Biochimica.

Risultano presenti i Professori: A.Falasca, S.Hrelia, S.Iotti, G.Lenaz, A.Pagliarani, G.Solaini, V.Tugnoli.

Risultano assenti giustificati i Professori: D.Fiorentini, F.Flamigni, C.Guarnieri, .

Risulta assente il Professore: E.Carpenè

Risultano presenti i Professori a titolo personale: C.Muscari, C.Stefanelli.

Risultano assenti giustificati i Professori a titolo personale: A.Baracca, R.Fato, C.Prata, G.Romeo, B.Tantini, F.Trombetti.

Risultano assenti i Professori a titolo personale: R.Agati, A.Bordoni, E.D.Giordano, G.Isani, P.Parchi, A.Pession, B.Vaira

Presiede la seduta il Prof. Giorgio Lenaz.

Assume le funzioni di Segretario il Prof. Giancarlo Solaini.

Il Prof. Lenaz riconosce valida la seduta e la dichiara aperta per trattare, come dagli avvisi di convocazione, il seguente ordine del giorno:

1. Comunicazioni.
2. Presentazione Dottorandi XXIV Ciclo da allegare alla tesi di Dottorato.
3. Designazione docenti per la composizione della Commissione Giudicatrice per il conferimento del titolo di Doctor Europaeus
4. Varie ed eventuali

---OMISSIS---

2. Presentazione Dottorandi XXIV Ciclo da allegare alla tesi di Dottorato.

Il Prof. Lenaz fa presente al Collegio dei Docenti che i dottorandi, iscritti all'ultimo anno di corso, hanno provveduto a presentare, nei termini previsti, le dissertazioni finali scritte.

Il Collegio è chiamato a redigere, per ciascuno di essi, la "presentazione" da allegare alla tesi finale

Si invitano, a tal fine, i componenti del Collegio, che prevalentemente hanno guidato le attività di ricerca dei dottorandi, a voler illustrare i contenuti delle predette tesi ed i risultati conseguiti dagli allievi.

Dopo ampia discussione, il Collegio dei Docenti decide, unanime, di approvare le "presentazioni" di seguito riportate le quali illustrano la personalità di ciascun dottorando e l'attività scientifico-formativa svolta durante il corso, mettendone in luce gli aspetti positivi.

---OMISSIS---

Dott.ssa Carmela Iosco. Tema di Ricerca: Biochimica di cellule, organi e tessuti e dei mediatori cellulari. Titolo tesi Dottorato: "Caratterizzazione di nuovi bersagli molecolari coinvolti nel flusso di ioduro nella tiroide: le anoctamine". Tutore Prof. Giovanni Romeo (allegato n° 2).
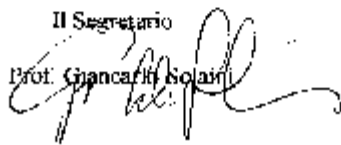
---OMISSIS---

Le deliberazioni prese in questa seduta sono state redatte, lette, approvate e sottoscritte seduta stante.
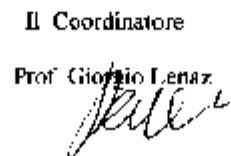
La seduta è tolta alle ore 16.

Il Segretario

Prof. Giancarlo Solaini

Il Coordinatore

Prof. Giorgio Lenaz

ALMA MATER STUDIORUM · UNIVERSITA' DI BOLOGNA
DIPARTIMENTO DI SCIENZE GINECOLOGICHE OSTETRICHE E PEDIATRICHE

CATTEDRA DI GENETICA MEDICA
Presso Pad. 11 Policlinico S. Orsola-Malpighi
Via Massarenti 9 - 40138 Bologna
Tel. 051/306474 - Fax. 051/6964004

Seduta del 9 febbraio 2012
All'attenzione: **Collegio dei Docenti del Dottorato in Biochimica**

Dottorato di Ricerca in Biochimica
XXIV Ciclo - III Anno
Dottorando: Dott. Sa Carmela Iosco
Tutor e Relatore: Prof. Giovanni Romeo
Correlatore: Prof.ssa Kerry Rhoden

Relazione di presentazione

Caratterizzazione di nuovi bersagli molecolari coinvolti nel flusso di ioduro nella tiroide: le anoctamine

Durante i tre anni di dottorato la Dott.sa Carmela Iosco ha analizzato il trasporto di ioduro (I⁻), concentrandosi su diversi tessuti e bersagli molecolari coinvolti, presso il laboratorio dell' U.O di Genetica Medica, Ospedale S.Orsola, Dipartimento di Scienze Ginecologiche, Ostetriche e Pediatriche, Università di Bologna, sotto la supervisione della Prof.ssa Kerry Rhoden.

La dottoranda si è soffermata su due bersagli molecolari: il trasportatore NIS, "Sodium Iodide (Na⁺/I⁻) Symporter", il primo e il secondo anno e il canale Cl⁻ Ca²⁺ attivato TMEM16A (o Anoctamina1), di recente scoperta, per tutto il corso del dottorato.

Argomento della ricerca. NIS (Sodium Iodide Symporter) è il trasportatore di ioduro espresso nella tiroide dove riveste il suo ruolo più importante, la sintesi degli ormoni tiroidei per il controllo del metabolismo dell'organismo. Lo ioduro entra nel tireocita per mezzo di NIS attraverso la sua membrana basale e fluisce attraverso quella apicale nella colloide tiroidea per mezzo di trasportatori

1

diversi, quali pendrina e altri non ancora ben caratterizzati. Poiché quelli noti non sono sufficienti per l'efflusso, l'attenzione è stata rivolta al canale TMEM16A, scoperto nel 2008, che è risultato essere il principale responsabile dell'attività di trasporto Cl^- Ca^{++} dipendente, attività nota ma priva di un responsabile fino ad allora. Avendo TMEM16A una affinità per lo ioduro ancora più elevata di quella per il cloruro, si è ipotizzato che potesse avere un ruolo nell'efflusso di ioduro a livello tiroideo, tessuto in cui è risultato essere presente (portale BioGPS, banca dati di espressione genica). TMEM16A/ANO1 appartiene alla famiglia delle anoctamine. Tale famiglia nell'uomo è costituita da 10 membri, le cui funzioni sono da approfondire (TMEM16A, B, C, D etc).

Scopo della ricerca. La dottoranda ha caratterizzato, a livello trascrizionale, traduzionale e funzionale, trasportatori anionici in cellule tiroidee ed extratiroidee, localizzando l'attenzione sul flusso dell'anione ioduro e sui suoi interattori conosciuti e meno conosciuti.

Inizialmente, oltre alla tiroide, la dottoranda aveva preso in esame anche altri tessuti coinvolti nel flusso di ioduro: la placenta umana, per conoscere il trasporto di ioduro transplacentare putativamente attraverso NIS, poco noto, e la ghiandola mammaria murina, dove TMEM16A risulta essere espresso, per individuare un modello sperimentale cellulare di lattazione e di concentrazione di ioduro nel latte. In seguito è stato preso in analisi l'epitelio bronchiale umano, dato che il suo ruolo nella sterilizzazione delle vie aeree si esplica attraverso formazione di intermedi reattivi dell'ossigeno come lo ioduro ossido (OI) contenenti I, potenzialmente trasportato da NIS.

Nel corso del lavoro la dottoranda ha ampliato gli obiettivi in base ai risultati ottenuti. Ha trovato risultati positivi nello studio delle linee cellulari di ghiandola mammaria murina HC11, che si sono dimostrate un ottimo modello di lattazione e differenziamento.

Durante l'intero periodo di dottorato, invece, la dottoranda ha rivolto l'attenzione al flusso di ioduro soprattutto nel tessuto tiroideo attraverso la membrana apicale (efflusso), che si è rivelato l'obiettivo più promettente, analizzando il canale Cl^- Ca^{++} attivato TMEM16A. Ha analizzato sotto molteplici aspetti questo argomento, tanto da meritare una esclusiva, completa e dettagliata trattazione nella tesi finale di dottorato.

Il fine ultimo del progetto di ricerca della dottoranda, per mezzo della caratterizzazione dei trasportatori studiati, è stato anche fornire dettagli sul loro uso quali nuovi target molecolari: regolando canali coinvolti nell'efflusso di I si potrebbe aumentare l'efficacia della terapia radioablativa del cancro alla tiroide in quanto, inibendo l'efflusso di ^{131}I, i tireociti ne avrebbero una aumentata ritenzione.

2

Materiali e metodi. La dottoranda si è rivelata capace di adoperare adeguatamente le tecniche usate per i diversi tipi di esperimento. Ha ottimizzato le condizioni di reazione di RT-PCR e analizzato con precisione e con diversi metodi i risultati di Real Time PCR, per verificare l'espressione del trascritto dei trasportatori studiati. Ha effettuato esperimenti di clonaggio per produrre una proteina di fusione tra il canale studiato e la proteina fluorescente EYFP (*Enhanced Yellow Fluorescent Protein*) e analizzare così la sua espressione esogena in cellule modello. Ha caratterizzato in maniera approfondita l'espressione proteica dei trasportatori studiati con la tecnica di Western Blot, sia per mezzo di elettroforesi monodimensionale che bidimensionale (separazione delle proteine per punto isoelettrico e peso molecolare). La dottoranda ha mostrato notevoli capacità di adattamento e desiderio di ampliare il pannello di approcci sperimentali: ha espresso, infatti, la volontà di trascorrere un periodo di ricerca all'estero nel corso del dottorato, per imparare e utilizzare le tecniche di clonaggio e di elettroforesi bidimensionale, recandosi nel laboratorio del Dott. Diego Alvarez De La Rosa Rodriguez (Unità di Farmacologia, Hospital Universitario de Canarias, Università de La Laguna, S. Cruz de Tenerife, Spagna).

Ha studiato la funzione dei trasportatori studiati con il saggio di fisiologia cellulare ottimizzato e adoperato da anni dalla Prof.ssa Kerry Rhoden. Il saggio si basa sulla proteina YFP (*Yellow Fluorescent Protein*, variante YFP-H148Q/I152L), come biosensore di alogenuri, fatta esprimere stabilmente dalle linee cellulari FRTL-5, provenienti da tiroide normale di ratto Fischer, perfuse con soluzioni contenenti agonisti e antagonisti recettoriali.

Risultati. La dottoranda è stata in grado di ottenere risultati positivi impiegando le diverse tecniche descritte. In breve, ha rilevato l'espressione del trascritto di TMEM16A nelle cellule tiroidee studiate, studiato l'espressione proteica in un sistema esogeno in maniera preliminare, e ha mostrato che l'efflusso di I in esse caratterizzato possiede proprietà assimilabili alla conduttanza al Cl attivato da Ca⁺⁺ mediata da TMEM16A.

La dottoranda ha mostrato senso critico, abilità nel ragionamento e nell'adattamento agli eventuali imprevisti sorti durante il periodo di ricerca, capacità nel fronteggiare i problemi e nell'organizzare le diverse attività portando a termine il lavoro. Possiede un senso del dovere e di responsabilità molto profondi e desiderio di completare ogni compito assegnatole. Dopo alcune difficoltà iniziali che incontra nello svolgimento di determinate attività, cerca di risolverle in ogni modo possibile. Inoltre è capace di seguire diversi studenti sia nel progettare e svolgere esperimenti sia nell'insegnare nozioni teoriche di base, anche in contesti pubblici. Tale capacità è stata dimostrata sia con gli studenti interni al laboratorio, sia con studenti esterni, in quanto ha diretto con serietà, entusiasmo e impegno un corso di laboratorio per due anni di seguito (Laboratorio didattico

3